SLAC-125
UC-34
(EXP)

MEASUREMENT OF THE TWO PHOTON DECAY OF THE K_L^o MESON

JAMES E. ENSTROM

STANFORD LINEAR ACCELERATOR CENTER
STANFORD UNIVERSITY
Stanford, California 94305

PREPARED FOR THE U.S. ATOMIC ENERGY
COMMISSION UNDER CONTRACT NO. AT(04-3)-515

September 1970

Reproduced in the USA. Available from the Clearinghouse for Federal Scientific and Technical Information, Springfield, Virginia 22151.
Price: Full size copy $3.00; microfiche copy $ .65.

Print-70-2608

ABSTRACT

A measurement of the rate $\Gamma(K_L^o \rightarrow 2\gamma)$ has been made relative to the rates $\Gamma(K_L^o \rightarrow 3\pi^o)$, $\Gamma(K_L^o \rightarrow \pi^{\pm}\mu^{\mp}\nu_{\mu})$, and $\Gamma(K_L^o \rightarrow \pi^{\pm}e^{\mp}\nu_e)$ using a spark chamber scintillation counter experiment. Using published branching ratios of the three body decays relative to the rate $\Gamma(K_L^o \rightarrow \text{all})$, the branching ratio $\Gamma(K_L^o \rightarrow 2\gamma)/\Gamma(K_L^o \rightarrow \text{all})$ has been found to be $(4.5 \pm 1.0) \times 10^{-4}$, based on 23 valid decays, which were separated from a small background. The result is compared with theoretical predictions and other experimental measurements.

ACKNOWLEDGEMENTS

It is a pleasure to acknowledge the contributions of the many people who made this experiment possible. The experiment was under the direction of Professor Melvin Schwartz, who served as my advisor and who was a major source of help and inspiration to me. The very careful and precise work of Professor Stanley Wojcicki and Dr. Kenneth Riley, a visitor from Cambridge University, made possible the massive amount of data taking and data analysis necessary for the execution and completion of the experiment. I would especially like to thank Professor Wojcicki for his patience, perseverance, and thoroughness in helping me with the analysis of the experiment.

I appreciated very much the help, cooperation, and company of the other graduate students, David Raymond, Gideon Akavia, Robert Piccioni, and Allan Rothenberg. They, along with all those mentioned above, are to be especially thanked for having done most of the scanning of the spark chamber film. Dr. Dan Porat, Karl Hense, and Dale Ouimette are to be thanked for designing, building, and maintaining most of the electronics used in the experiment. Roger Coombes and Don Clark are to be thanked for designing and assembling most of the mechanical apparatus used in the experiment. George Ike and Jeff Hobson are to be thanked for measuring the spark chamber film. Professor William Bardeen is to be thanked for a critical discussion of the theory. Also, Drs. David Dorfan, David Fryberger, and Harry Saal are to be thanked for their valuable contributions to the experiment. In addition, I would like to indicate my gratitude to Karl Hense and Jeff Hobson for their help and encouragement when it was needed the most.

Many thanks go to the other facilities at SLAC which assisted the experiment. The machine shop and the heavy fabrication shop constructed the spark chamber,

the lead box, and the optical system. The high energy electronics shop provided and maintained the fast logic modules and high voltage power supplies. The accelerator staff developed the beam knockout system and successfully maintained the K_L^o beam during our data taking. The Computation Center made possible all the data processing.

Above all, I would like to thank my parents for the tremendous amount of patience, encouragement, and support they gave me during my graduate years.

This work was supported in part by the U. S. Atomic Energy Commission and the U. S. Air Force Office of Scientific Research, Contract No. F 44620-67-C-0070.

TABLE OF CONTENTS

LIST OF TABLES

LIST OF FIGURES

CHAPTER I

INTRODUCTION

A. Theory

The motivation behind studying the two photon decay mode of the K_L^o meson is to gain a better understanding of the weak interaction. The K_L^o meson is useful in this study because it is one of the few particles with both weak decay modes and a life time long enough that it can be separated from a background of strongly interacting particles and studied in an intense beam at a practical distance from the point of production. Specifically we can check the validity of various models which predict its rate. Also a complete study of this decay, coupled with the decay $K_S^o \rightarrow 2\gamma$, might provide a better understanding of the source of CP violation.

1. Theoretical Models for $K_L^o \rightarrow 2\gamma$

All models for this decay assume the K_L^o undergoes an intermediate transition via a strangeness changing weak interaction and converts to two photons via an electromagnetic interaction. The theoretical arguments are well summarized by J. Todoroff,[1] P. Kunz,[2] and J. Pilcher,[3] and presented in detail in the original papers.[4-15]

We shall discuss the widely used pole model in which the pseudoscalar bosons π^o and η^o have been considered as intermediate states. The basic formula for the rate is

$$\Gamma(K_L^o \rightarrow 2\gamma) = \frac{m_K^3}{16\pi} \left| M(K_L^o \rightarrow 2\gamma) \right|^2$$

where $M(K_L^o \to 2\gamma)$ is the decay matrix element, which can be written as

$$M(K_L^o \to 2\gamma) = f_{K\pi} \frac{m_K^2}{m_K^2 - m_\pi^2} M(\pi^o \to 2\gamma) + f_{K\eta} \frac{m_K^2}{m_K^2 - m_\eta^2} M(\eta^o \to 2\gamma)$$

where m_K, m_π, and m_η are the masses of the K_L^o, π^o, and η^o, $f_{K\pi}$ and $f_{K\eta}$ are properly normalized constants which measure the strength of the $K_L^o \pi^o$ and $K_L^o \eta^o$ vertices, and $M(\pi^o \to 2\gamma)$ and $M(\eta^o \to 2\gamma)$ are the matrix elements for the electromagnetic transitions.

Following Kunz,[2] we assume the exact SU(3) relation for the vertex constants

$$f_{K\eta} = \frac{1}{\sqrt{3}} f_{K\pi}$$

and relate the electromagnetic matrix elements by the formula

$$\frac{\Gamma(\eta^o \to 2\gamma)}{\Gamma(\pi^o \to 2\gamma)} = \frac{|M(\eta^o \to 2\gamma)|^2}{|M(\pi^o \to 2\gamma)|^2} \left(\frac{m_\eta}{m_\pi}\right)^3$$

Using the measured decay rates[16]

$$\Gamma(\pi^o \to 2\gamma) = (1.1 \pm 0.2) \times 10^{16} \text{ sec}^{-1}$$

$$\Gamma(\eta^o \to 2\gamma) = (1.5 \pm 0.4) \times 10^{18} \text{ sec}^{-1}$$

we obtain a rate in terms of $f_{K\pi}$ of

$$\Gamma(K_L^o \to 2\gamma) = (4.3 \pm 1.9) \times 10^{18} f_{K\pi}^2$$

or a branching ratio of

$$BR_{\gamma\gamma} \equiv \frac{\Gamma(K_L^o \to 2\gamma)}{\Gamma(K_L^o \to \text{all})} = (2.3 \pm 1.0) \times 10^{11} f_{K\pi}^2$$

Again following Kunz and assuming the estimated strength of the $K_L^o \pi^o$ vertex is given correctly as $f_{K\pi} = 4.2 \times 10^{-8}$,[15] we obtain

$$BR_{\gamma\gamma} = (4.0 \pm 1.8) \times 10^{-4}$$

The above value of $f_{K\pi}$ is based on current algebra and the hypothesis of partially conserved axial vector current (PCAC), but it is sensitive to the method of computation. For instance, we have recomputed $f_{K\pi}$, using the method of Oneda and Pati,[15] and obtained a value different from their quoted value above. We use the PCAC relation

$$m_K^2 f_{K\pi} = \frac{2g_A m_p}{g_r} M(K_S^o \to 2\pi^o)\Big|_{q(\pi^o) \to 0}$$

$$\simeq C_0 \frac{2g_A m_p}{g_r} M(K_S^o \to 2\pi^o)$$

where g_A is the ratio of the axial vector to vector β-decay coupling constant, g_r is the renormalized pion-nucleon coupling constant, m_p is the mass of the proton, and $q(\pi^o)$ is the four-momentum of one of the π^o mesons in the $K_S \to 2\pi^o$ decay, and

$$C_0 = \frac{\left(3m_\pi^2 + 4m_K^2 + m_\eta^2\right)}{16\left(m_K^2 - m_\pi^2\right)}$$

is a correction factor which is obtained in the PCAC expression corresponding to the $K^+\pi^+$ vertex.[15] We obtain $M(K_S^o \to 2\pi^o)$ from the expression

$$\Gamma(K_S^o \to 2\pi^o) = \frac{1}{32\pi} \frac{1}{m_K} \left(1 - 4\frac{m_\pi^2}{m_K^2}\right)^{1/2} |M(K_S^o \to 2\pi^o)|^2$$

using the experimental value for $\Gamma(K_S^o \rightarrow 2\pi^o)$. This yields

$$f_{K\pi} = 9.4 \times 10^{-8}$$

or

$$BR_{\gamma\gamma} = (20.0 \pm 9.0) \times 10^{-4}$$

Using a similar model by Savoy and Zimerman,[12] but ultimately assuming that the electromagnetic matrix elements are related by the SU(3) prediction

$$M(\eta^o \rightarrow 2\gamma) = \frac{1}{\sqrt{3}} M(\pi^o \rightarrow 2\gamma)$$

which is known to be not experimentally true, we obtain

$$f_{K\pi} = (3.7 \pm 0.6) \times 10^{-8}$$

or

$$BR_{\gamma\gamma} = (3.5 \pm 1.2) \times 10^{-4}$$

From the above estimates we see that the branching ratio is most sensitive to the value of $f_{K\pi}$, which is dependent on the validity of the PCAC hypothesis, and to the relationship between $f_{K\eta}$ and $f_{K\pi}$, which may or may not be correctly given by the SU(3) prediction. Basically in order to get a theoretical value which agrees with the experimental results there has to be a large amount of cancellation between the π^o and η^o pole term contributions. The π^o pole term above gives much too small a value and the η^o pole term alone gives much too large a value. But, improvements will have to be made in the details of the theoretical model before it will lead to a single accurate prediction of the branching ratio.

2. CP Implications

Because of the observed CP violation in the two pion decay mode of the K_L^o,[17] a study of the two photon decay mode has certain interesting implications. The

K_L^o decays into two gammas which must either be in a CP even or CP odd eigenstate:

$$\text{CP even:} \quad |1\rangle = \frac{|LL\rangle + |RR\rangle}{\sqrt{2}}$$

$$\text{CP odd:} \quad |2\rangle = \frac{|LL\rangle - |RR\rangle}{\sqrt{2}}$$

where $|LL\rangle$ and $|RR\rangle$ are the two photon final states of left- and right-hand polarization respectively. With no CP violation we would expect $|K_S^o\rangle$ to decay to $|1\rangle$ and $|K_L^o\rangle$ to $|2\rangle$. However, since CP is violated $|K_S^o\rangle$ and $|K_L^o\rangle$ can decay into the same CP eigenstate and there can be interference between the two states, with the size of the interference depending on the source of the CP violation and the relative size of $M(K_S^o \rightarrow 2\gamma)$ and $M(K_L^o \rightarrow 2\gamma)$, the matrix elements for the respective weak interaction transistions. The details of this interference have been worked out in the literature[9,10,13] and are summarized by P. Kunz[2] and J. Pilcher.[3] However, the decay $K_S^o \rightarrow 2\gamma$ has yet to be observed and any interference effect in the photon decays would be even harder to measure. Estimates of the size of this effect have been made,[14,18] and the prospects for studying it more completely are improving with the capability for more statistics and better resolution.

B. Basic Method of Experiment

The basic approach of this experiment was to use scintillation counters and a large optical spark chamber to detect and photograph the presence of electromagnetic showers originating from the two photon decay of the K_L^o. We measured the rate of $K_L^o \rightarrow 2\gamma$ by geometrically reconstructing the events with two showers to find a best fit vertex. Then using measured time-of-flight for the kaon to obtain its momentum, we transformed the decay to the center-of-mass system

and determined whether the gamma rays were collinear, and hence whether they originated from $K_L^o \rightarrow 2\gamma$ decays. The total rate at which all decays occurred was determined by detecting decay modes of the K_L^o whose branching ratios are well known. We measured the rate of $K_L^o \rightarrow 3\pi^o$ by analyzing the resultant gamma shower events in the spark chamber. Concurrently, we measured the rate of the leptonic decays, $K_L^o \rightarrow \pi\mu\nu_\mu$ and $K_L^o \rightarrow \pi e\nu_e$, by analyzing the events with a pion and lepton in the chamber.

Using the number of genuine 2γ decays, the total number of K_L^o decays, and several efficiency factors which were determined by Monte Carlo programs, we were able to calculate the branching ratio

$$BR_{\gamma\gamma} = \Gamma(K_L^o \rightarrow 2\gamma)/\Gamma(K_L^o \rightarrow \text{all})$$

In addition we made an attempt to understand and estimate the background and all possible sources of systematic and random error.

C. Discussion of Previous Experiments

The first $K_L^o \rightarrow 2\gamma$ experiment was done by Criegee et al.,[19] in 1966 and used a beam of 1 BeV K_L^o mesons which decayed in a 1-ft × 1-ft × 4-ft long region 75 ft from the target. The resulting gammas were detected in two separate spark chambers placed symmetrically about opposite sides of the beam. The spark chambers were preceded by lead plates and followed by lead and total absorption scintillation counters. Normalization was obtained using the charged decay modes $K_L^o \rightarrow \pi\mu\nu_\mu$, $K_L^o \rightarrow \pi e\nu_e$, and $K_L^o \rightarrow \pi^+\pi^-\pi^o$. Monte Carlo programs were used to determine their triggering efficiencies, which were all of the order .002. The actual number of 2γ events obtained was approximately 30, but the 2γ decays were detected with an overall efficiency of only about 10^{-4} and, in addition, there were several cuts which made the result very sensitive to systematic effects.

In fact, the first published result of $BR_{\gamma\gamma} = (1.3 \pm .6) \times 10^{-4}$ [19] was five times smaller than the result of a reanalysis of the same experiment by Todoroff,[1] which was $BR_{\gamma\gamma} = (6.7 \pm 2.2) \times 10^{-4}$.

The heavy liquid bubble chamber experiment by Arnold et al.,[20] in 1968 studied 2γ and $3\pi^0$ decays observed in CF_3 Br. Its result rested on only 16 measured events, with a number of factors such as the gamma conversion efficiency and the scanning efficiency which had to be introduced as corrections, increasing the number of expected 2γ events by roughly a factor of two. The normalization was determined from the number of $3\pi^0$ decays, which were counted in a way similar to the 2γ events. The result was $BR_{\gamma\gamma} = (5.3 \pm 1.5) \times 10^{-4}$.

The two spark chamber gamma ray spectrometer experiments, written up in the theses of P. Kunz[2] and J. Pilcher,[3] yielded the largest number of 2γ events in the final sample, namely 115. But the overall number of normalizing events was dependent on certain momentum cuts and also dependent on the detection efficiency ratio $\epsilon(K_L^0 \rightarrow 3\pi^0)/\epsilon(K_L^0 \rightarrow 2\gamma) \simeq .02$. Thus a small error in the efficiency ratio could cause a large error in the final value of $BR_{\gamma\gamma} = (4.7 \pm .6) \times 10^{-4}$.[3]

The present experiment had the intrinsic advantage that it had a relatively high efficiency for detecting both the 2γ events, $\epsilon(K_L^0 \rightarrow 2\gamma^0) \simeq .2$, and the $3\pi^0$ events $\epsilon(K_L^0 \rightarrow 3\pi^0) \simeq .4$ and the ratio of efficiencies was fairly insensitive to other parameters such as the gamma conversion probability. Also a normalization independent of the $3\pi^0$ decays was determined by using the leptonic decay modes.

CHAPTER II

APPARATUS

A. Accelerator and Beam

The data for this experiment was taken at the Stanford Linear Accelerator Center during 200 hours of running time in December, 1968 and 350 hours during April and May, 1969. The B beam line of the accelerator provided 16 BeV electrons in 1.5 μsec bursts which occurred at a rate of 180/sec with an average current of 1.5 mA. Coming from the injector the electrons were bunched within a phase of less than 5° of the sinusoidal rf electromagnetic field which oscillated at the accelerator frequency of 2856 MHz.[21] In order to obtain an unambiguous measure of the time-of-flight of the kaons produced at the target it was necessary to decrease the rate at which bunches passed down the accelerator. This was achieved by the use of a knockout system[21] which consisted of a transverse electric field developed between two metal plates on either side of the beam, which deflected all the bunches into the accelerator wall except the ones which passed through the plates during a null in the sinusoidal electric field. The plates were located in the injection system and were supplied with rf power at 40 MHz, so that only one electron bunch passed through every 12.5 nsec. A second set of plates supplied with rf power at 10 MHz reduced the bunch rate to one every 50 nsec.

The chopped electron beam then hit a 1-1/2-in. diameter, 21-in. long cylindrical beryllium target, and the subsequent electromagnetic interactions produced a secondary beam of K_L^o mesons, along with a background of charged particles, such as muons, pions, and charged kaons, in addition to neutrons and photons. The spectrum of K_L^o mesons coming from the target at a production angle of 3° beam was determined in a previous experiment[22] and is given in Fig. 1.

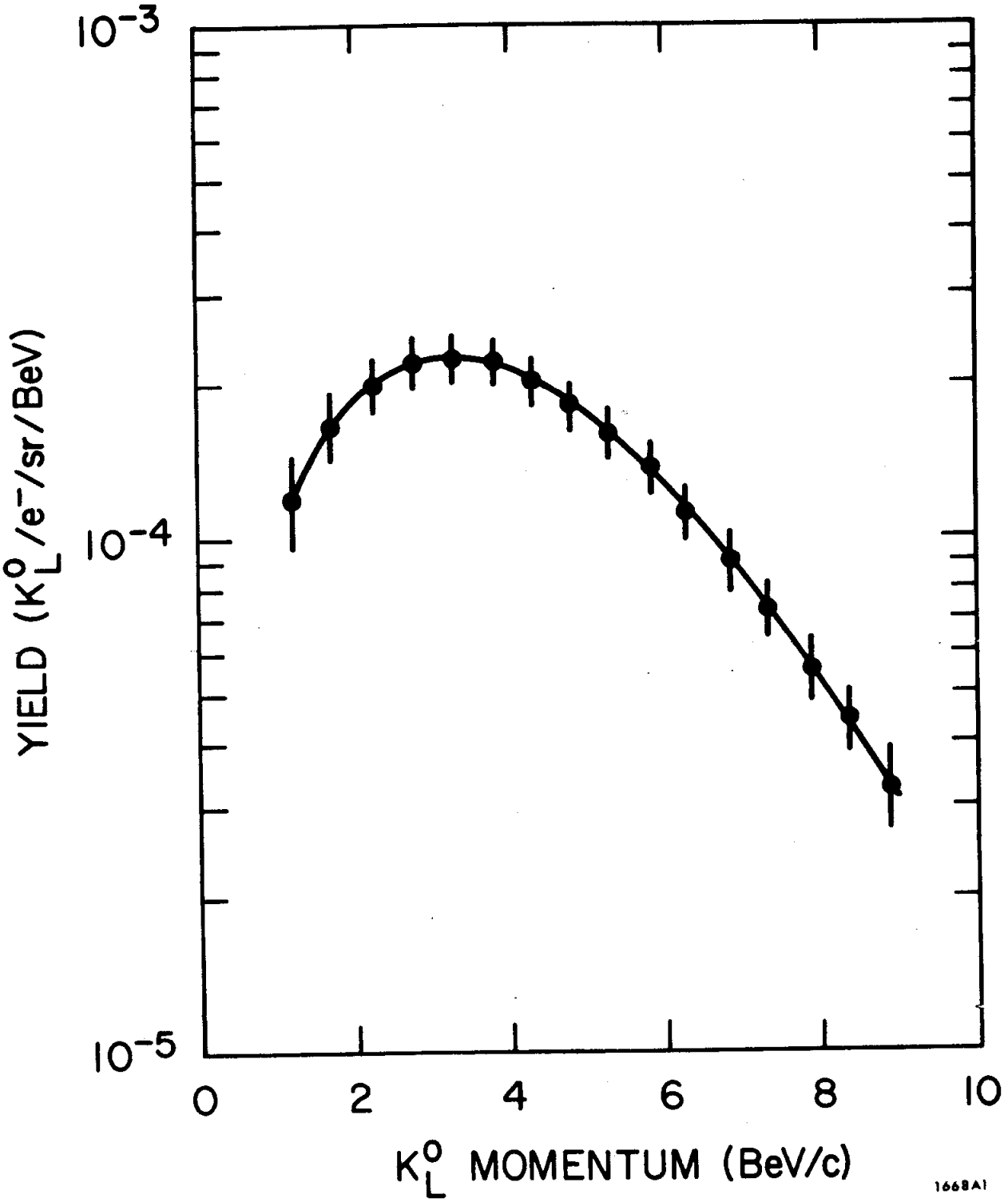

FIG. 1--K_L^o momentum spectrum at target.

The electron beam continued through the target and was absorbed in a 20 kW, water-cooled beam dump. The bare end of a coaxial cable was placed immediately after the target and before the dump. A current was induced in the cable by virtue of the fact that more electrons were ejected than were incident. This current formed a well defined pulse which was sent via an air core cable to the detection apparatus area and was used for timing the kaons produced at the target.

The secondary beam, which traveled in air at 3^{o} to the right of the electron beam, passed into End Station B through a 3-in. × 3-in. hole in a 2-ft high and 12-ft long steel layer, which was located at the beam height of 7 ft above the ground, in an otherwise concrete wall. To eliminate the photon component of the beam, 12 in. of lead converter was placed immediately after the wall. Charged particles in the beam were removed by four horizontal sweeping magnets. Two 18D36 (18 in. × 36 in.) magnets were located along the beam line approximately 45 ft and 140 ft, respectively, from the target. Downstream from the first sweeping magnet was a 30-ft long cylindrical iron and steel shield which attenuated the charged particles, mainly pions and muons, which did not pass through its 16-in. diameter hole. Upstream of the second sweeping magnet was a 6-in. diameter, 4-ft long lead collimator which further attenuated photons and charged particles. Located approximately 180 ft from the target was a third 18D36 magnet, which was part of another experiment that was conducted along our beam line.[23] The beam then passed through the far wall of End Station B and through a final 12D60 magnet located 230 ft from the target. The basic beam layout is shown in Fig. 2.

The beam remaining after the last magnet was composed of K_L^o mesons and neutrons, which were approximately equal in intensity,[22] and a small photon

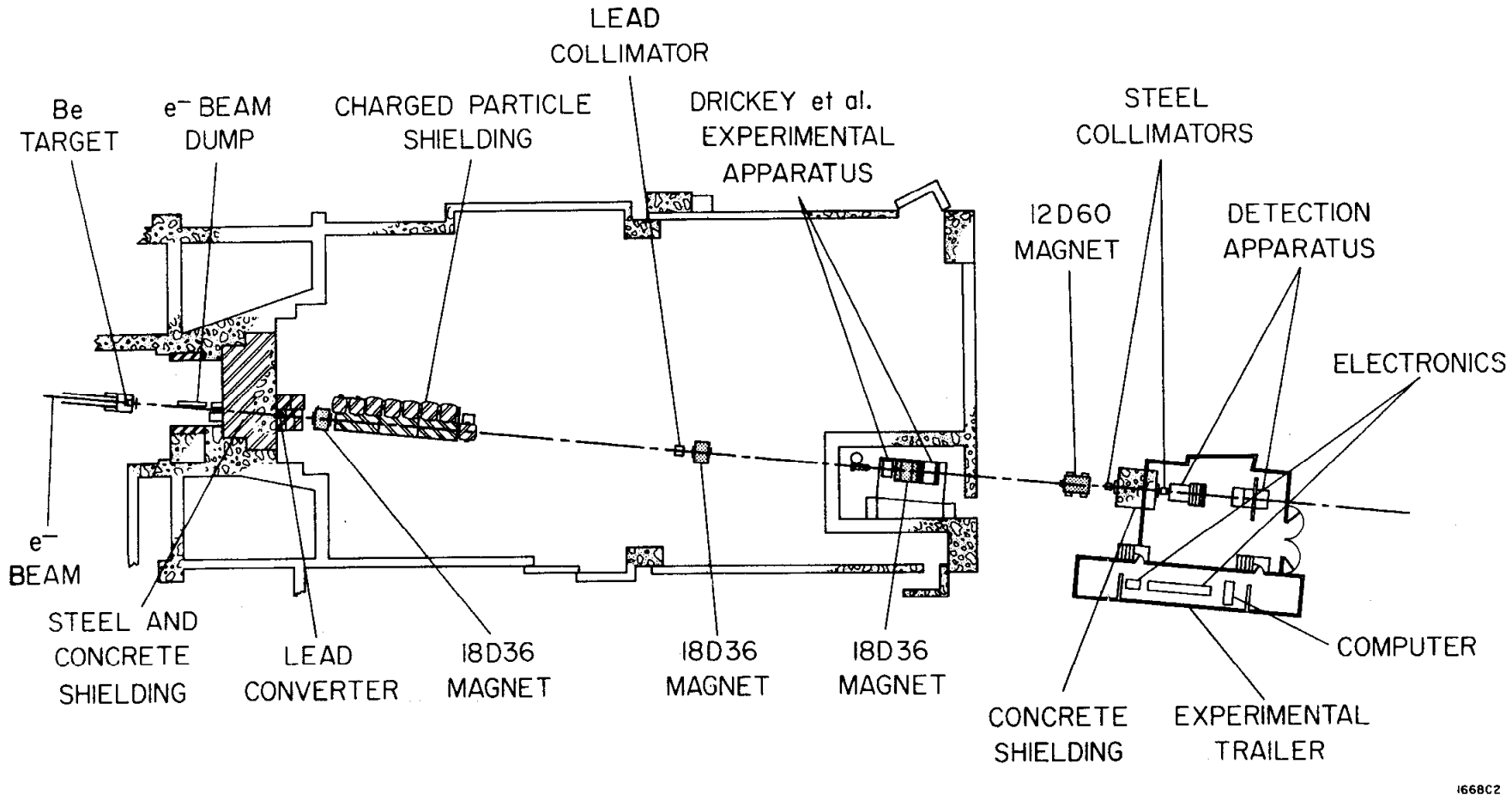

END STATION B

FIG. 2--K_L^o beam line.

component. This beam then passed through a defining collimator and a shadow collimator. The collimators in the December, 1968 data taking period, known as Run 4, were located 8 ft and 20 ft downstream of the 12D60 sweeping magnet, with a 9-ft long concrete block between them. The defining collimator was made of 7-in. high × 15-in. wide × 24-in. long mild steel with a 1-in. thick hevimet lining surrounding a 1-in. high × 8-in. wide opening centered in the steel. The shadow collimator was made of 7-in. high × 15-in. wide × 18-in. long mild steel with a 2-in. high × 10-in. wide opening centered in it. Located 6 in. upstream of shadow collimator were two pairs of small 1/8 in. × 20 in. scintillation counters, with two above the beam and two below the beam and separated by 3 in. These were called M* counters and were used to scale the charged decays of the kaons which passed between them; they are discussed in more detail later. The relative location of the collimation equipment for Run 4 is shown in Figs. 2 and 3.

During the April-May, 1969 data taking period, known as Runs 6 and 7, the position of the collimators was changed to increase the efficiency for triggering on kaon decays. The defining collimator was placed 12 ft upstream of the 12D60 sweeping magnet and the shadow collimator was placed at the former location of the defining collimator. The data for Run 6 was taken with a 1-in. × 5-in. opening in the defining collimator. The data for Run 7 was taken with two 1-in. × 1-in. holes, separated by 6-in. brass shims in order to reduce the size of the collimator openings. Two 1/2-in. × 6-in. × 33-in. scintillation counters were added 6 in. downstream of the M* counters. They had a layer of 1/2-in. thick lead, covering their upstream face, and were placed horizontally about the beam and separated by 3 in. They were called B counters and they effectively served as a collimator because they vetoed the triggering of any event whenever

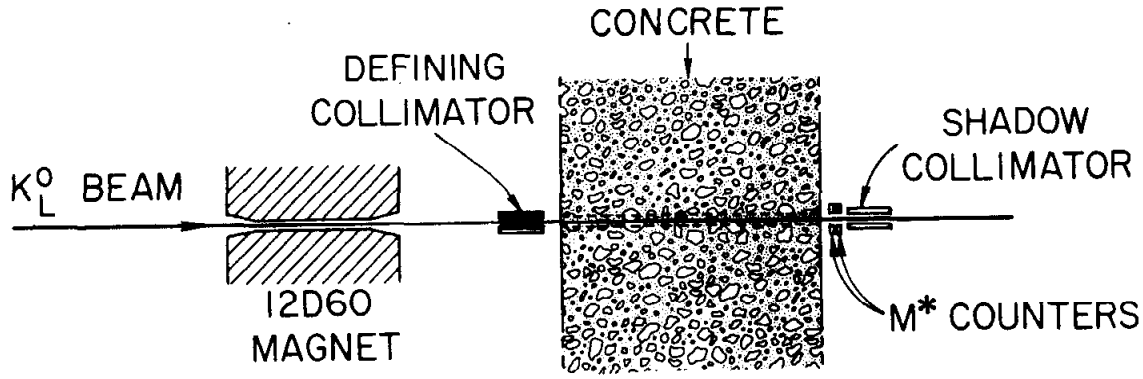

RUN 4

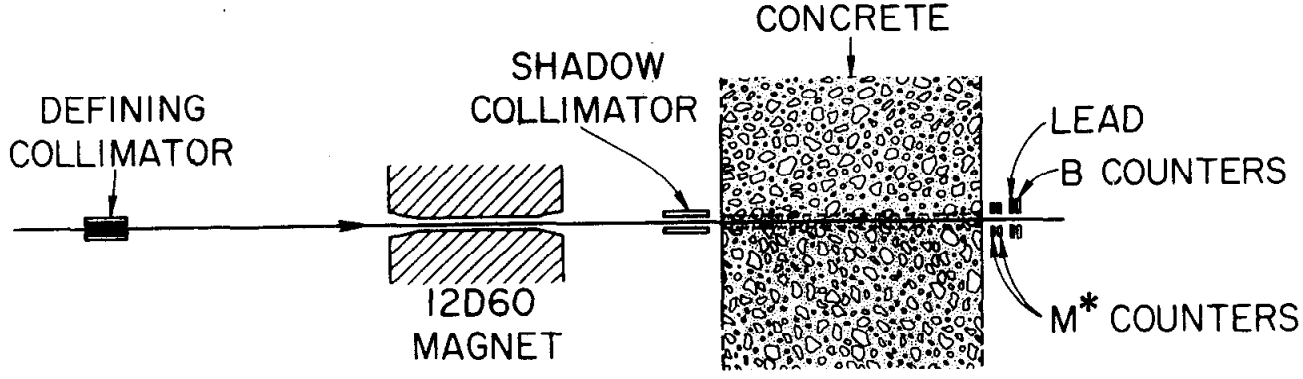

RUNS 6 AND 7

SIDE VIEW

166883

FIG. 3--Collimation of K_L^0 beam.

a charged particle or converted photon passed through them. The location of the collimators and counters for Runs 6 and 7 is shown in Fig. 3.

B. Decay Region and Detection Counters

The decay volume immediately following the second collimator in Run 4 was a four-sided aluminum frame box centered about the beam, with a 47-in. × 47-in. internal cross section and 48-in. length. The inside of the box was lined with a 1/2-in. thick layer of lead. Within the lead box was a heavy duty polyethylene bag which was inflated with helium gas to fill the decay region. The probability of a kaon interacting in helium as it traversed the decay volume was about a factor of seven smaller than that of interacting in air. Each of the four sides on the outside of the box were covered with three pairs of 1/2-in. × 12-in. × 60-in. scintillation counters. There were two additional counters placed on the top and bottom sides of the box to make a total of twenty-six counters, called latch (L) counters. The downstream vertical end of the box was covered with six 1/2-in. × 11-in. × 60-in. scintillation counters, two above beam level and two below beam level, and two 1/2-in. × 6-in. × 33-in. counters at beam level. These were known as veto (V) counters and were arranged as shown in Figs. 4 and 5. The lead box and latch counters were used to convert and detect the presence of photons, which originated from the neutral decay modes of kaon and did not enter the spark chamber. They also detected accidental tracks which occurred at the same time as the decays. The veto counters were used to detect the presence of charged particles which occurred in the charged decay modes. These plastic scintillation counters were equipped with a lucite light pipe and a 56 AVP photomultiplier tube at one end. At the opposite end was imbedded a gallium phosphide photodiode connected to a pulsing unit via a 50 ohm impedance coaxial cable. The photodiode was used to provide a standard light pulse to the

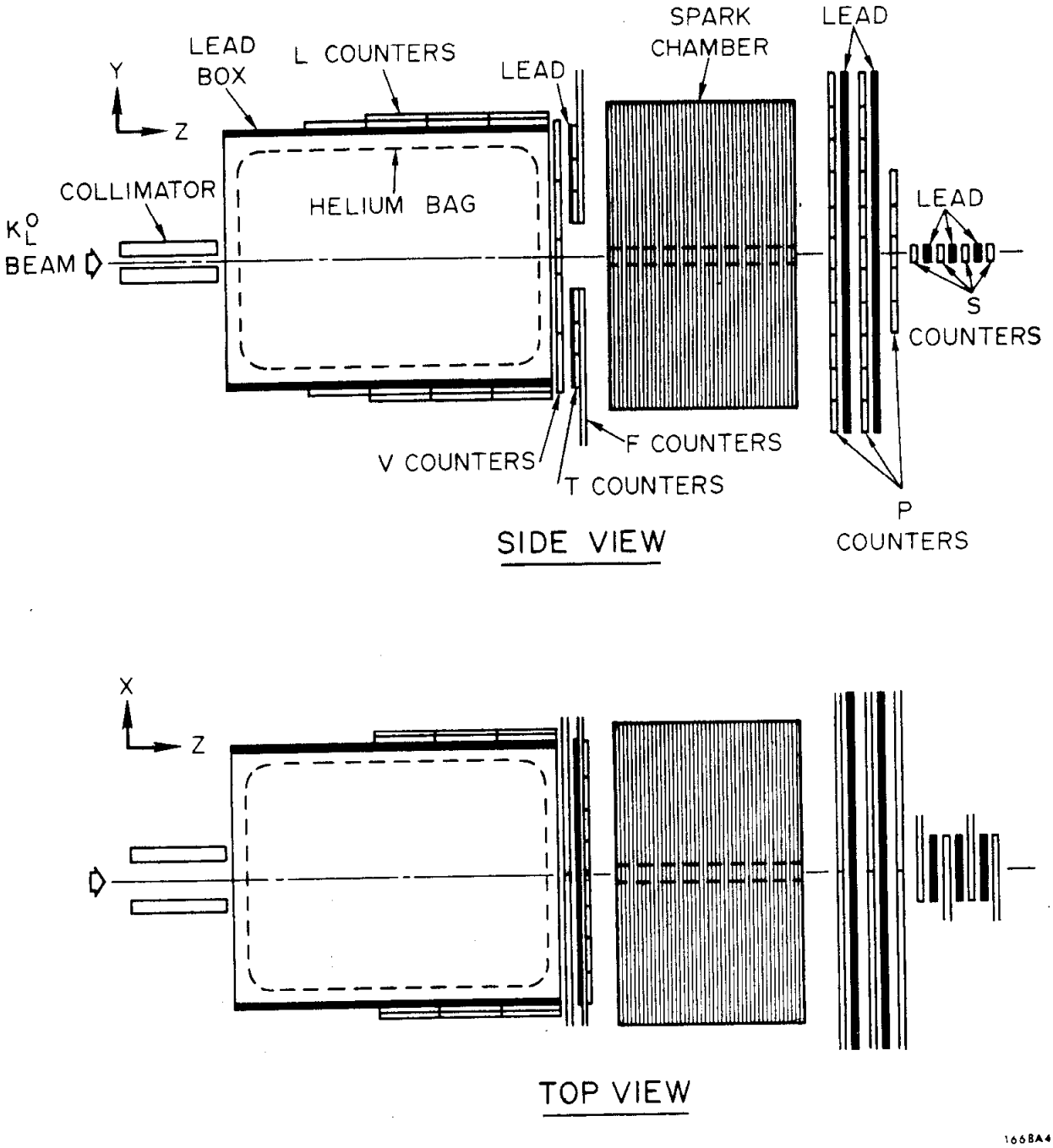

FIG. 4--Detection apparatus (Run 4 collimation).

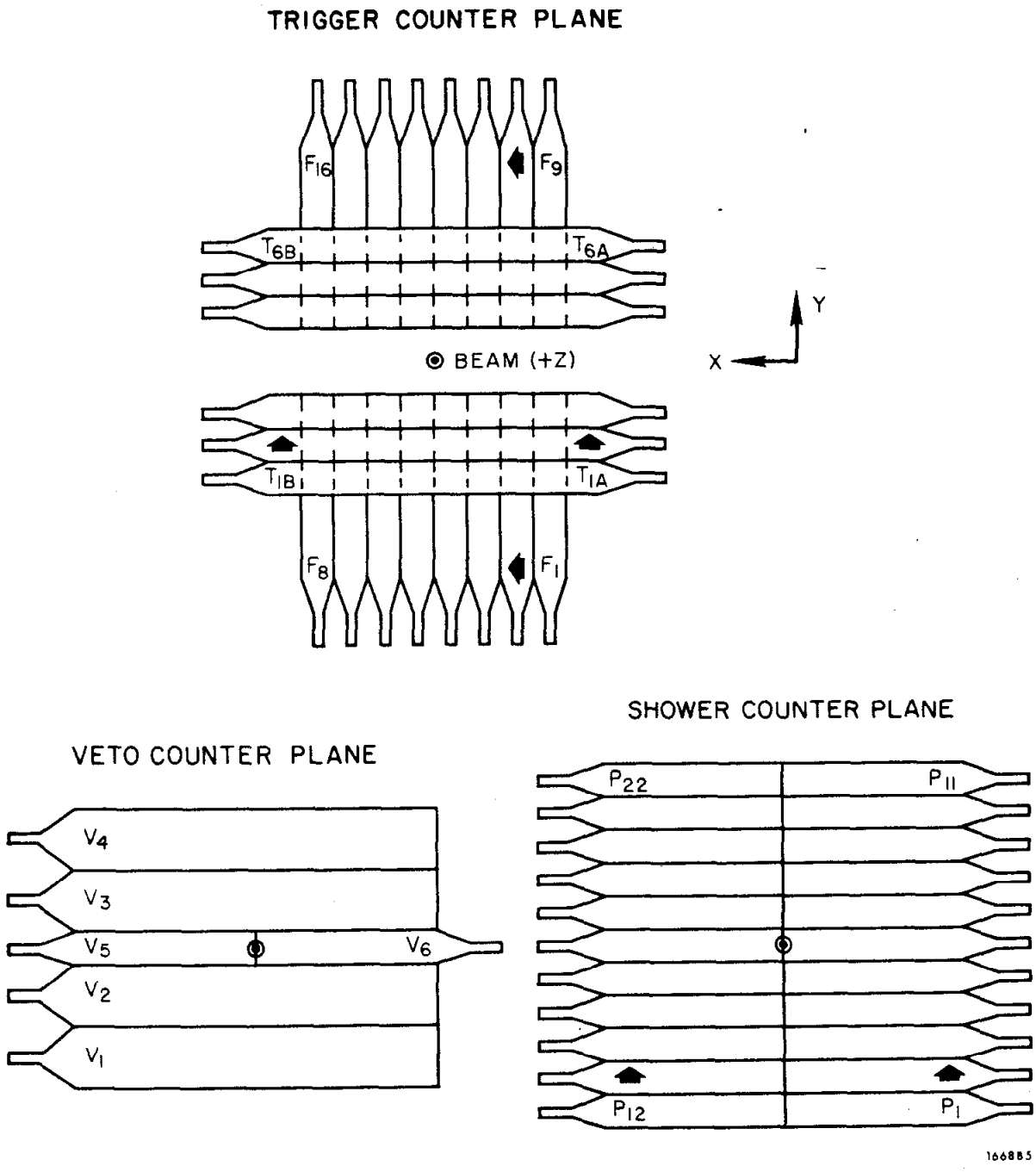

FIG. 5--Scintillation counter banks.

counter in order to monitor its proper operation. The photomultiplier tubes were operated with approximately 2000 Vdc to give an output signal of approximately -0.5 V amplitude and 20 nsec width for a minimum ionizing track passing through the counter.

Downstream of the veto counters were two 1/4-in. × 18-in. × 60-in. slabs of lead, each supported by an aluminum frame and displaced 6 in. vertically from the center of the beam line, which acted as converters for photons which came from the neutral kaon decays. Immediately downstream of the lead was the bank of counters called T counters, consisting of three horizontal counters above and three below the beam, again displaced 6 in. from the center of the beam. These counters were 1/2-in. × 6-in. × 60-in. and were equipped with light pipes and 56 DVP photomultiplier tubes at both ends, with a photodiode located at the center. They were each supported with a backing of 1/2-in. thick wood. In a plane immediately downstream of the T counters were sixteen vertical counters, called F counters, eight below the beam and eight above the beam. These counters were 1/2-in. × 6-in. × 33-in. and were equipped with a light pipe and an XP 1021 photomultiplier tube at one end and a photodiode at the other. The arrangement of these is shown in Figs. 4 and 5. The T and F counters were used to determine the time-of-flight of the kaon. Hence on each counter it was necessary to minimize the time jitter due to the finite rise time of the output pulse. This was done by operating the T and F counter photomultiplier tubes at about 2500 Vdc, which gave about a -2 V output pulse.

C. Spark Chamber

The spark chamber was located downstream of the T and F counter planes and consisted of twenty-one 63-in. × 63-in. cross section, 1/2-in. thick aluminum ground plates alternated with twenty 63-in. × 63-in. cross section, 1/2-in. thick plates made of a copper covered laminate called G10.[24] Each G10 plate

was a fiberglass substance made of 65% SiO_2, 25% AlO, and 10% MgO with a total density of 1.8 gm/cm^3 and with a .002-in. thick layer of copper covering each side of the plate. The plates were separated from one another at their perimeter by a 3/8-in. thick × 1-in. wide border of transparent lucite with 1/16-in. deep O-ring grooves cut into them. The plates were made gas tight by 1/8-in. diameter soft rubber O-rings, which were seated in the grooves and pressed tight against the aluminum plates. All the plates were held together with steel rods which passed through the four corners of each plate and were bolted at the end aluminum plates and grounded.

For specifying the boundaries of the chamber, fiducials were located in each corner of the first and last aluminum plates at the corners 28-in. horizontally and 28-in. vertically from the center of the plate, and along the vertical sides 28 in. from the center and 2 in. above and below the center line. They consisted of 3/4-in. long plastic tubes which were inset into the aluminum plates through 1/8-in. diameter holes. The eight fiducials at each end of the chamber were then supplied with light from a 120 V neon flash tube via fiber optics light pipes. The fiducial plane on the first aluminum plate was located 71.4 in. from the downstream edge of the shadow collimator in Run 4. The fiducial plane was 87 in. downstream of the B counters used in Runs 6 and 7. The fiducial plane was also 6 in. from the T and F counters and 9 in. from the V counters. The second fiducial plane was 34.6 in. downstream from the first plane. The location of the spark chamber with respect to the other apparatus is shown in Fig. 4.

The copper on each side of the G10 was separated into four horizontal strips with 1/8-in. wide separations which were located at the center and 12 in. above and below the center. The original motivation for separating the copper was to increase the multitrack efficiency[25,26] of the spark chamber by providing four

independently charged copper strips per plane which would each be discharged only by the gamma showers which passed through them. Monte Carlo simulations of the $K_L^o \rightarrow 3\pi^o$ decay indicated that for a typical kaon decay, the gammas would distribute themselves roughly uniformly within the four sections by the time they had traveled half way through the chamber. This would have increased the multitrack efficiency, since there would have been only one or two showers in each segment. After much experimentation using tests with cosmic ray muon tracks, it was discovered that the segments were not well separated electrically and hence instead of discharging to the ground plate when pulsed, they would break down from one section to another and create spurious sparks. The fact that the segments were not completely decoupled decreased the expected good multitrack efficiency. The breakdown could not be stopped completely even when layers of epoxy up to 1/2-in. thick were spread over the separations in the copper, because the epoxy simply acted as a dielectric and carbon deposits formed on its surface whenever breakdown occurred and hence tended to form in places where repeated breakdown would occur. The end result of the tests was that the segments above and below the center were directly coupled at the ends of the plates, although the epoxy remained on the separation along the plates. This effectively left two independent halves in each spark gap plane. There was no direct breakdown between the two halves because in addition to the epoxy there was also opaque mylar in a V-shaped trough, which was epoxied horizontally across the chamber. The mylar acted both as an insulator and as an optical divider which kept sparks in the upper half of the chamber visible only in the top view and sparks in the lower half visible in the bottom view.

There were ten wire electrode high voltage spark gaps and each gap was connected in parallel to eight 5000 pf charging capacitors, one of which was

connected to each of eight half segments of four adjacent copper planes. Each aluminum ground plate was connected to the adjacent copper plate by a 50 ohm, 1/4 watt terminating resistor which gave the pulse which went onto the plates a decay time of roughly 200 nsec. Due to the inductance in the connections of the capacitor to the copper plate and the intrinsic inductance in the spark gap itself, which totaled about 30 nh, the rise time of the pulse going onto the plates was about 50 nsec, with the best rise time as short as 30 nsec and the poorest around 80 nsec. The spark gaps were powered by a high voltage supply set at about 9000 V and triggered with a driver amplifier which used a Marx generator to develop a negative high voltage trigger pulse. The basic operation of this spark chamber was the same as that of other plate spark chambers.[25,26]

A commercial spark chamber gas of 90% neon-10% helium was mixed with the vapor from propenol alcohol in a bath at -15% and circulated through the chamber with a pump and purification system that had a liquid nitrogen trap which the spark chamber gas passed through to keep the oxygen contamination in the gas to less than .1%. The alcohol vapor was added to the gas mixture in an attempt to increase the spark development time and hence improve the multitrack efficiency, if there were several showers in one half plane. The effectiveness of this procedure was not really known, but qualitatively an improvement was noted in the quality of the showers.

D. Shower Counters

Following the spark chamber were two full banks of twenty-two horizontal counters, called P counters, which absorbed the showers originating in the spark chamber. They were separated by a slab of lead converter. The counter-lead-counter sandwich was followed by a second slab of lead and a partial bank of ten more counters, centered about the beam line. Each slab of lead was

60-in. × 60-in. in cross section and 1/2-in. thick and had a 2-in. high × 10-in. wide hole in the center to let kaons from the beam pass through without interacting. The P counters were 1/2-in. × 6-in. × 33-in. and came with a photodiode at one end and a light pipe and 56 AVP photomultiplier tube at the other end, which was operated at about 2000 Vdc. The output current from the photomultiplier tubes for counters in the same vertical position in each of the three banks was summed directly to obtain a combined pulse, which was roughly proportional to the total energy deposited in those counters. The P counter banks only absorbed part of the energy from the photon showers because 1 in. of lead represented only 5 radiation lengths, or 4 conversion lengths, of converter. The highest fraction of energy was absorbed for showers which were below about 1.5 BeV in total energy and which developed early in the spark chamber. The shower energy calibration is discussed later.

Following the P counters were four small 1/8-in. × 2-in. × 18-in. counters, with each of the last three preceded by a 1/4-in. thick piece of lead. These were called S counters and were used to convert and detect any gammas which had gone through the hole in the chamber and P counter lead. They were equipped with 56 AVP photomultiplier tubes and were operated like the P counters. The arrangement of the P and S counters is shown in Figs. 4 and 5.

E. Camera and Photography

Photographs containing a top, bottom and side view of the spark chamber gaps were taken of each event using a mirror system which focused the light from the sparks, fiducials and chamber plates on a lens. Each of the forty gaps was numbered in all three views, with the first gap being the one containing the upstream fiducials. Also recorded in each picture was the run-roll-frame number in octal and the presence of a special light for certain events which will be

discussed later. Silver-coated strip mirrors, 1.9 in. wide, extended the full length of each individual gap and were adjusted so that the light from consecutive gaps converged to the lens to give a uniform reproduction of the spark chamber itself. In addition to the strip mirrors, two sets of focusing mirrors were used to direct the light onto the lens. The pictures were taken on 70 mm wide Kodak Plus X Panchromatic film, which was unperforated and came in 400 ft rolls. It was mounted in a motor driven camera which advanced at a maximum speed of 2 frames/sec, using vacuum suction to hold the film in place and a release of the vacuum to advance the film. The camera and other apparatus was located in a wooden building and was kept completely dark when in use. The camera was operated with an open shutter and background illumination was provided by four lights which were directed at the spark chamber plates and were flashed on for each picture long enough to produce an outline of the spark chamber on film.

A perspective view sketch of all the apparatus as it was actually set up, using the collimator positions for Runs 6 and 7, is shown in Fig. 6. The concrete wall following the shadow collimator has been removed from the sketch for clarity. A side view picture of apparatus, including the camera, focusing mirrors and background lights is shown in Fig. 7. A back view of the spark chamber, showing the strip mirrors and shower counters, is shown in Fig. 8.

F. High Voltage System and Electronics

The high voltage system was used to supply dc power to the photomultiplier tubes, which were each run at about 2000 to 2500 Vdc. It consisted of seven commercial power supplies, each with a 3000 Vdc, 20 mA capacity. The output from the power supplies was fed into nine separate distribution boxes, which in turn sent the proper voltage to each phototube. Within each distribution box the individual output voltages could be adjusted over a 200 to 500 Vdc range.

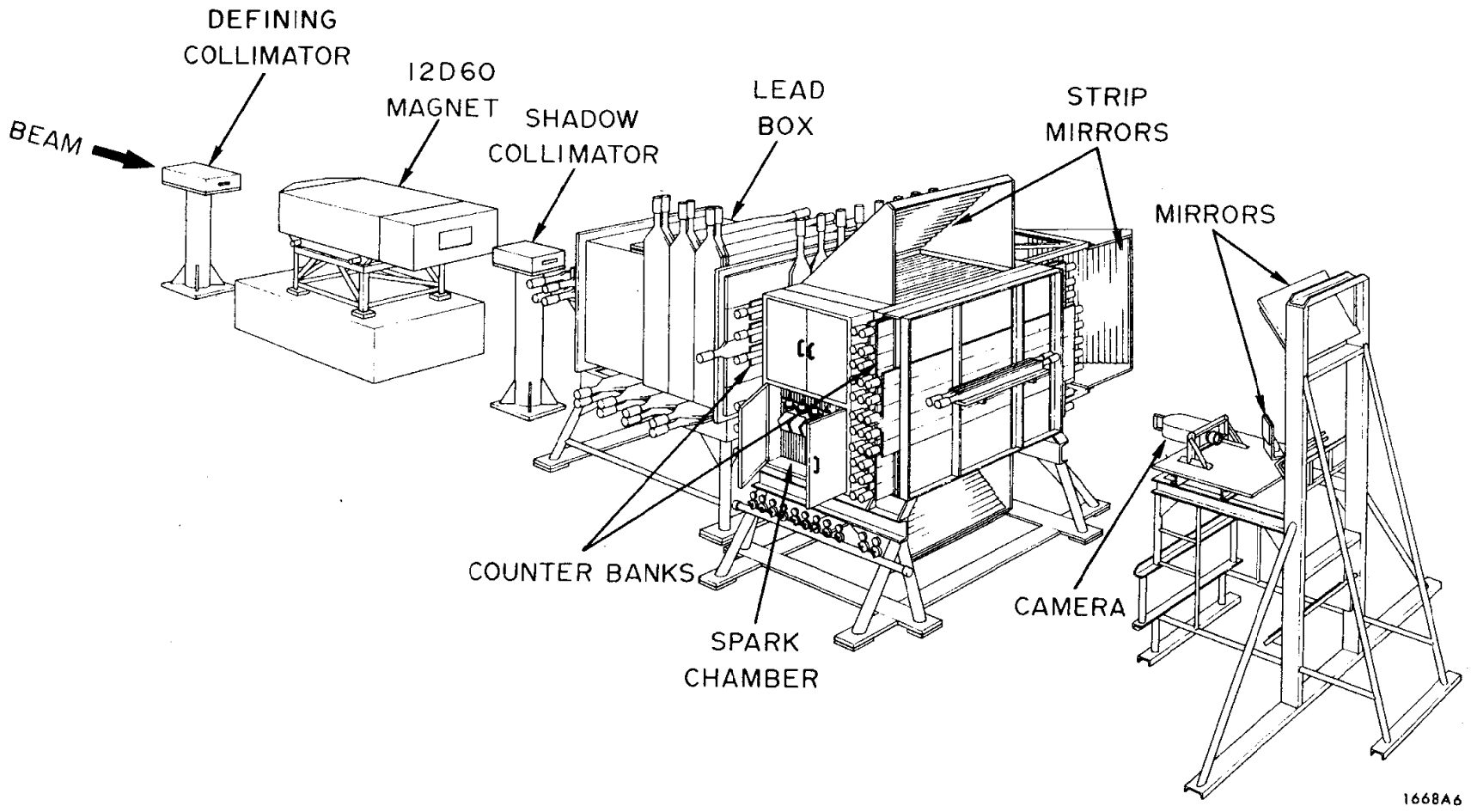

FIG. 6--Perspective view of detection apparatus (Runs 6 and 7 collimation).

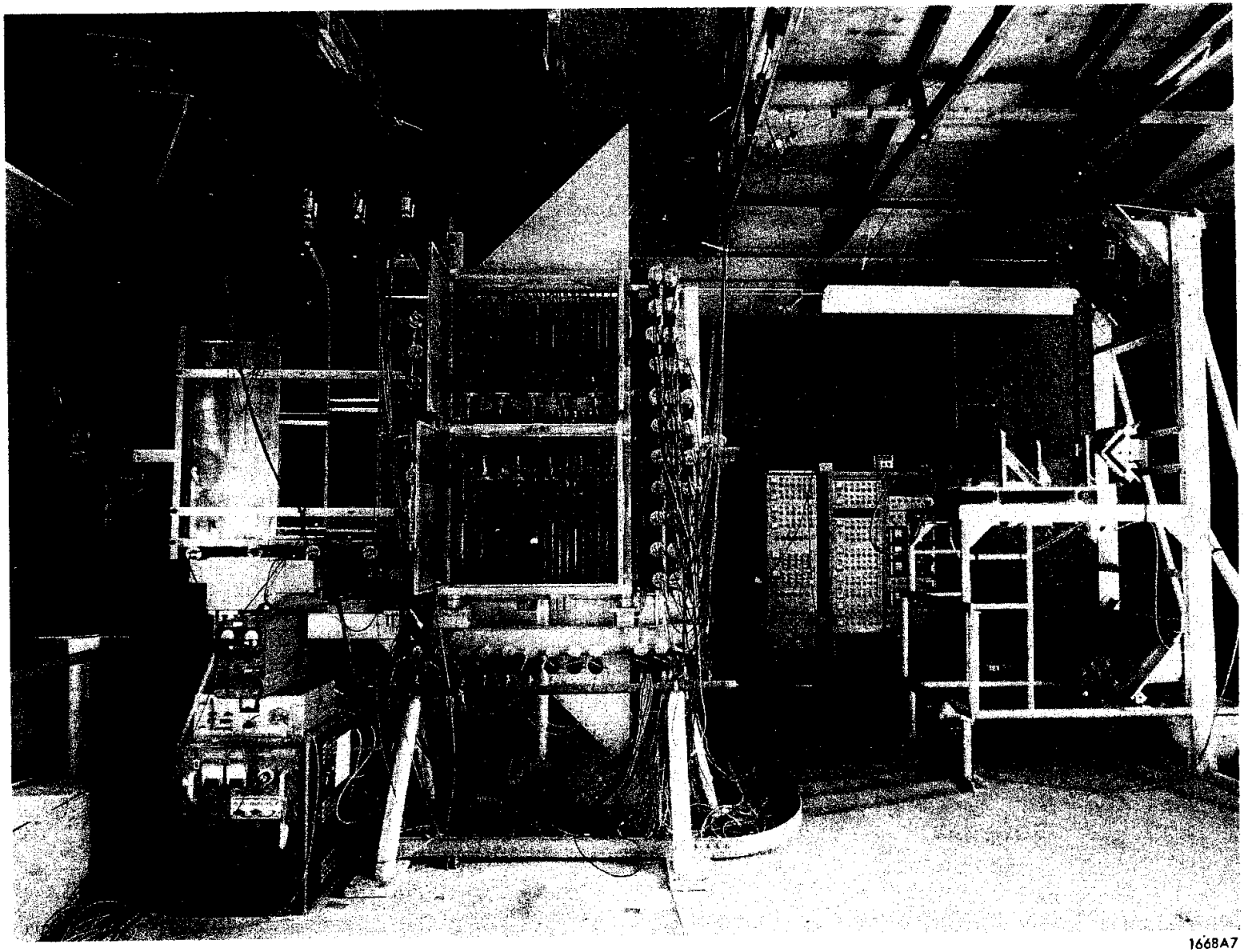

1668A7

FIG. 7--Photograph of detection apparatus (side view).

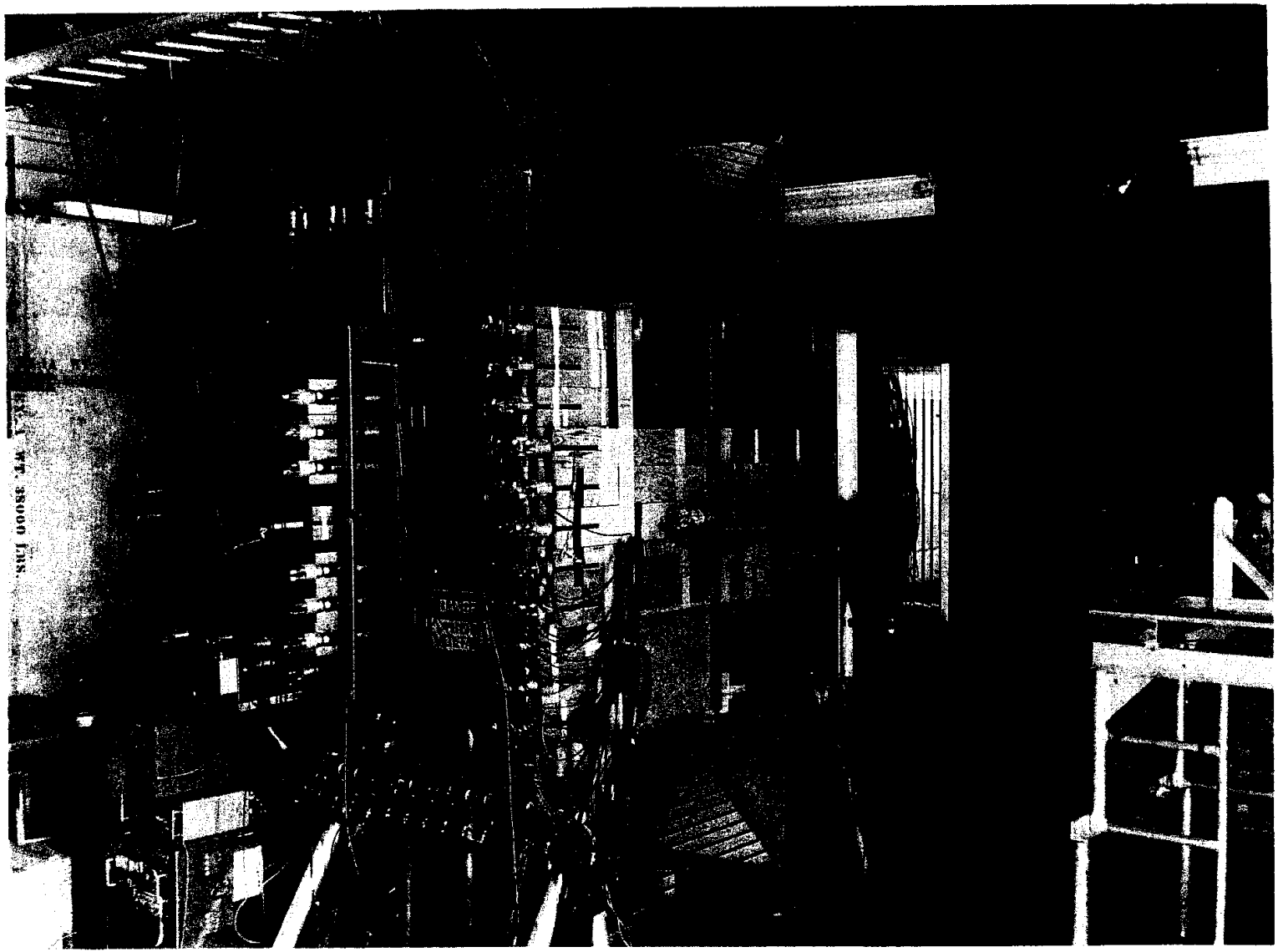

1668A8

FIG. 8--Photograph of detection apparatus (back view).

A pulser of the mercury reed relay type was used to produce a standardized electrical signal of roughly 1000 V total amplitude and 5 nsec width at a rate of 60 Hz. This pulse was divided up and sent to one or more groups of a dozen or so counters, with each photodiode receiving a pulse of about 50 V, which in turn produced a pulse of about -.5 V from the photomultiplier tube. The counters were divided into the following groups: P_1 to P_{11}, P_{12} to P_{22}, V_1 to V_4, L_1 to L_{13}, L_{14} to L_{26}, T_1 to T_3, T_4 to T_6, F_1 to F_8, and F_9 to F_{16}. An eight step telephone stepping relay was used to determine which of the above groups were to be pulsed at a given time.

Various electronic modules were used to standardize the pulses received from the counters and to form logic circuits which triggered the apparatus. These fast logic modules were commercially made and resolved input signals up to a rate of 150 MHz. The basic modules were: discriminators which produced a standard output signal of -.7 V amplitude and variable width up to 200 nsec upon receiving an input pulse which exceeded the threshold of -.1 V; standard coincidence units for forming logical "and" or "or" coincidences up to three inputs; specialized coincidence units with up to four inputs and a veto; gate generators with outputs up to 2 sec duration; standard analog-to-digital converters (ADCs), which gave a digitized output proportional to the total time integral of the input pulse; improved, high quality analog-to-digital converters designed especially for this experiment;[27] current integrators for linearly summing two separate input current pulses; inverters for reversing the polarity of the input pulse; special relay controlled units whose output depended on the input relay being on or off. The use of all these devices is shown in the logic diagrams of Figs. 9 and 10, which are discussed in detail later.

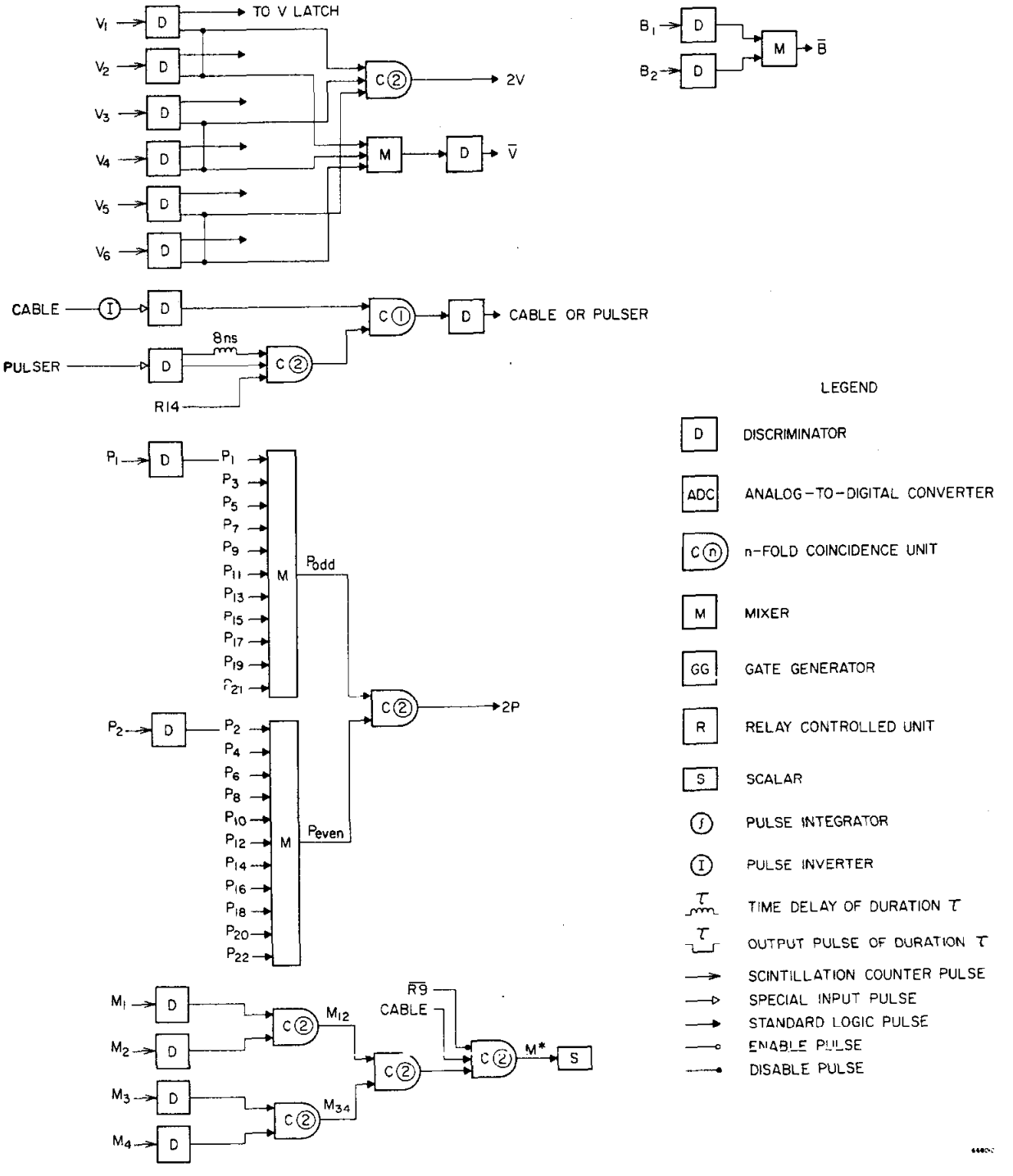

FIG. 9--Logic diagrams for parts of event trigger.

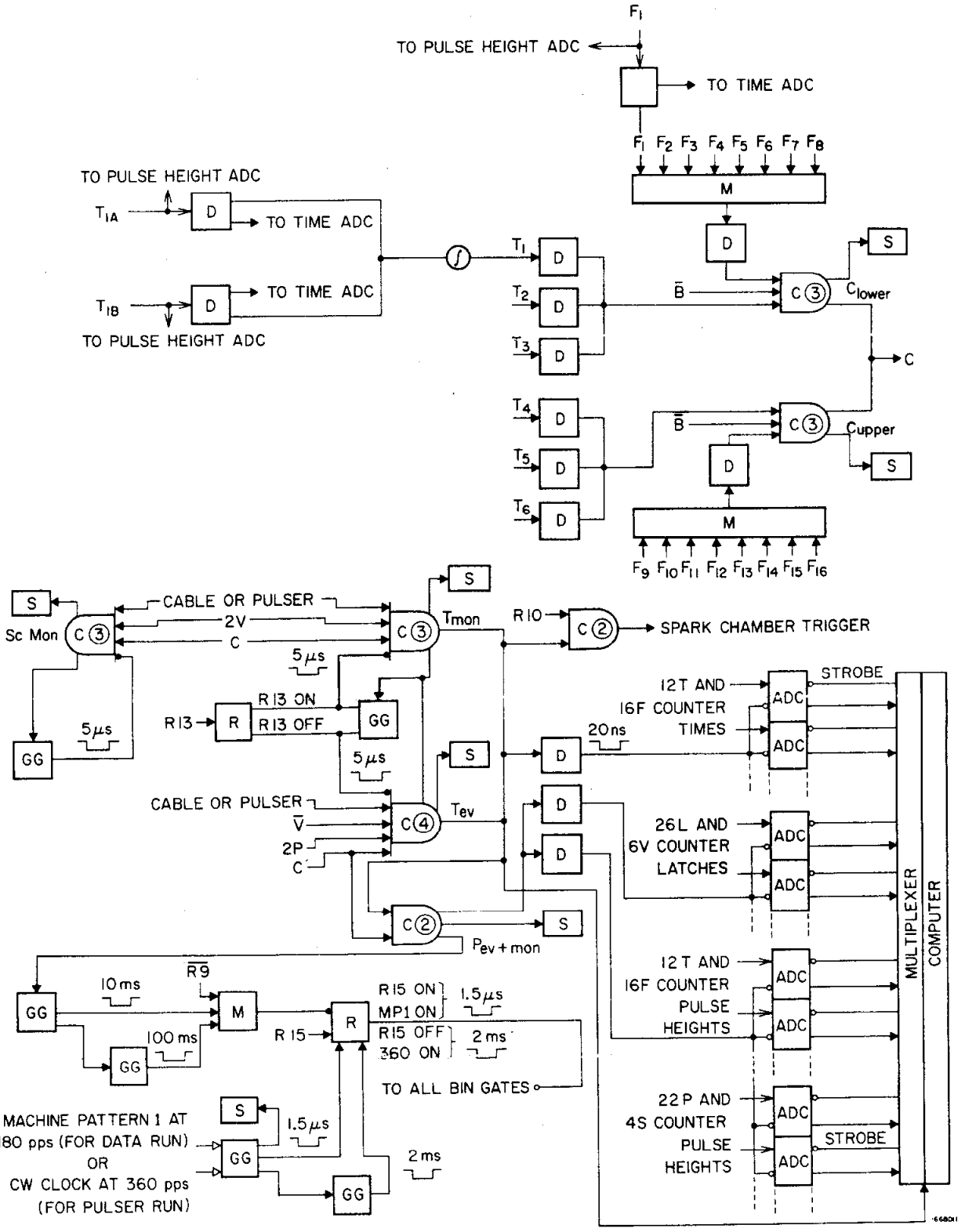

FIG. 10--Master logic diagram for event trigger.

G. Computer

A PDP-9 computer[28] was used for the on-line storage and display of data taken during the occurrence of events. For each event, the basic computer programs[29] instructed the computer to: (1) strobe the data out of the various ADCs via a multiplexer and store it, (2) histogram the data on an event by event basis, and (3) display, if desired, the individual event data or the histograms on either the Teletype Teleprinter or on the Precision CRT Display.[28]

Each time an event occurred, a certain number of quantities were first stored in the ADCs and then strobed into the computer buffer as data words. These included the run number, the roll-frame number, the latch and veto counter bits, the times from the T and F counters and the pulse heights from the T, F, P, V, and S counters. When the buffer of the computer was full, typically after every ten to fifteen events, all the nonzero words in the stored events were then transferred to a block of 10-track magnetic DEC tape.[28] After the DEC tape was filled with data, its contents were transferred directly to IBM compatible 9-track tape using a Magnetic Tape Transport.[28] All further data processing was done on an IBM Series 360, Model 91 Computer.

The computer programs were controlled by various console switches. There were basically two functions for these switches: one was to operate the data taking procedure, and the other was to display the contents of the data currently stored in the computer or on DEC tape. Specifically, there were switches for initiating light pulser tests, advancing the camera, enabling the camera, enabling the spark chamber, enabling the background lights and fiducials, enabling the event logic, enabling the writing on DEC tape, and terminating a DEC tape with an end of file mark. In addition, there were switches for typing out on the Teletype specific counter histograms which showed the frequency with which certain

counters had fired or showed the timing and pulse height distributions for certain counters. Finally, there were switches for displaying data on the CRT scope which showed the counters that fired in an individual event.

In addition to the controls given explicitly by the computer, there were also manual relays which could be turned on or off to override the corresponding computer command; if the relays were left in a neutral position the computer command was used. The various relays and their respective functions were: R1, camera enable; R2, enable of fiducials; R3, enable of background lights; R4, enable of roll-frame number lights; R5, camera vacuum enable; R6, out of film alarm; R7, general alarm; R8, internal enable of input; R9, external enable of input; R10, spark chamber enable; R11, latch and scalar reset; R12, pulser power supply enable; R13, monitor trigger enable; R14, time calibration delay; and R15, pulser run enable. The specific use of some of these relays is shown in the circuit diagrams of Figs. 9 and 10.

CHAPTER III

DATA COLLECTION

A. Running Conditions

Most of the data taking was done systematically in consecutive eight hour shifts. To initiate a data taking run all apparatus was checked for proper operation. The camera was loaded and placed in position, the electron beam was adjusted so that it was hitting the target and the coaxial cable properly, the beam knockout system was phased so that only one full bunch, and not two fractional bunches, went down the accelerator every 50 nsec, and the computer was enabled for recording data.

During the running the following quantities were checked every two hours for their proper functioning: the filled helium bag, the nitrogen pressure to the spark chamber, the spark chamber gas flow rate, the liquid nitrogen trap, the alcohol bubbler temperature, the spark chamber high voltage, the background lights and fiducial lights.

Whenever the requirements for triggering an event were satisfied the spark chamber was fired and sparks were recorded on the film. A gating pulse from the event trigger was sent to the ADC modules which allowed the pulse height and timing data from the counters to be stored in them. The triggering logic was then disabled and the data in the ADC modules was transferred into the computer. Then the film was advanced to the next frame and the background lights, fiducial lights, and roll-frame number were flashed on. The event logic was again enabled and ready to accept the next event.

There were basically two triggers used in the data taking. The neutral event trigger was satisfied by all the neutral decay modes of the kaon and the monitor event trigger was satisfied by all the charged decay modes. The monitor trigger

was used once after every ten neutral events to obtain an independent sample of kaon decay events, and whenever it was used a special light was flashed onto the film. These triggers will be explained in detail later.

Histograms of the number of individual counter firings were displayed on the Teletype to make sure that all the counters were firing properly, and also a regular watch was kept on the beam knockout signal to make sure that only one complete bunch was present every 50 nsec. The average event rate was about 10/min with an electron beam current of 1.5 mA and a beam rate of 180 bursts/sec. It took about three hours to complete a 400 ft roll of roughly 1600 pictures. After each roll was developed, the general exposure, the background lights, fiducials, and spark clarity were checked, and if any problems were observed they were corrected on the then current roll. After each roll a "pulser run" was taken as a monitor on proper counter operation, and after every other roll a "muon run" was taken to give a calibration reference for the kaon time-of-flight. Pulser runs and muon runs are described in detail later.

B. Triggers

1. Neutral Events

The neutral event trigger was used to obtain the neutral decay modes of the K_L^o, namely, 2γ, $2\pi^o$, and $3\pi^o$. The same trigger was used for all the data taking. The requirements were the presence of: no pulse from the collimation counters ($\bar{B}$), a requirement which was understood to be satisfied in Run 4, when there were no B counters; no veto counter pulse ($\bar{V}$); at least one trigger counter triplet pulse (C), defined as TA and TB pulses from the two ends of a T counter along with the pulse from a corresponding F counter; pulses from at least two "adjacent" shower counters ($\bar{2P}$), a requirement which meant one even counter and one odd counter from the bank shown in Fig. 5; a properly timed pulse from

the coaxial cable behind the target ("Cable"); and no dead time pulse from the processing of the preceding event ($\overline{DT}$). The trigger was written symbolically as

$$\overline{B} \cdot \overline{V} \cdot C \cdot 2P \cdot \text{Cable} \cdot \overline{DT}$$

The $\overline{B}$ and $\overline{V}$ requirements eliminated charged decays, interactions, and other charged particles. The C requirement indicated the presence of a gamma which converted in the preceding lead. The 2P requirement eliminated nonshowering tracks, such as muons, which would fire only one counter and not any adjacent ones. The Cable requirement signaled the time when K_L^o mesons were being produced at the target. The $\overline{DT}$ requirement implied the presence of an overall enable pulse, which occurred when no events were being processed and when the K_L^o beam was being produced. This enable pulse was called a bin gate pulse and is discussed in detail later. A logic diagram for each of the above parts of the trigger, showing the counter pulses and electronic modules involved, is given in Figs. 9 and 10.

2. Monitor Events

The monitor event trigger was used to obtain the charged decay modes of the K_L^o, namely, $\pi\mu\nu_\mu$, $\pi e\nu_e$, and $\pi^+\pi^-\pi^o$. Two variations of this trigger were used during the data taking. The first trigger was used up to Roll 26 of Run 4, and consisted of requiring pulses from one upper veto counter, one lower veto counter, and one trigger counter triplet, along with a Cable pulse and no dead time pulse. This was written symbolically as

$$2V \cdot C \cdot \text{Cable} \cdot \overline{DT}$$

where

$$2V = (V_1 + V_2) \cdot (V_3 + V_4)$$

The second trigger was used beginning at Roll 26 of Run 4 for all remaining data on Run 4, and for Runs 6 and 7. It was the same as the first trigger, except for the additional B counters in Runs 6 and 7 and another pair of veto counters, which were located between the earlier four and were used to increase the triggering probability. This trigger required that any two of the three veto counter pairs had to fire. This was written symbolically as

$$\bar{B} \cdot 2V \cdot C \cdot \text{Cable} \cdot \bar{D}\bar{T}$$

where

$$2V = \{2 \text{ of } (V_1 + V_2),\ (V_3 + V_4),\ (V_5 + V_6)\}$$

The second trigger is shown in Figs. 9 and 10.

3. Pulser Runs

The pulser runs were used to check the stability and consistency of all the counters throughout the data taking and to provide a time calibration in terms of ADC counts/nsec for each counter. The pulser run events were triggered by firing counter pulsers in groups such that either the neutral or monitor trigger was always satisfied. The triggers were modified so that the Cable pulse was replaced by a "Pulser" pulse, which was generated for every pulser event. Also, the dead time between bin gate enable pulses was decreased by a factor of ten to facilitate a faster data taking rate, and the spark chamber and camera were disabled. Written symbolically, the trigger was

$$V \cdot C \cdot 2P \cdot \text{Pulser} \cdot \overline{(DT/10)}$$

or

$$2V \cdot C \cdot \text{Pulser} \cdot \overline{(DT/10)}$$

The pulser run logic is shown in Figs. 9 and 10.

Half of the pulser events gave a reference number of counts in each of the timing ADC modules, as determined by the arrival of the Pulser pulse in the

event trigger. The other half of the events gave a different number of counts in each of the timing ADC modules, as determined by adding 8 nsec of delay to the arrival of the Pulser pulse. Using the two sets of events it was possible to determine the number of ADC counts/sec for each T and F counter. Also, continuous pulse height histograms of the pulser events were made to monitor the stability of all the counters.

4. Muon Runs

The muon runs were used to provide a zero time reference for the calibration of the K_L^o time-of-flight. The trigger was changed to fire on single muon tracks, which required one veto counter, one trigger counter triplet, and one shower counter. The dead time was again decreased by a factor of ten from that for normal events, the spark chamber and camera were disabled, and the sweeping magnets were turned off so that muon could come down the beam line. We then collected events at a rate of about 2/sec up to a total of about 1500 for each run. Written symbolically, the trigger was

$$V \cdot C \cdot P \cdot \text{Cable} \cdot \overline{(DT/10)}$$

The muon run logic required modification of the normal event triggers and hence is not actually shown in Figs. 9 and 10.

In order to use these events for the time calibration, we had to select a clean sample of muon events, since the trigger was so unrestrictive that most of the events resulted from decays, interactions or cosmic rays. We used only those events with one valid triplet, consisting of pulses from TA, TB, and F counters. Also we eliminated those events with one or more latch counters and more than one P counter fired. Each of these clean events was binned according to which of the forty-eight different triplets it fired. The pulse height histogram for each of the three counters involved in each triplet was Landau distributed[30,31]

about a peak which corresponded to minimum ionizing muons. Thus for each counter in each triplet we determined PH_{MI}, the number of ADC units which corresponded to the pulse height of a minimum ionizing muon. Similarly we binned the time ADC values for each triplet to determine a zero of time for each counter, which was actually a time average over the 6 in. × 6 in. area of each triplet. By comparing the shift in time ADC peaks by moving from one F counter to the next along a given T counter, we obtained the number of ADC counts/6 inches. Combining this with the information obtained from the pulser runs on the number of ADC counts/nsec we determined the effective speed of light in the scintillator for each counter, which was roughly .44c.

C. Gating and Timing

The normal state of all the logic modules was such that they could not accept data, unless a 1.5 μsec gating pulse was present during the beam bursts when kaons were being produced at the target. This gating pulse controlled the modules through the bins in which they were electrically powered and acted as an enable pulse. The bin gate pulse was generated either by the presence of a "Machine Pattern 1" (MP1) pulse during the real event data taking or a "360 Clock" (360) pulse during the pulser run data taking. The MP1 pulse was produced by the accelerator at the beam repetition rate of 180 Hz. The 360 pulse was a continuous 360 Hz pulse which was used as a substitute for MP1 during the pulser runs.

During the time the bin gate pulse was on, it was possible for an event trigger pulse to be generated either as "T_{ev}" for neutral events or as "T_{mon}" for monitor events. It required the presence of a Cable pulse during real event data taking or a Pulser pulse during pulser run data taking. The trigger pulse served four purposes, which are shown schematically in Fig. 10. First, the trigger pulse sent a 20 nsec pulse to gate on the ADC modules which received the

timing pulses from the T and F counters. The gating pulse was initiated upon the arrival of the Cable pulse, which arrived last in the trigger coincidence. The Cable pulse served as a zero time reference for the production of kaons at the target. The kaon time-of-flight was determined by the overlap between the gating pulse and the timing pulses for the T and F counters which arrived any time up to 20 nsec later. The time-of-flight calibration is described later.

Second, the trigger pulse formed a coincidence with the C pulse to yield a "P_{ev+mon}" output, that gated on the ADCs which received the L and V counter latch pulses and the T, F, F, P, and S counter pulse heights. This pulse was initiated upon the arrival of the C pulse, which to first order was determined by the kaon time-of-flight. The gating pulse thus overlapped completely with all the counter pulses due to the kaon decay. Third, the trigger pulse initiated the firing of the spark chamber and initiated the computer program which transferred the event data from the ADCs to the computer. Fourth, the trigger pulse, through the P_{ev+mon} output, generated a dead time pulse that disabled the bin gate pulse until the processing of the current event was completed.

D. Scaled Quantities

As a continuous monitor on the beam intensity and triggering conditions, we scaled several quantities which gave information summarizing the events on each roll of film. All the scalars used for recording these quantities were gated on during the same time the triggering logic was gated on, and they were set to zero at the beginning of each new roll. The location of the scalars is shown in the logic diagrams of Figs. 9 and 10.

M* gave the number of charged decays of the kaon causing a coincidence in the four M counters. This number was directly proportional to the intensity of the kaon beam. T_{ev} (triggered events) gave the number of neutral events

triggered. T_{mon} (triggered monitors) gave the number of monitor events triggered; this was simply one-tenth of T_{ev}. Sc Mon (scaled monitors) gave the number of decays which satisfied the monitor event trigger during the combined time the neutral and monitor event triggers were gated on. P_{ev+mon} (triggered events and monitors) gave the total number of events which triggered the neutral event and monitor event logic.

The scaled quantities were generally used to verify consistency from roll to roll during the data taking. As an example of this, the ratios (No. of Sc Mon)/(No. of M*) and (No. of P_{ev+mon})/(No. of M*) are plotted in Fig. 11 for rolls from Runs 6 and 7. Although there are some fluctuations, there are no systematic shifts within the data for either Run 6 or Run 7. The ratios for Run 7 are somewhat larger than those for Run 6, most likely because of the different collimator openings in the two runs. The scaled quantities Sc Mon, T_{ev}, and T_{mon} are used to relate the time which the triggering logic accepted neutral events to the time which it accepted monitor events. This is used in determining the total number of kaon decays, as is discussed later.

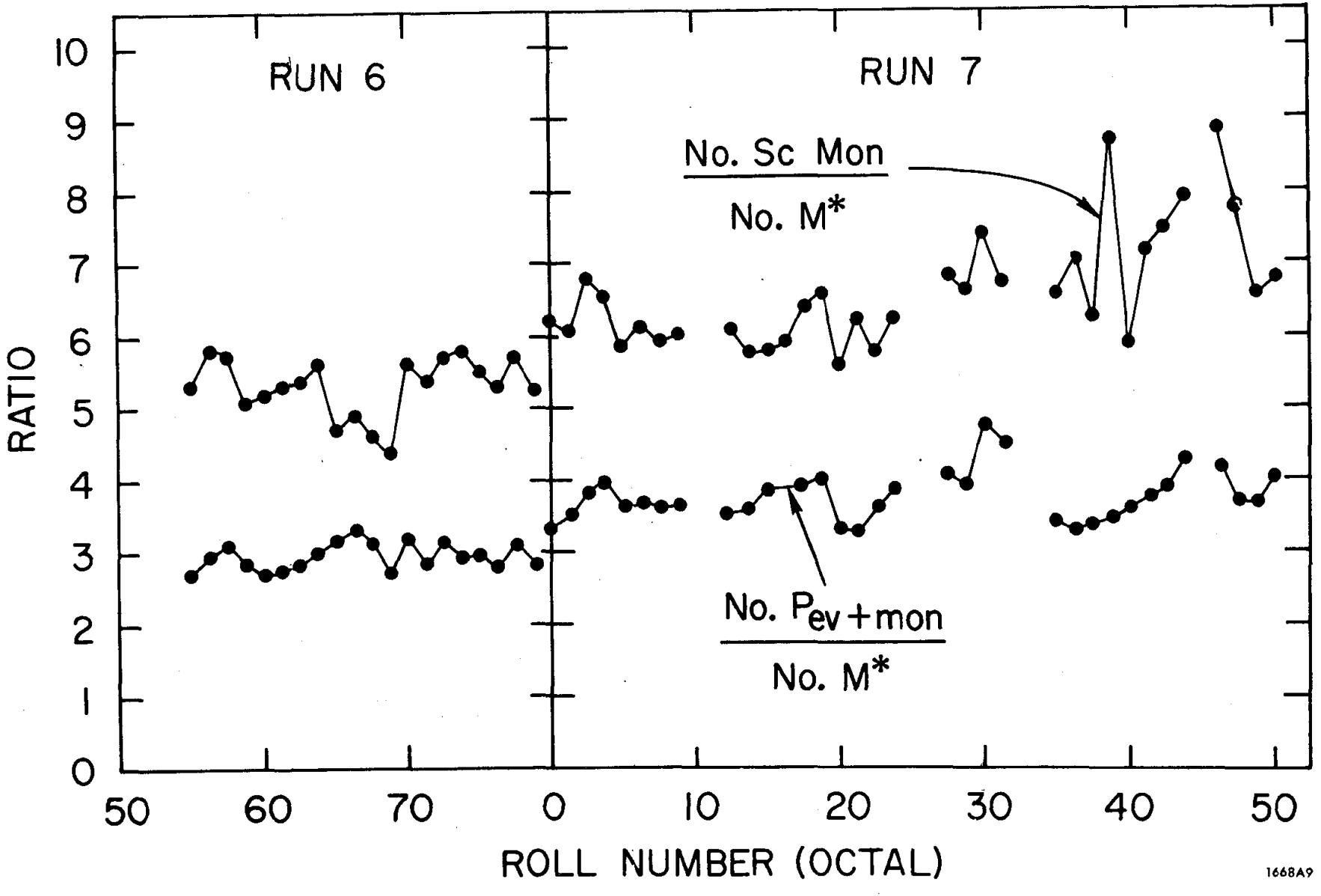

FIG. 11--Ratios of scaled quantities for Runs 6 and 7.

CHAPTER IV

DATA REDUCTION

A. Scanning

Of the approximately 300,000 pictures taken in this experiment, only about the last 200,000 were used for further analysis. These were on rolls from Runs 4, 6, and 7 where all the apparatus was functioning properly. Every roll of film with usable pictures was scanned by physicists and each picture was classified as a valid kaon decay or as unusable background. The unusable background represented about 70% of all the pictures scanned and it consisted of events where there was an obvious interaction of a kaon or neutron either in the collimator, air, helium, counters or spark chamber producing a number of tracks generally concentrated in the center of the spark chamber, where the spark chamber fired randomly or not at all, or where accidental cosmic rays or beam correlated particles photons triggered the logic.

The valid kaon decays consisted of the neutral events and the monitor events. The neutral kaon decays were classified by the number of gammas (2 to 6) observed in the chamber. The monitor events were classified as the decays $K_L^o \rightarrow \pi\mu\nu_\mu$ or $K_L^o \rightarrow \pi e\nu_e$ by the pion and lepton tracks observed in the chamber. The events $K_L^o \rightarrow \pi^+\pi^-\pi^o$ were ignored. Of the total number of leptonic decays we only used for further analysis the sample where the pion did not interact before the fifth plate in the chamber and where the muon penetrated all the way through the chamber or the electron did not interact with the trigger counter lead. A summary of the total number of events scanned and counted as valid is given in Tables 1, 2, and 3 for each run. There we have listed the raw number scanned along with various cuts imposed to give a well defined sample of valid events. All the entries in each table are discussed in detail later.

TABLE 1

NEUTRAL EVENT NORMALIZATION

$3\pi^0$ Decays

		Run 4 (Rolls 0-24)	Run 4 (Rolls 26-61)	Run 6 (Rolls 54-77)	Run 7 (Rolls 0-75)
(1)	No. 3-6γ Events Scanned	8700	6400	7800	14,500
(2)	No. 3-6γ Events with Valid Triplets	8300	6100	7400	13,700
(3)	Fraction of Unlatched 6γ Events	.87 ± .02	.88 ± .02	.85 ± .05	.80 ± .05
(4)	No. Unlatched 3-6γ Events with Valid Triplets [(2) · (3)]	7000	5400	6300	11,000
(5)	No. Valid 3-6γ Events Measured	0	0	292	714
(6)	Average Triggering Efficiency	.33 ± .03	.33 ± .03	.38 ± .04	.38 ± .04
(7)	Total No. Kaon Decays	99,000 ± 10,000	76,000 ± 8,000	77,000 ± 8,000	135,000 ± 14,000

TABLE 2

MONITOR EVENT NORMALIZATION

$\pi\mu\nu_\mu$ Decays

		Run 4 (Rolls 0-24)	Run 4 (Rolls 26-61)	Run 6 (Rolls 54-77)	Run 7 (Rolls 0-75)
(1)	No. Events Scanned and Sketched	173	119	222	304
(2)	No. Events Measured	165	103	214	270
(3)	No. Measured Events that are Unlatched with Valid Triplets	110	76	173	187
(4)	No. Events After Removing from (3) Events with $\|z\| > \|z_{MC}\|$	69	53	173	187
(5)	No. Events After Scaling (4) by (1)/(2)	72 ± 8	62 ± 8	179 ± 13	210 ± 15
(6)	$\left[(\text{No. Sc Mon}) - (\text{No. } T_{mon})\right]/(\text{No. } T_{mon})$	29	53.1	19.8	22.2
(7)	(Total No. M*)/(No. M*)	1	1	1	$\frac{19,500}{16,000}$
(8)	Average Triggering Efficiency	.065 ± .006	.143 ± .014	.163 ± .016	.163 ± .016
(9)	Total No. Kaon Decays	120,000 ± 16,000	86,000 ± 14,000	81,000 ± 10,000	130,000 ± 16,000

TABLE 3

MONITOR EVENT NORMALIZATION

$\pi e \nu_e$ Decays

	Run 4 (Rolls 0-24)	Run 4 (Rolls 26-61)	Run 6 (Rolls 54-77)	Run 7 (Rolls 0-75)
(1) No. Events Scanned and Sketched	57	40	103	163
(2) No. Events Measured	57	37	98	129
(3) No. Measured Events that are Unlatched with Valid Triplets	42	31	77	104
(4) No. Events After Removing From (3) Events with $\|z\| > \|z_{MC}\|$	35	26	77	104
(5) No. Events After Removing From (4) Events with e in Lead	32	25	74	103
(6) No. Events After Scaling (5) by (1)/(2)	32 ± 6	27 ± 5	78 ± 9	130 ± 12
(7) $\left[(\text{No. Sc Mon}) - (\text{No. } T_{mon})\right]/(\text{No. } T_{mon})$	29	53.1	19.8	22.2
(8) (Total No. M*)/(No. M*)	1	1	1	19,500/16,000
(9) Average Triggering Efficiency	.021 ± .002	.060 ± .006	.063 ± .006	.063 ± .006
(10) Total No. Kaon Decays	114,000 ± 25,000	62,000 ± 15,000	63,000 ± 9,000	144,000 ± 18,000

Besides recording a list of usable events in a log, we also sketched the tracks of these events on a 22 in. × 28 in. piece of thick white drawing paper which had an outline of the three views of the spark chamber plates and fiducial locations as they appeared when projected from the 70 mm film onto the measuring table. A sample drawing sheet is shown in Fig. 12 and a sample frame of film containing a 2γ event is shown in Fig. 13. The purpose of the sketch was to define the individual sparks or series of sparks in each track which were to be measured. Sparks were chosen to give the best approximation to the initial direction of the track. All good monitor events were sketched. All potential 2γ candidates were sketched, as were a representative sample of 3-6 γ events, called "supersketched" events.

B. Measuring

The events which were sketched were then measured on a measuring table using an image plane digitizer. The measurement data, along with event identification information, was recorded on an incremental magnetic tape.[32] The digitizer measured in two dimensions on the table with a resolution which corresponded to one count/0.01 in. in real space. The procedure was to measure two fiducials in the side view and each track in the side view, then measure one fiducial from each of the top and bottom views and the tracks in the top and bottom views. The four fiducials which were measured are indicated by large circles in Fig. 12. In measuring the gamma tracks, the direction was determined from the first several sparks and the central core of the resulting shower, and the range was determined by the distance between the first and last sparks. In measuring the pion and muon tracks, the direction was determined by the sparks from the initially unscattered portion of the track.

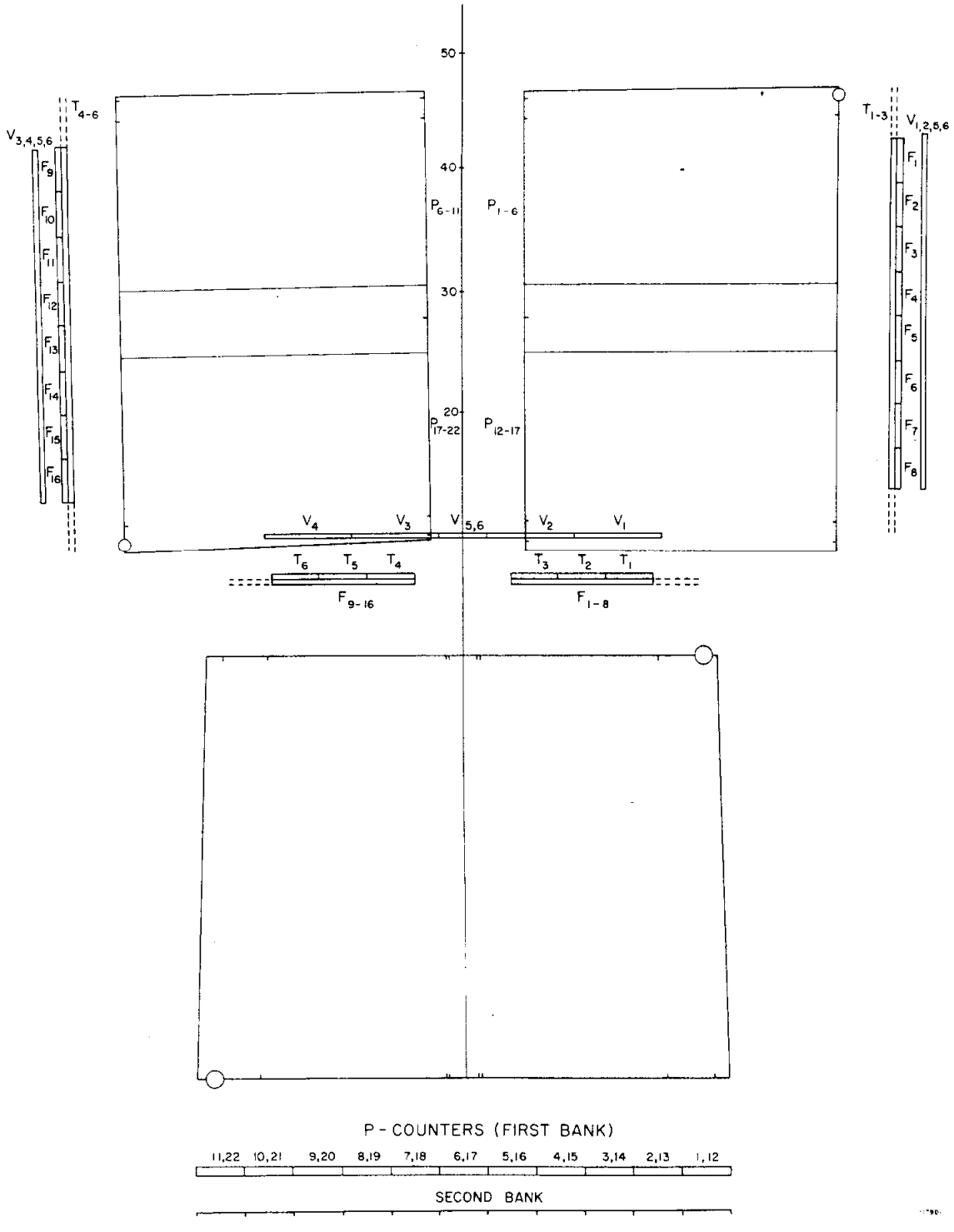

FIG. 12--Event measuring sheet.

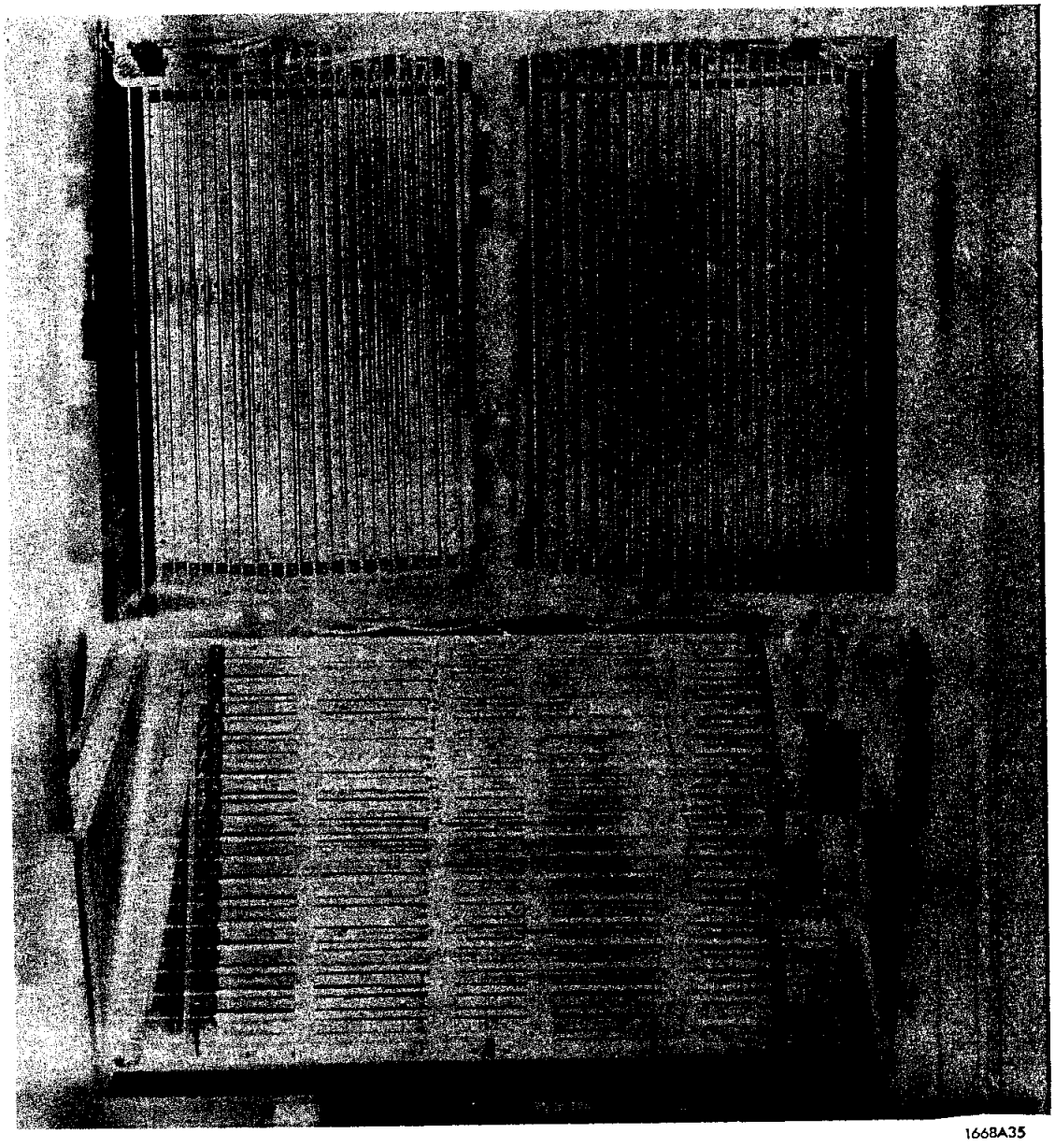

FIG. 13--Frame of spark chamber film.

C. Reconstruction

Using the digitized data for the spark coordinates of each measured event the tracks are reconstructed from the plane of the measuring table into a three dimensional coordinate system which had the z-axis horizontally along the beam line, the y-axis vertically upwards, and the x-axis horizontally to the left looking down the beam line. The zero of the coordinate system was defined as the center of the fiducial plane on the upstream end of the spark chamber. The transformation was based on using the known position of each fiducial in real space and its corresponding position on the film, and then extrapolating between the fiducials to obtain a given spark position. Care was taken to account for depth of field, which meant that the apparent spark position in one view had to be corrected for the position of the same spark in the corresponding perpendicular view. We assumed there were no significant local distortions in the lucite and other nonlinear effects which could have systematically affected the reconstructed direction of a measured track. The accuracy of the reconstruction program was tested by using the tracks of high energy muons, which traveled straight through the chamber without scattering appreciably. The same track was remeasured several times and it was found that the track reconstructed to a straight line and was reproducible to within a spark location error of roughly 0.1 in. in real space. A discussion of measurement and reconstruction errors is given later.

D. Fitting

Using the spark locations as obtained by reconstructing the data points from the measurement tape, we determined raw gamma direction cosines by doing a least squares fit for each track. For each event, the direction cosines and the other event identification information contained on the measurement tape were then combined with the corresponding counter and identification information

contained on the PDP-9 generated 9-track tape, and the merged result was then recorded on a third tape, known as the Master Tape, which contained all the completely processed events.

Using the events on the Master Tape we proceeded with the fitting. The fit determined the decay vertex from the raw direction cosines by minimizing a chi square function which was formed from the difference between the raw and fitted direction cosines, subject to the constraint that all the tracks had to originate from the same vertex point, which had to lie in the appropriate x-y region defined by the collimators in Runs 4, 6, and 7. From the vertex and the fitted direction cosines, it was possible to reconstruct where the tracks crossed the trigger counter plane and thus determine if the triplets which fired corresponded to the observed tracks. Using this procedure, events with the wrong triplets or excess triplets were eliminated.

E. Timing Calibration

In order to obtain valid time-of-flight information from the trigger counter bank, each T and F counter had to be calibrated so that when struck by a particle or shower originating from a K_L^o decay, its time ADC value could be translated into a time-of-flight for the K_L^o. We have defined the time-of-flight as the difference between the time it took a kaon moving with $\beta < 1$ to travel 250 ft from the target to the trigger counter bank and the time it took a reference particle moving with $\beta = 1$ to travel the same distance. The relationship between the kaon time-of-flight, t_{TOF}, and the kaon energy, E_K, is as follows:

$$t_{TOF} = \frac{d}{\beta c} - \frac{d}{c} = \frac{d}{c}\left((1 - 1/\gamma^2)^{-1/2} - 1\right)$$

$$\cong \frac{d}{c}\left(\frac{1}{2\gamma^2}\right) = \frac{250 \text{ ft}}{1 \text{ ft/nsec}}\left(\frac{1/2}{(E_K/m_K)^2}\right) = 125\ m_K^2/E_K^2$$

As reference particles we used muons and the zero time value for each counter was defined as the average number of ADC units for muon events in that counter, where we used the results of the muon runs to determine these values. The K_L^o decays all had ADC values of less than the corresponding muon value and we obtained the time-of-flight for an event from the difference between the muon value and the event value, after a series of corrections was made to standardize the values.

We made geometrical corrections from a given triplet location to a standard position in the center of the trigger bank. We corrected to a position that was in the middle of counters T3 and T4, located 9 in. directly below and above the center of the beam line in the trigger counter bank shown in Fig. 5. We modified the ADC value for each triplet counter according to the number of 6-in. counter shifts which had to be made in order to reach the standard position, using the muon runs to give us the ADC counts/6 in. Then we obtained a raw time-of-flight for each triplet counter by converting the difference between the event ADC value and the muon run ADC value into nsec, using the pulser runs to give us the ADC counts/nsec. Then we corrected the gamma time-of-flight from the kaon decay point (taken to be z = -5 ft) to the triplet location, to a time-of-flight from the decay point to the standard position.

The next correction was one which adjusted the three raw times obtained from each valid counter triplet so that they were internally consistent with one another. We looked at events with at least one standard triplet, which was arbitrarily defined as a triplet with individual pulse heights, PH_{MI}^{TA}, PH_{MI}^{TB}, and PH_{MI}^{F}, in the range (2.5 ± 0.7) and a triplet average, PH_{MI}^{C}, in the range $(2.5 \pm .25)$, where PH_{MI}^{X} was the pulse height in counter X in units of PH_{MI}, the pulse height corresponding to minimum ionizing muon tracks. For each T and

F counter combination we compiled a distribution of $\Delta t_S = \left(t_S^X - t_S^C\right)$, where X = TA, TB, or F and t_S is the event time-of-flight computed using counter X, including only the geometrical corrections and t_S^C is the average of the three times from the standard triplet. From the distribution of these differences, the individual counter times were adjusted so that each Δt_S distribution had a zero mean. This meant that each counter on a given triplet gave the same average value for the event time-of-flight. Because the T and F counters crossed one another, this procedure standardized all the counters in the lower bank with one another and all the counters in the upper bank with one another. To equalize the two banks we looked at events with two standard triplets, one in the upper bank and one in the lower bank. All the counter times in one bank were adjusted until the distribution of $\Delta t_{TOF} = \left(t_S^{C\,\text{upper}} - t_S^{C\,\text{lower}}\right)$, the difference in the two triplet times, had a zero mean.

The remaining correction was the pulse height slewing correction, which corrected the time-of-flight according to the counter pulse height, where we arbitrarily defined 2.5 in units of PH_{MI} as the pulse height corresponding to zero slewing correction. Slewing is the finite time it takes a counter pulse to go from zero to a threshold level (-0.1 V) in order to trigger a fast discriminator, which in turn sends a logic pulse to a gated ADC module. This correction was made by looking at the events with two valid triplets, but only one standard triplet. We plotted the difference $\Delta t_{slew} = \left(t^X - t_S^C\right)$ vs PH_{MI}^C, where t^X is the time for the individual counters X = TA, TB, and F in the nonstandard triplet and t_S^C is the standard triplet time. This yielded a curve which measured the

slewing correction, Δt_{slew} (nsec), which is given by the following formula

$$\Delta t_{slew} = -1.60 + .64\ PH^{C}_{MI} \qquad \text{where } 0 \leq PH^{C}_{MI} \leq 2.5$$

$$= -.50 + .20\ PH^{C}_{MI} \qquad \text{where } 2.5 \leq PH^{C}_{MI} \leq 5.0$$

We then verified the accuracy of the slewing correction by recomputing all the triplet times, t^{X}, including the above correction to produce a plot of time difference vs PH^{C}_{MI}, which had zero average difference for all values of PH^{C}_{MI}.

A final correction was one which corrected the zero time from one obtained by the muon events to one which corresponded to true $\beta = 1$ particles which came straight down the beam line. This correction was necessary because most of the muons striking the trigger counters did not come straight down the beam line, but scattered and penetrated through the large amounts of shielding along the beam line. The correction was obtained by adjusting the time-of-flight distribution of the measured gamma events from the $K^{o}_{L} \rightarrow 3\pi^{o}$ decays with the time distribution obtained from a Monte Carlo simulation of these decays. The correction was to add $+1.0 \pm .2$ seconds to the measured time-of-flight difference for all events. For more details refer to the treatment by D. J. Raymond.[33] We have verified this correction by our study of the $3\pi^{o}$ decay momentum distribution, which is discussed later.

As a measure of the intrinsic error in the time-of-flight calculation, we took a sample of events from Run 4, each with two valid triplets, and plotted the difference in the times of flight as computed using the two triplets for each event, including all the corrections given above. Such a plot is shown in Fig. 14, which shows a standard deviation in the difference of $\overline{\Delta t}_{TOF} = (0.5 \pm 0.1)$ nsec. This corresponds to an error in the individual triplets of $\overline{\delta t}_{TOF} = \overline{\Delta t}_{TOF}/\sqrt{2} =$ $(.35 \pm .07)$ nsec.

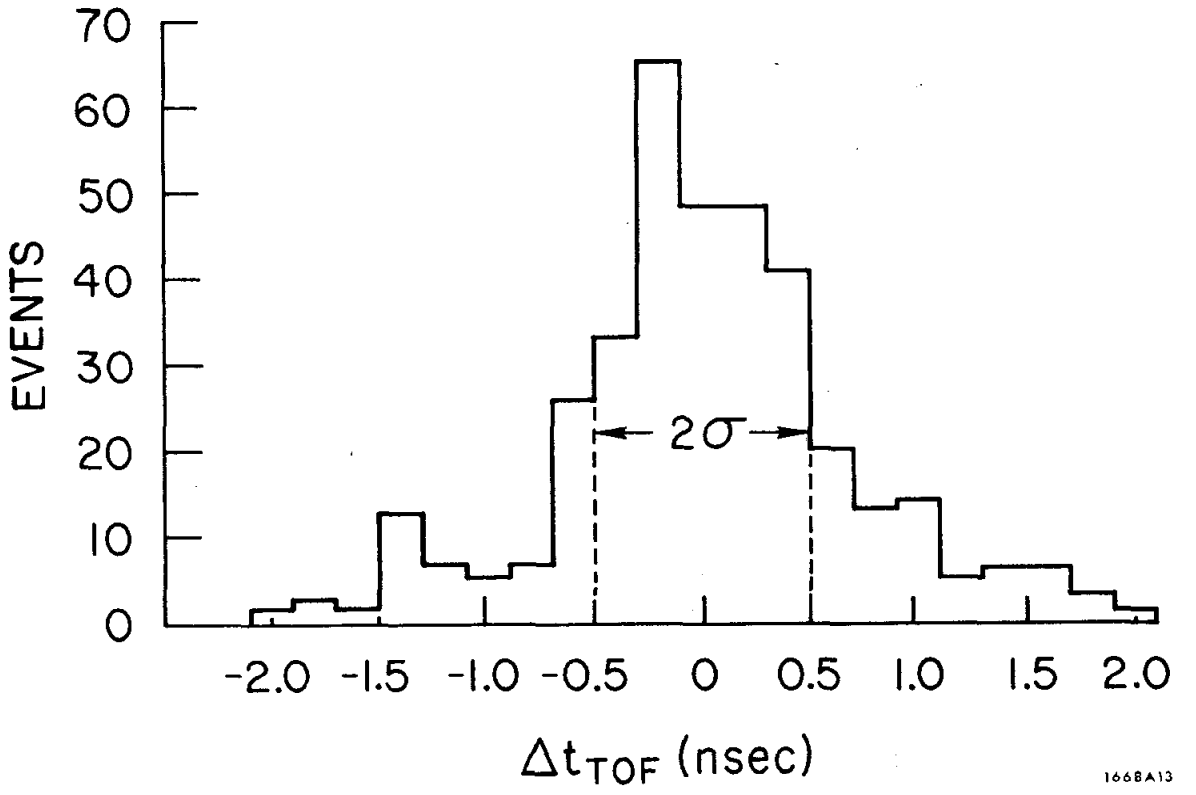

FIG. 14--Difference between corrected triplet times for Run 4 3-6γ events.

CHAPTER V

DATA ANALYSIS

A. Normalization

The normalization measured the total number of K_L^o decays which occurred during the data taking. First, the number of neutral decays, $K_L^o \rightarrow 3\pi^o$, was determined and then the number of leptonic decays, $K_L^o \rightarrow \pi\mu\nu_\mu$ and $K_L^o \rightarrow \pi e\nu_e$, was independently determined. Both determinations were based on comparing measured events with Monte Carlo simulated events and verifying that they were consistent with one another. The number of K_L^o decays was then determined from the number of measured events, from an average triggering efficiency, and from a known branching ratio.

1. Neutral Events

A Monte Carlo program was used to simulate the neutral decay, $K_L^o \rightarrow 3\pi^o$, as it occurred in our decay region, using the geometrical configuration of the counters and spark chamber as shown in Figs. 4 and 5, and using the momentum spectrum for our K_L^o beam at the decay region. The momentum spectrum at the decay region was modified from the spectrum at the target, as shown in Fig. 1, by the proper decay probability factor. Each simulated decay was generated in the K_L^o center-of-mass frame by selecting uniformily within three-body phase space to determine the three pion energies and directions. These pion directions were given three independent rotations to obtain a final arbitrary orientation in space. To complete the decay, each neutral pion was allowed to decay independently according to two-body phase into two photons, and then the six photons were Lorentz transformed to the K_L^o lab frame. The triggering efficiency for decays of given momentum and given decay point was equal to the fraction of such decays which satisfied the neutral event trigger, $\bar{B} \cdot \bar{V} \cdot C$, discussed earlier.

For the Monte Carlo event trigger, the Cable and $\overline{D}\overline{T}$ requirements were not necessary and the 2P requirement was assumed to be always satisfied. The average efficiency was obtained by integrating over the momentum spectrum in .5 BeV/c steps from 1 BeV/c to 8 BeV/c and over the decay points in .5 ft steps from -1 ft to -7 ft for Run 4, and from -1 ft to -9 ft for Runs 6 and 7.

The two important quantities which went into this Monte Carlo program and were also used in the Monte Carlo program for the 2γ decays, were the gamma conversion probability in the trigger counter lead and the gamma conversion probability in the spark chamber. These quantities were estimated using known photon absorption cross sections and then checked with actual measured decays. The total absorption cross sections for photons in lead and aluminum[34] are plotted in Fig. 15, as a function of photon energy. Using the value at .5 BeV as a good average, the absorption coefficients are $\bar{\mu}_{Pb} \simeq \mu_{Pb}$ (.5 BeV) = .112 cm^2/gm and $\bar{\mu}_{Al} \simeq \mu_{Al}$ (.5 BeV) = .029 cm^2/gm. Thus the number of conversion lengths for a photon going through 1/4 in. of lead ($\ell_{Pb} = 7.2$ gm/cm^2) is $\bar{\mu}_{Pb} \cdot \ell_{Pb} = .81$, which corresponds to a conversion probability of $1 - e^{-\mu\ell} = .55$. Also the conversion probability in the 1/2-in. thick veto counters is $\mu_{CH_2} \ell_{CH_2} = .022$. The absorption coefficient for the G10 laminate was estimated by using the following composition[24]: .34 Si, .29 C, .13 Ca, .09 Al, .065 B, .065 O, and .02 (H+N+Na+K). Averaging the known absorption coefficients for these elements,[34] we obtained: $\bar{\mu}_{G10} \simeq \mu_{G10}$ (.5 BeV) = .027. An approximate curve for the absorption cross section of G10 is plotted in Fig. 15.

Thus the number of conversion lengths for a photon going horizontally through the chamber, which was composed of 10 in. of Al ($\ell_{Al} = 70$ gm/cm^2)

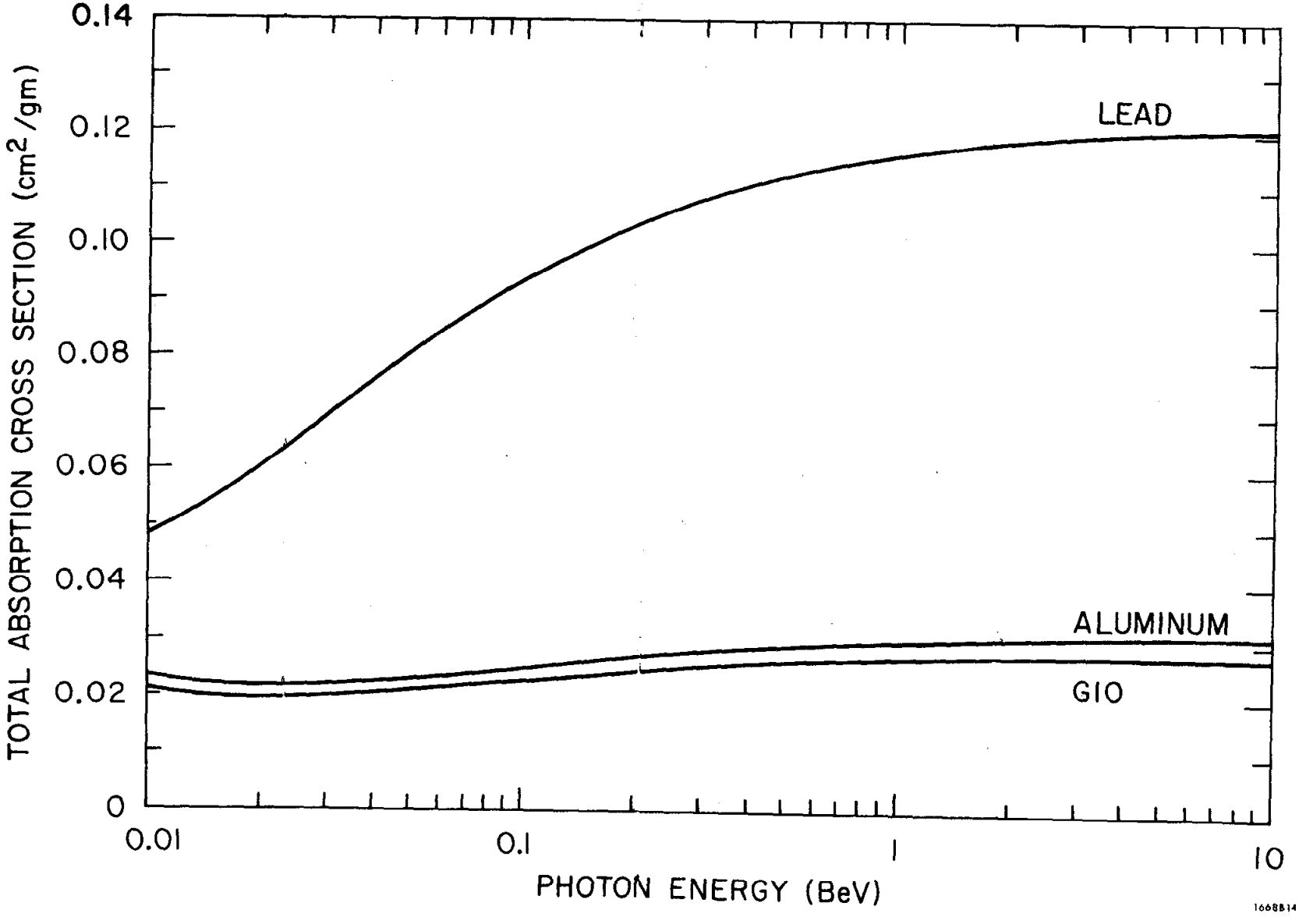

FIG. 15--Photon total absorption cross sections.

and 10 in. of G10 ($\ell_{G10} = 45$ gm/cm^2), is

$$\bar{\mu}_{Al} \cdot \ell_{Al} + \bar{\mu}_{G10} \cdot \ell_{G10} = 2.0 + 1.2 = 3.2 ,$$

which corresponds to a conversion probability of $1 - e^{-\mu\ell} = .96$.

We performed checks on the conversion probability in the lead and on the number of conversion lengths in the chamber in the following way. We collected the supersketched 6γ events from Runs 6 and 7, which showed six gammas converted in the chamber. Using the fitted direction cosines of the gamma showers, we obtained the points at which the gammas passed through the trigger counter plane. We then compared the triplets which fired with the total number of gammas which went through the counters. To first order we assumed the gammas went through the trigger counter at normal incidence and we neglected the energy dependence of the photon absorption cross section, which changed appreciably only for photons of energy less than 0.2 BeV. Our sample of 6γ events included only those which were unlatched and which had only triplets that could each be associated with a converted gamma. This gave us a total of 106 events where at least one gamma went through the counters and 84 events where more than one gamma went through the counters. In Fig. 16a we show the distribution of number of gammas which went through the trigger counters and in Fig. 16b we show the distribution of number of gammas which converted in the trigger counters.

The efficiency was calculated in the following way. First we assumed that the probability for j out of i gammas to convert in the lead in front of the trigger counters was given by the binomial distribution

$$p(j,i) = \binom{i}{j} p^j (1 - p)^{i-j}$$

where $1 \leq j \leq i$ and $1 \leq i \leq 6$, and p is the probability for a single photon converting in the lead. We computed the ratio of expected number of nontriggering converted gammas to total number of nontriggering gammas in the following way

$$\bar{r} = \sum_{i=2}^{6} n_i \left\{ \sum_{j=1}^{i} (j-1)\, p(j,i) \Big/ \sum_{j=1}^{i} (i-1)\, p(j,i) \right\} \Big/ \sum_{i=2}^{6} n_i$$

$$= \sum_{i=2}^{6} n_i \frac{ip - (1 - (1-p)^i)}{(i-1)(1 - (1-p)^i)} \Big/ \sum_{i=2}^{6} n_i$$

where n_i is the number of events with i gammas going through the counters. By nontriggering gamma we mean any gamma in addition to the one converted gamma necessary to trigger each event. We chose to calculate the ratio in this way because it was much more sensitive to the value of p, than, for instance, a similar ratio computed using all the gammas.

Using the sample of events shown in Fig. 16a and assuming p = .5, we obtained the following expected ratio

$$\bar{r} = [28\ (.33) + 34\ (.36) + 16\ (.38) + 6\ (.40)]/[28+34+16+6] = .35$$

assuming p = .4, $\bar{r}$ = .27; and assuming p = .6, $\bar{r}$ = .46. The corresponding experimental ratio was calculated from Fig. 16b as

$$\bar{r}_{exp} = \sum_{i=2}^{6} (i-1)\, n_i^{conv} \Big/ \sum_{i=2}^{6} (i-1)\, n_i$$

$$= [1 \cdot (37 \pm 6) + 2 \cdot (8 \pm 3)]/[1 \cdot 28 + 2 \cdot 34 + 3 \cdot 16 + 4 \cdot 6] =$$

$$= \frac{53 \pm 8}{168} = .32 \pm .05 ,$$

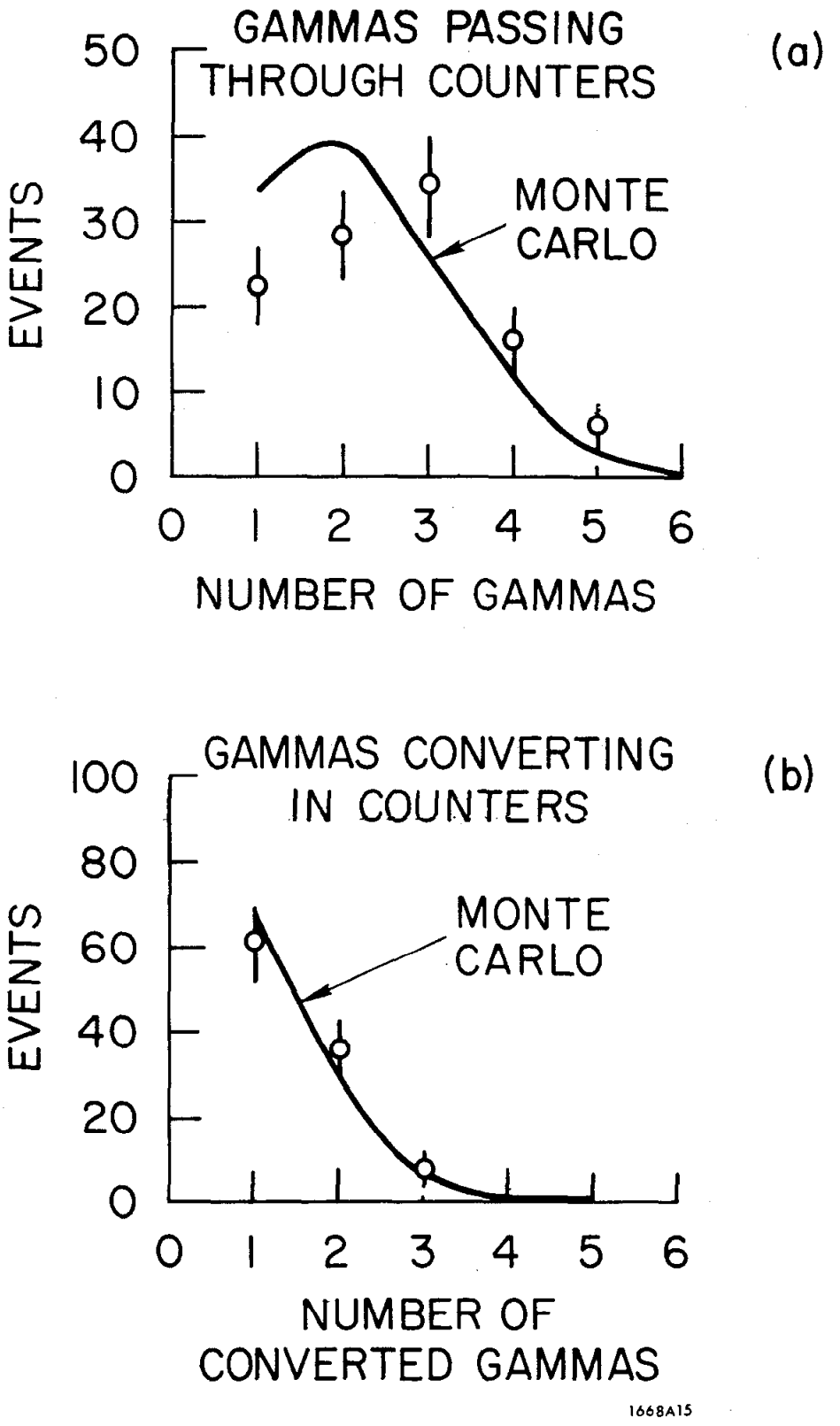

FIG. 16--Gamma distributions in trigger counters for good 6γ events from Runs 6 and 7.

where the error is statistical. This ratio corresponds to an experimental conversion efficiency of $p = .48 \pm .07$, which is consistent with our calculated value of $p = .55$.

In our Monte Carlo programs we assumed the value $p = .5$ for the conversion probability. The Monte Carlo curves for the distribution of the number of gammas going through and converting in the trigger counters are shown in Fig. 16, and the agreement is sufficiently good to verify that we were indeed studying a valid sample of 6γ events.

As an additional test we studied the distribution of conversion points of the gammas in all the supersketched $3\text{-}6\gamma$ events from Runs 6 and 7. We selected only those gammas which are directed toward the center of the chamber and neglected the small angular correction ($\sim 2\%$) to the thickness of the material actually traversed. In Fig. 17 we show the number of gammas converting in groups of gaps 3-10, 11-18, 19-26, and 27-34. From the best fit slope we obtained the result that following each group of eight gaps, the number of gamma conversions dropped by an average factor of $1.93 \pm .1$. For the entire chamber, consisting of five groups, we obtained the number of conversion lengths as $5\ \ell n\ (1.93 \pm .1) = 3.3 \pm .3$, which agrees with the calculated number of 3.2.

2. Monitor Events

A Monte Carlo program was also used to simulate the leptonic decays, $K_L^o \rightarrow \pi\mu\nu_\mu$ and $K_L^o \rightarrow \pi e\nu_e$. Following the same procedure as with the neutral events, the leptonic events were generated by taking the K_L^o at rest and selecting from three-body phase space weighted according to the probability factor[35]

$$dw = \left\{\left[2m_K E_\ell E_\nu - m_K^2 (W-E_\pi)\right] f_+^2 - 2m_\ell^2 E_\nu f_+ f_2 + m_\ell^2 (W-E_\pi) f_2^2\right\} dE_\ell\, dE_\nu$$

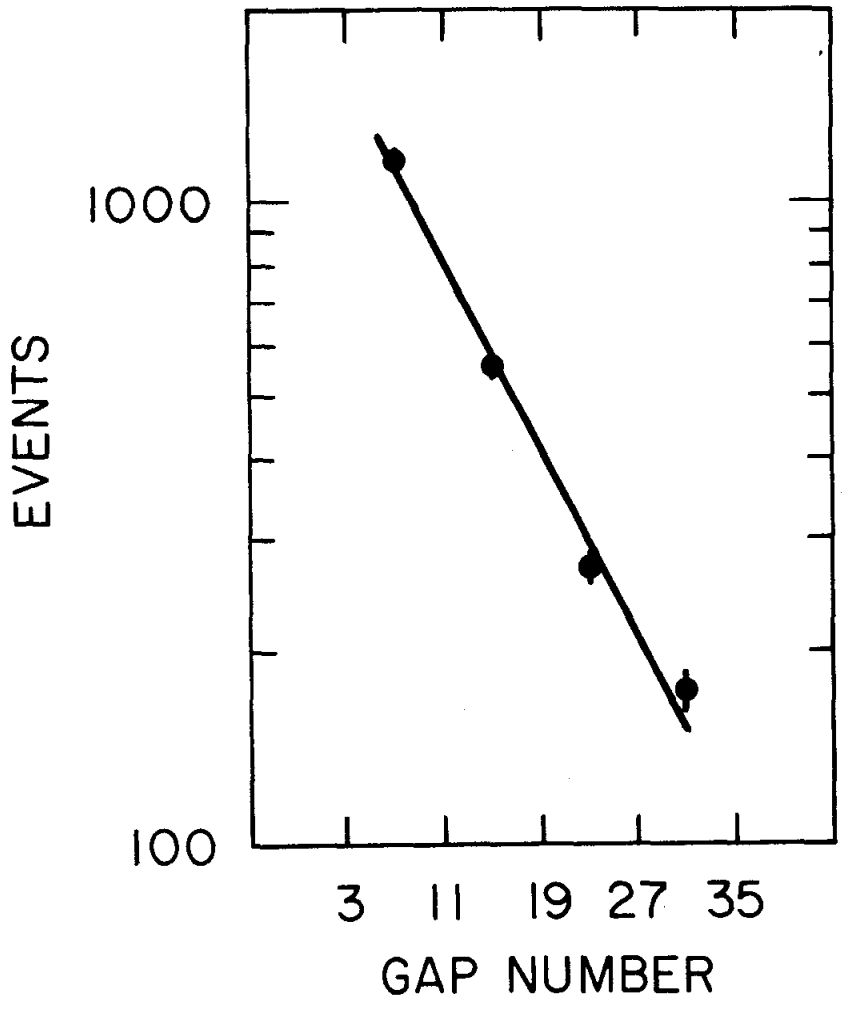

FIG. 17--Distribution of gamma conversion points for good 3-6γ events from Runs 6 and 7.

where E_π is the pion energy, E_ℓ ($\ell = \mu$ or e) is the lepton energy, E_ν is the neutrino energy, $f_2 = \frac{1}{2}(f_+ - f_-) = \frac{1}{2} f_+ (1-\xi)$, $\xi = f_-/f_+$, $f_+ \equiv f_+(q^2) = f_+(0)\left[1+\lambda_+\left(\frac{q}{m_\pi}\right)^2\right]$, $q^2 = m_K^2 + m_\pi^2 - 2m_K E_\pi$, and $W = \left(m_K^2 + m_\pi^2 - m_\ell^2\right)/2m_K$. We used the following experimental values[16] for the parameters: $\lambda_+ = .017 \pm .007$ and $\xi = -1.59 \pm .26$ (determined from muon polarization). The value of ξ had only a negligible effect on dw because ξ appears only in terms proportional to m_ℓ^2. The spectrum was somewhat more sensitive to the value of λ_+, but we used the number given above as a compromise. Next, the decay particles were given an arbitrary orientation in space with three independent rotations, and then transformed to the K_L^o lab frame.

For purposes of more accurate reconstruction, we limited the sample of measured monitor events to those where the pion did not interact before the fifth gap, which meant that the pion had to penetrate two aluminum plates and two G10 plates, corresponding to 11.5 gm/cm^2 of material. If the pion also went through the 1/4 in. of lead and the three 1/2-in. thick layers of T counters, support wood, and F counters, this represented an additional 11.1 gm/cm^2 of material. The interaction length of pions in aluminum is 80 gm/cm^2 and in lead is 160 gm/cm^2.[16] For the muonic decays, we required that the muon had to be energetic enough to travel through the lead and trigger counters and the entire spark chamber, which corresponded to a range of about 125 gm/cm^2 and a muon energy of at least .35 BeV. For the electronic decays, we required that the electron not hit the lead. These requirements, which we used in selecting the measured events, were also used in the Monte Carlo program, so that we obtained the triggering efficiency for the same class of events which we actually measured. The trigger used for these decays was $\bar{B} \cdot 2V \cdot C$, where

$2V = (V_1 + V_2) \cdot (V_3 + V_4)$ up to Roll 26 of Run 4 and $2V = \{2 \text{ of } (V_1 + V_2), (V_3 + V_4), (V_5 + V_6)\}$ for all remaining data. We obtained an average efficiency by integrating over the same momentum range and decay point range as was used for the neutral decays.

As a subsidiary test on the leptonic decays, to check the accuracy of one of our calculated parameters, we measured the number of pion interaction lengths in the chamber and compared it with the number expected from geometrical cross sections. This study is presented in Appendix B, and the agreement between the measured and calculated values was found to be good.

3. Normalization Calculation

To determine the K_L^o flux we used the sample of scanned and measured events for both the neutral and leptonic decay modes. In Tables 1, 2, and 3 we have summarized the number of events for each run and each decay mode subjected to various cuts which improved the quality of the sample. The final number for K_L^o flux was based on unlatched events with valid triggers.

For the neutral decays the total number scanned is listed first in Table 1, and the number of these that were sketched and measured is listed next. From the number of scanned events we selected only those events which were not accidentally latched. The fraction of accidentally latched events for each run was computed by taking the sample of scanned events for that run which had been designated as 6γ events and determining the latch distribution for such events. In principle, if six gammas were present in the chamber then it was not possible for any of them to have triggered the latch counters, but we found that in fact 10 to 20% of these events had one or more latches. Thus we have assumed that such events were accidentally latched, most likely by some beam correlated photons or particles which are not associated with the kaon decay itself. Next

we removed from the remaining sample of scanned events of fraction which did not have valid triggers, i.e., the timing counters which fired could not be properly associated with the tracks that appeared in the chamber. This error affected about 5% of the events, as determined by studying the measured events. Out of a total of about 37,000 scanned 3-6γ events, 30,000 passed our selection criterion and of these a sample of 1006 supersketched events from Runs 6 and 7 were measured.

To show that we were truly studying $3\pi^0$ decays, for the measured events we plotted distributions of the kaon momentum, obtained from the time-of-flight, and of the decay point, obtained from a geometrical fit of the gamma directions subject to the constraints of the collimator. These distributions are shown in Fig. 18 along with the corresponding curves obtained from the Monte Carlo program which simulated these decays. The agreement is sufficiently good that we are justified in assuming that our entire sample of scanned events originated from $3\pi^0$ decays. To compute the total number of $3\pi^0$ decays which occurred during our data taking period, we calculated the average efficiency for a $3\pi^0$ decay to trigger the detection apparatus using our Monte Carlo program, and this value is given in Table 1 for each run. Finally, to compute the total number of kaon decays we used the previously measured branching ratio[16]

$$\Gamma(K_L^0 \rightarrow 3\pi^0)/\Gamma(K_L^0 \rightarrow \text{all}) = .215 \pm .007$$

For the monitor decays all of the scanned events were also sketched; the numbers of events are listed in Tables 2 and 3. Out of the total of sketched events a high percentage were measured and this number is listed. Of the measured events we selected only those which had no latches fired and no counters fired other than those which corresponded to visible tracks. Note that any valid leptonic decay with two tracks visible in the chamber, could only have accidental

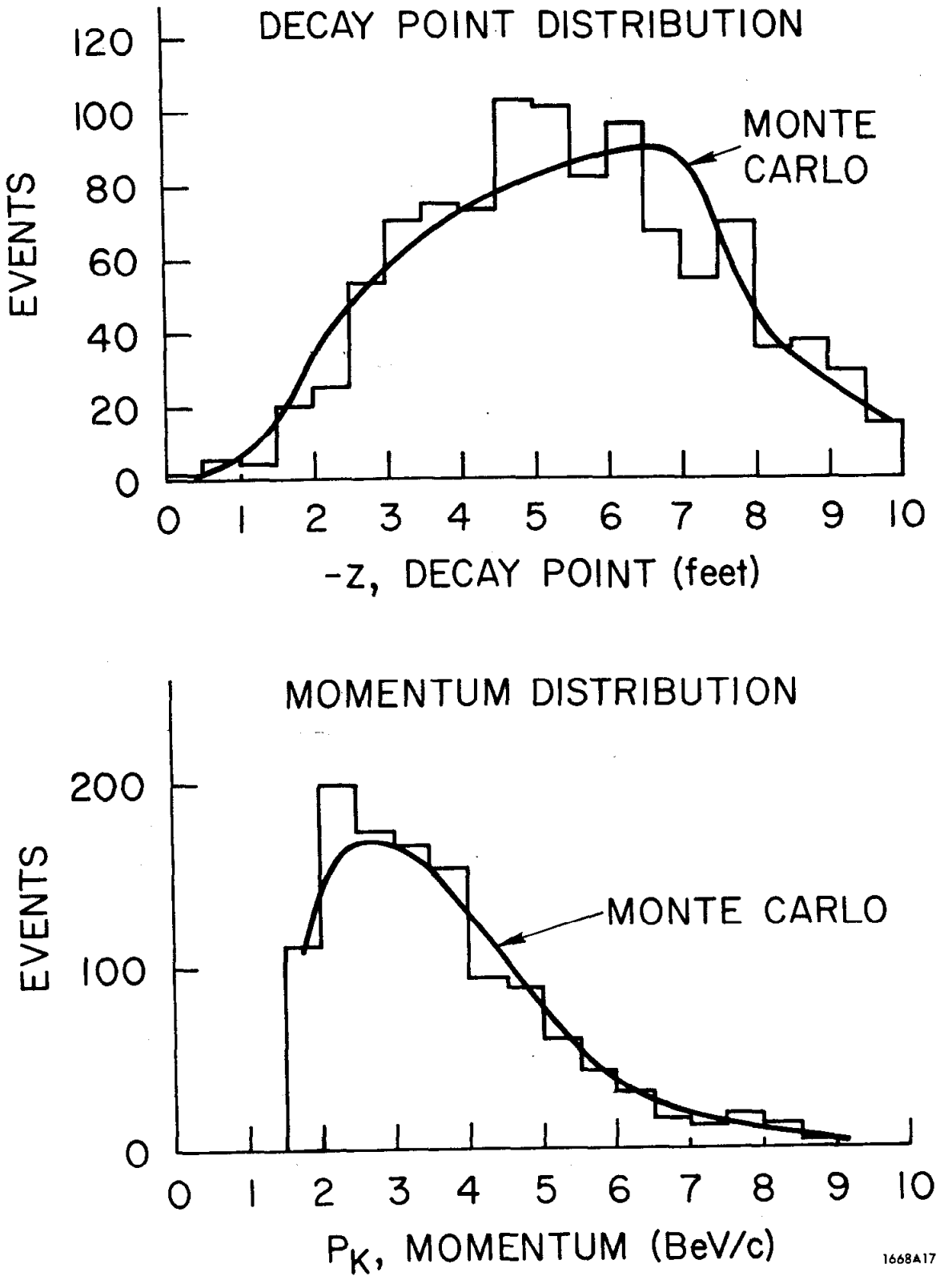

FIG. 18--K_L^o decay point and momentum distributions for good 3-6γ events from Runs 6 and 7.

latches associated with it. For Run 4 we eliminated those events which had a fitted vertex with $z < -7.5$ ft, which was the limit obtained from the Monte Carlo program, which accounted for the presence of the collimator at $z = -6$ ft. For the electronic decays we finally eliminated those events which supposedly satisfied our selection criterion, but which were found after geometrical fitting to have an electron which passed through the lead. This left samples of measured events which all satisfied the prescribed conditions discussed earlier. Of the muonic decays there were 122 events from Run 4 and 360 events from Runs 6 and 7, and for the electronic decays there were 57 events from Run 4 and 177 events from Runs 6 and 7. We finally scaled these samples by the number of scanned events divided by the number of measured events.

To verify that the samples of selected events originated from the leptonic decays, we plotted distributions of kaon momentum and decay point in Figs. 19 to 22. We compared them with the corresponding Monte Carlo curves and the agreement is quite good. In order to determine the total number of kaon decays, we first corrected for the fact that the trigger for the leptonic decays was different than that for the neutral decays and also was used for a different period of data taking. During the time that the neutral trigger was on, the number of decays which satisfied the monitor trigger was scaled and to this number was also added the number of decays which actually triggered the monitor logic. The sum is called "No. of Sc Mon" and the later quantity is called "No. of T_{mon}." Thus, to obtain the number of leptonic decays which would have occurred during the period of the neutral trigger we have multiplied the number of observed decays by the ratio $\left[(\text{No. of Sc Mon}) - (\text{No. of } T_{mon})\right]/(\text{No. of } T_{mon})$. The monitor events were not measured for all of Run 7 and so we scaled the number of measured events by the ratio of No. of M* counts for the entire run to No. of

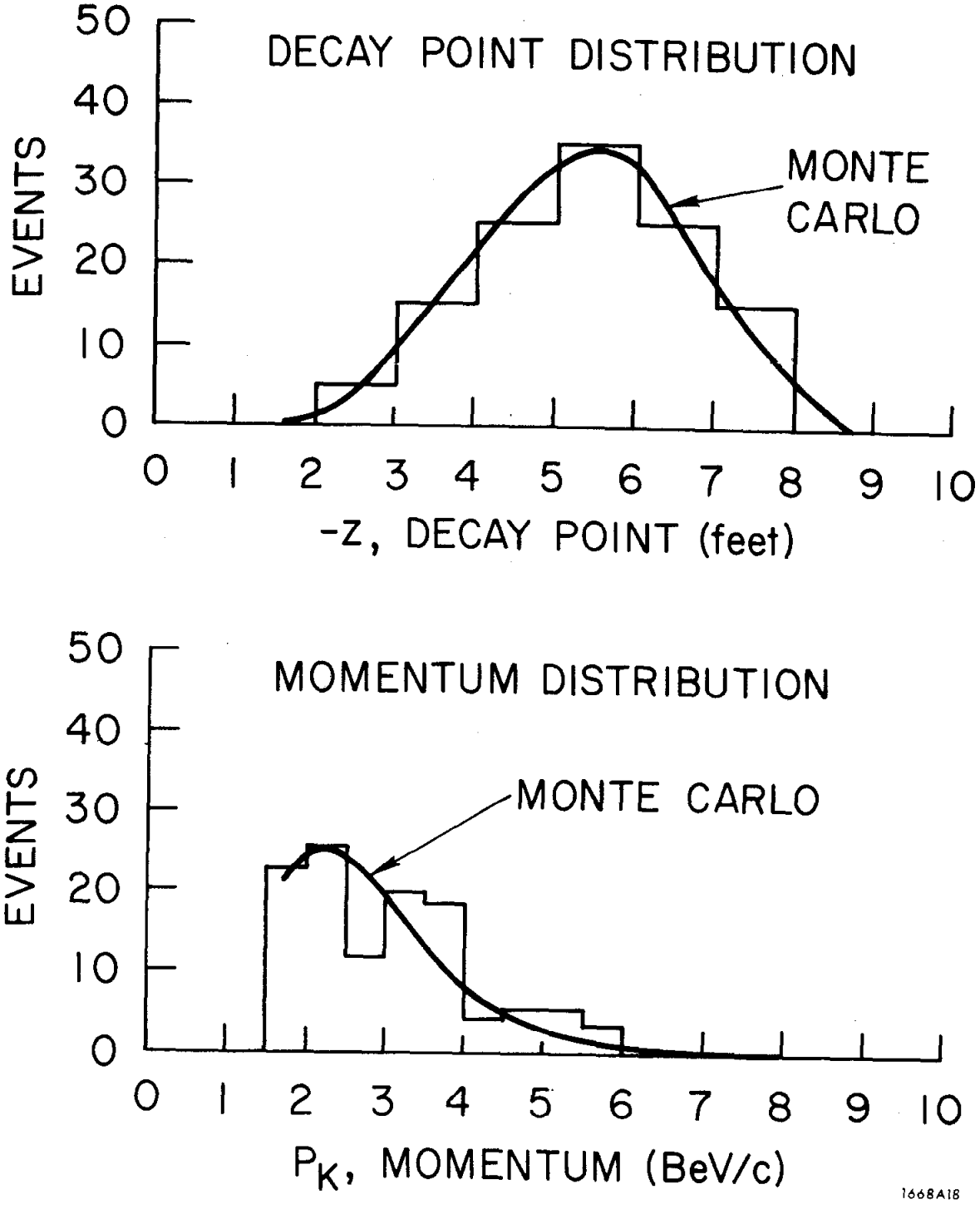

FIG. 19--K_L^o decay point and momentum distributions for good $\pi\mu\nu_\mu$ events from Run 4.

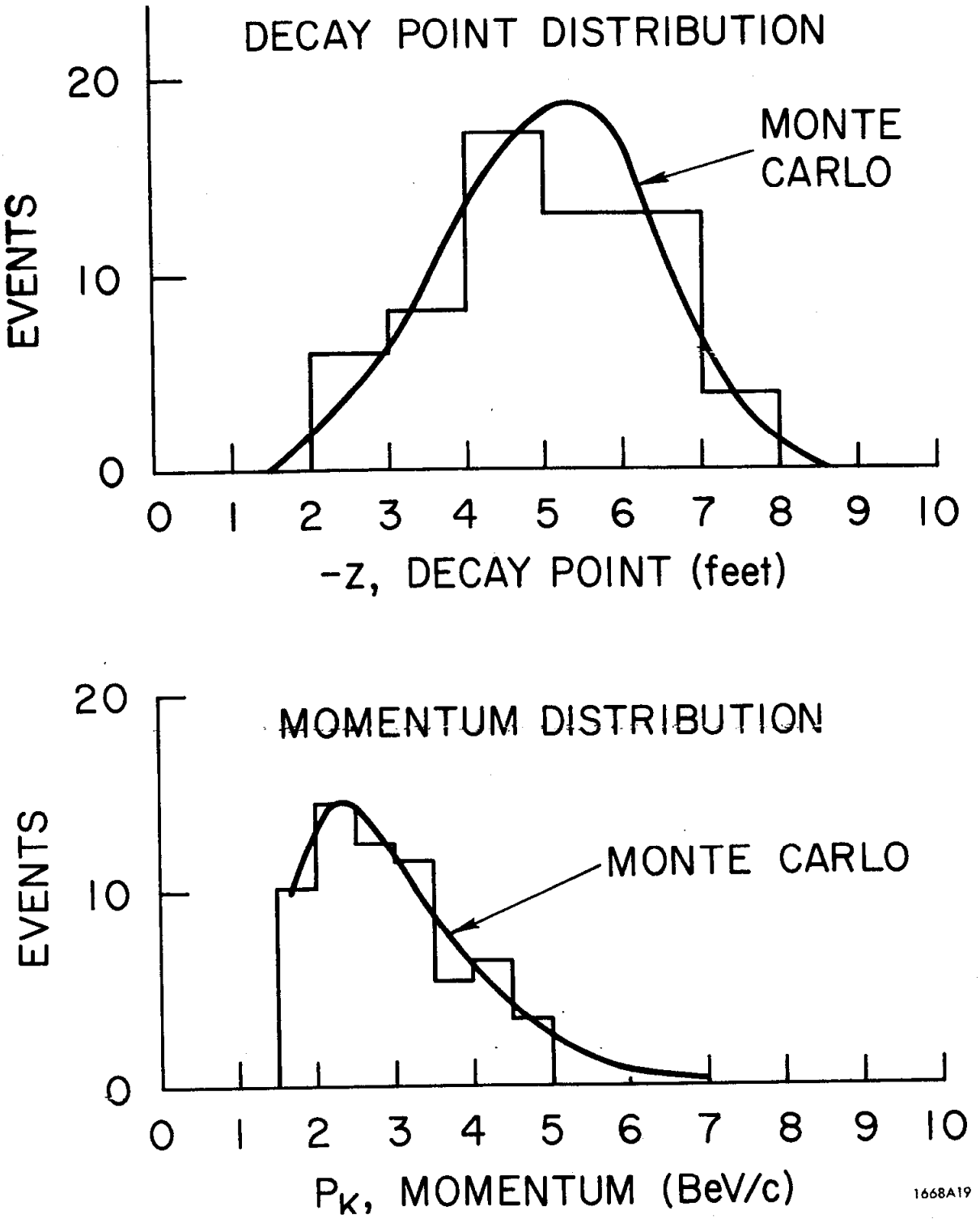

FIG. 20--K_L^o decay point and momentum distributions for good $\pi e \nu_e$ events from Run 4.

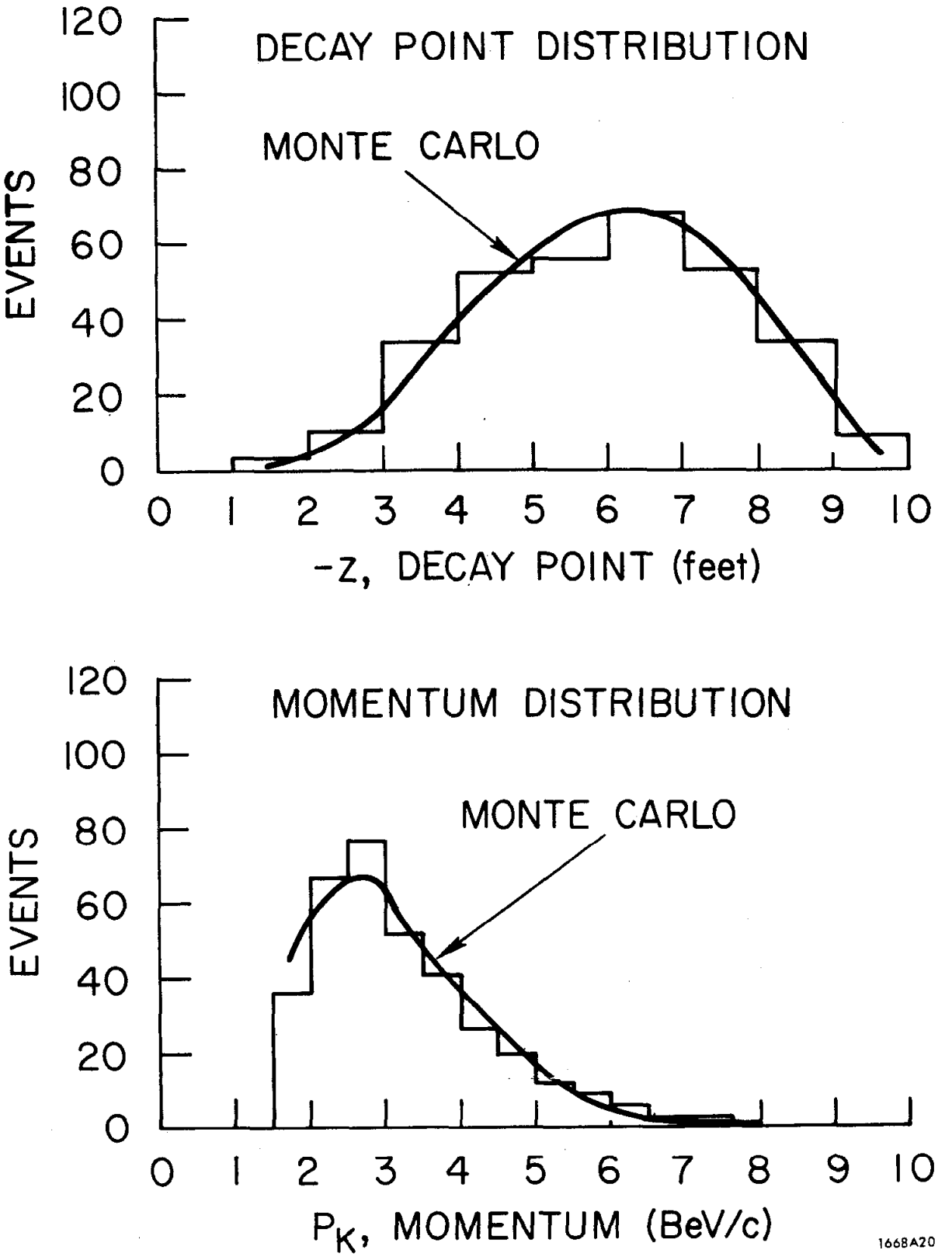

FIG. 21--K_L^o decay point and momentum distributions for good $\pi\mu\nu_\mu$ events from Runs 6 and 7.

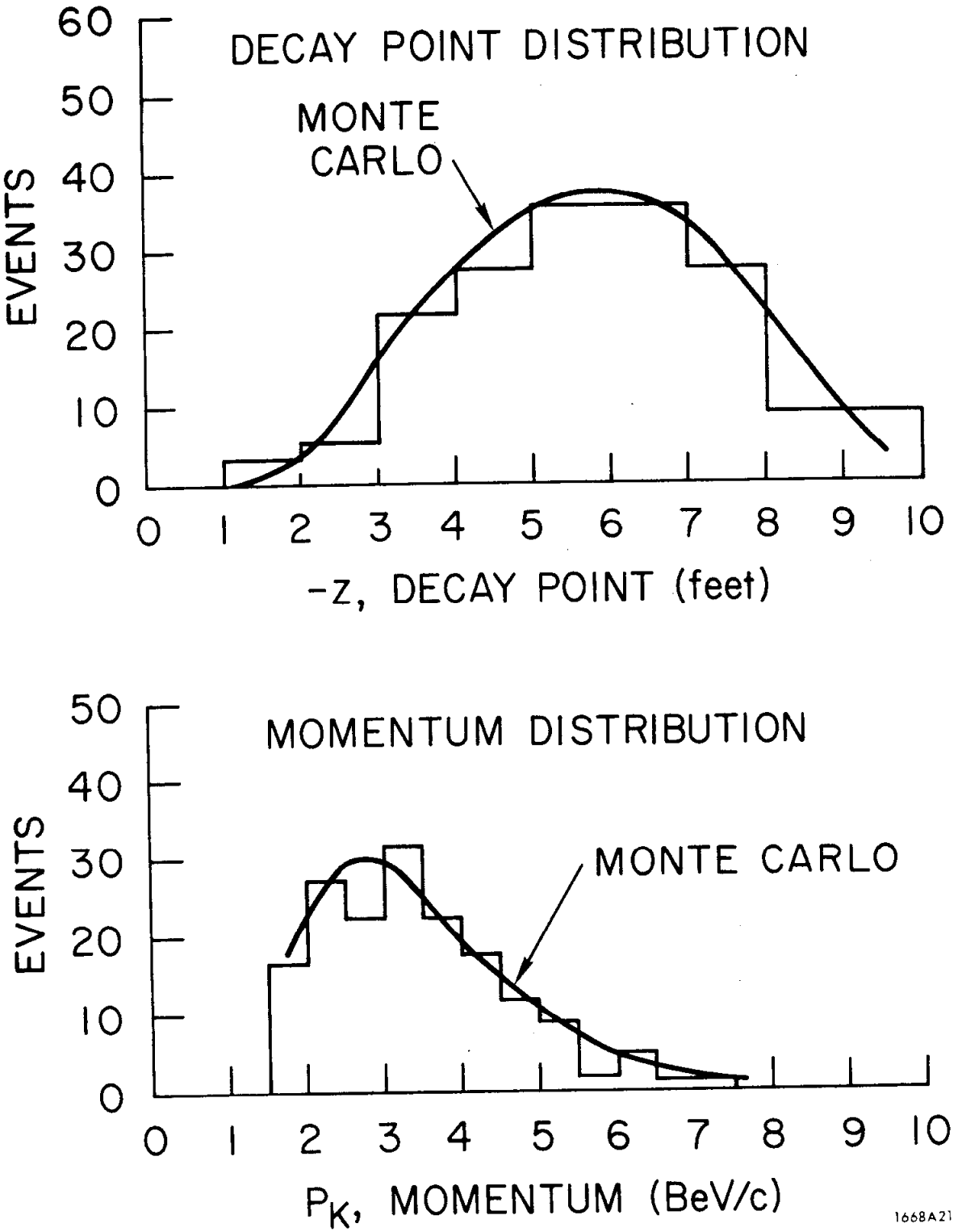

FIG. 22--K_L^o decay point and momentum distributions for good $\pi e \nu_e$ events from Runs 6 and 7.

M* counts for the measured part. We have chosen to scale with No. of M* counts because they are directly proportional to the number of events, as was shown earlier in Fig. 11. To obtain the total number of leptonic decays which actually occurred, we used the Monte Carlo triggering efficiencies calculated for each of the decay modes for each run. Finally, to obtain the number of kaon decays we used the published branching ratios[16]

$$\Gamma(K_L^o \rightarrow \pi\mu\nu_\mu)/\Gamma(K_L^o \rightarrow \text{all}) = .268 \pm .007$$

$$\Gamma(K_L^o \rightarrow \pi e\nu_e)/\Gamma(K_L^o \rightarrow \text{all}) = .388 \pm .008 \quad .$$

Thus for each run we have obtained three independent determinations of the number of kaons which passed through the decay region during the total period of data taking. These numbers are listed in Tables 1, 2, and 3. Averaging the three values, we obtain the following number of kaons, where the listed error is obtained from averaging the determinations

Run 4 (Rolls 0-11, 14-20, 22,24)	111,000 ± 10,000
Run 4 (Rolls 26, 27, 44-50, 52-61)	75,000 ± 7,000
Run 6 (Rolls 54-63, 70-77)	74,000 ± 5,000
Run 7 (Rolls 0-7, 12-23, 26-32, 34-43, 45-75)	136,000 ± 9,000

This gives a total of $N(K_L \rightarrow \text{all}) \cong 396,000 \pm 16,000$. The fact that all three normalizations are in agreement with one another, although they were obtained using distinctly different calculations, is a good indication that there were no large systematic effects, such as scanning inefficiencies, present but unaccounted for.

B. Selection of 2γ Events

1. Scanning and Measuring

All film from Runs 4, 6, and 7 used in the normalization calculation was also scanned by physicists for possible 2γ candidates. The basic criteria for a picture to be listed as a 2γ event was that two and only two gamma showers be visible in the chamber. All these events were then rescanned and checks were made using the counter data which was obtained for each of the first scan candidates. In order not to be eliminated from further considerations each of the second scan candidates had to have at least one gamma which started at the front of the chamber and extrapolated back to a valid trigger counter triplet, and also the second gamma had to be directed in such a way as to not obviously violate momentum conservation, assuming that the gammas had originated from a K_L^o coming down the beam line. This meant that the gammas had to be in opposite quadrants of the x-y plane of the spark chamber. Also eliminated in the second scan were those events where the S counters indicated that an extra gamma had passed through the chamber hole.

All events which passed the second scan were sketched on the 18 in. × 22 in. measuring sheets. For each of the gamma showers on the film a straight line was drawn on the measuring sheet which started at the first spark, continued in the direction of the core of the shower and ended with a range point at the last spark of the shower or the last gap of the chamber. These events were then measured in the standard way.

2. Fitting Procedure and Selection Criterion

Using the sample of 2γ events which were sketched and measured, namely 114 from Run 4, 64 from Run 6, and 114 from Run 7, we have determined a number of properties which allow us to select the true 2γ candidates from the

background. The 292 events were divided into two classes, 159 with no latches, and 133 with one or more latches fired. Ideally, for a genuine 2γ decay, no latches should fire if the two gammas go into the chamber. But, as was seen with the 6γ events, a certain fraction of genuine 2γ decays could have been latched accidentally. Also, the latched events could have been due to other causes: they could have been $2\pi^o$ or $3\pi^o$ decays in which only two gammas appeared in the chamber and one or more of the other gammas converted in the latch counters; or they could have been interactions in which a π^o was produced which showed two gammas in the chamber, and other particles were produced which went into the latch counters. Following our criteria for the calculation of the normalization, we have used only the unlatched events for the calculation of the number of genuine 2γ events.

Each of the unlatched measured events was processed with its counter information to associate the proper trigger and shower counters with each gamma. The gamma laboratory energies were calculated using the formula:

$$E_\gamma = .03\ PH^C_{MI} + .025\ N_g + .28\ PH^P_{MI}\ (BeV)$$

where PH^C_{MI} is the pulse height in the trigger counters, N_g is the number of gaps which the shower traversed, and PH^P_{MI} is the pulse height in the shower counters. The derivation of this formula is given in Appendix A. The energy of the kaon was calculated from the measured time-of-flight. Using this information along with the measured direction cosines, the two gammas were fitted to the hypothesis $K^o_L \rightarrow 2\gamma$ by using two straight lines, originating from a common vertex which was within the constraints of the collimator. The vertex was constrained as follows: $|y| \leq .5$ in. for each run, and $x = \pm 3.1$ in. $\pm .4$ in. for Run 7 and x was not constrained in Runs 4 and 6. The geometrical fit was made in such a

way to minimize a chi square based on the difference between the measured and fitted direction cosines, including the associated errors in these quantities.

The quantity upon which we based the selection of our valid two gamma events is the collinearity of the decay in the K_L^o center-of-mass frame. The collinearity is defined as $\cos \theta^{cm}_{\gamma_1\gamma_2}$, the cosine of the opening angle between the two gamma rays after they have been transformed to the kaon center-of-mass frame, as determined by the measured time-of-flight. After our events were selected, we studied several other associated quantities to verify the hypothesis of $K_L^o \rightarrow 2\gamma$.

Of the 159 unlatched events, 38 events with first measurement giving $\cos \theta^{cm}_{\gamma_1\gamma_2} < -.90$ were measured a second time independently. After the second measurement a total of 30 events were found to have at least one measurement giving $\cos \theta^{cm}_{\gamma_1\gamma_2} < -.96$. When the value of $\cos \theta^{cm}_{\gamma_1\gamma_2}$ differed significantly between the two measurements, both measurements were compared on a spark by spark basis to determine if one of the measurements had been done incorrectly. In several cases it was found that two measurements of the same spark gave reconstructed positions which differed by up to 1 in. in real space. This caused a significant change in one or more of the raw values of direction cosines $\cos \theta_{x_i}$ or $\cos \theta_{y_i}$. We said a mismeasurement had occurred when

$$\left| \cos \theta^{(1)}_{x_i} - \cos \theta^{(2)}_{x_i} \right| \gtrsim .05$$

or

$$\left| \cos \theta^{(1)}_{y_i} - \cos \theta^{(2)}_{y_i} \right| \gtrsim .05$$

and this happened in approximately 10% of the events in both the first and second measurements. The mismeasured events were remeasured a third time and the bad measurement was eliminated by comparison with the other

two. In Fig. 23 we have plotted the first good measurement of cos $\theta^{cm}_{\gamma_1\gamma_2}$ for all unlatched events in the region cos $\theta^{cm}_{\gamma_1\gamma_2} < -.50$. In Fig. 24 we have similarly plotted all of the latched events.

With two good measurements for each event, it was found that of the sample of 30 events, 90% of the first measurements had cos $\theta^{cm}_{\gamma_1\gamma_2} < -.96$ and 85% of the second measurements had cos $\theta^{cm}_{\gamma_1\gamma_2} < -.96$. 75% of both measurements had cos $\theta^{cm}_{\gamma_1\gamma_2} < -.96$, and the other 25% had one measurement with cos $\theta^{cm}_{\gamma_1\gamma_2} < -.96$ and the other measurement with cos $\theta^{cm}_{\gamma_1\gamma_2} < -.90$. Hence, we concluded that a high percentage of all the events had been measured correctly and that there was no large systematic error in the measuring process. For the purposes of further discussion we shall define our sample of good events as those 27 which had a first measurement giving cos $\theta^{cm}_{\gamma_1\gamma_2} < -.96$. A picture of one of these good events is shown in Fig. 13. All of these good measured events were obtained from the complete scan of all the data for all decay modes. To check the scanning efficiency, an entirely independent scan was done, looking only for 2γ events. The independent scan found some additional candidates, but no new events which could be classified as good events after they were measured and fit.

In order to determine the total number of genuine 2γ events over all values of cos $\theta^{cm}_{\gamma_1\gamma_2}$, we had to determine the distribution of cos $\theta^{cm}_{\gamma_1\gamma_2}$, accounting for the measurement and timing errors that were present in the reconstruction and transformation to the center-of-mass. The measuring error originated from two independent sources. The first error was due to the scattering of the electron and position which were created when a gamma converted in the chamber. The

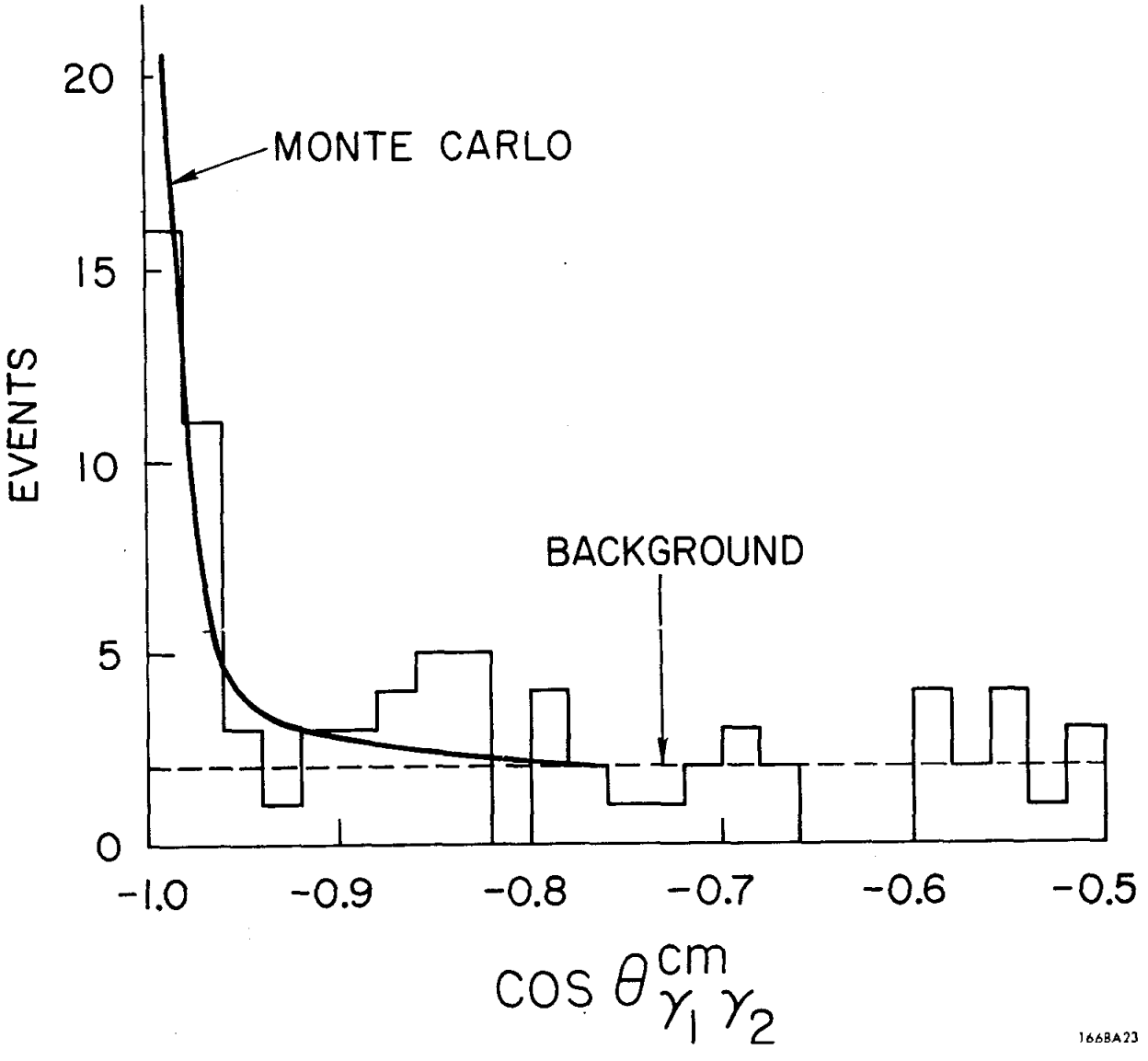

FIG. 23--Collinearity distribution for all unlatched 2γ events.

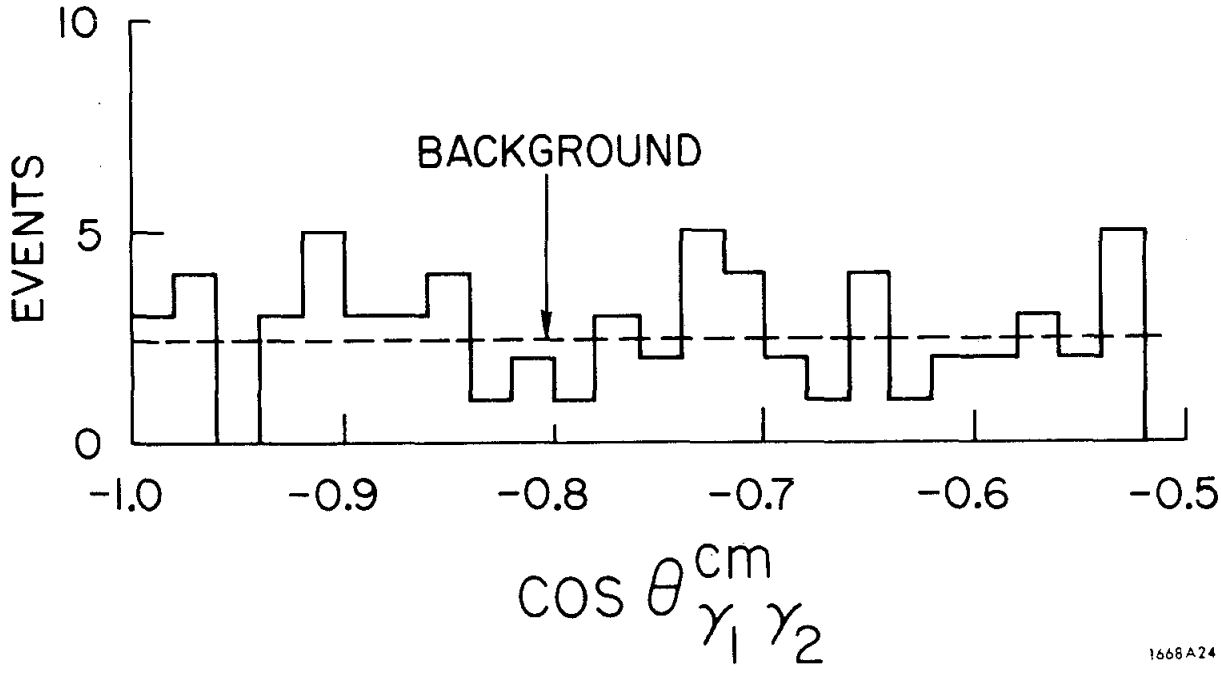

FIG. 24--Collinearity distribution for all latched 2γ events.

total angular error for the scattering process is[30]

$$\theta_{e^\pm} \simeq \frac{21\ \text{MeV}}{P_{e^\pm}}\sqrt{\frac{x}{X_0}} \approx \frac{21\ \text{MeV}}{P_e}$$

where P_e is electron momentum and $x/X_0 \simeq 1$ is the number of radiation lengths traversed which gives the most useful directional information. Since the electron and positron both scatter independently about the initial photon direction the average deviation is

$$\langle\theta^2\rangle = \frac{1}{2}\ \langle\theta^2_{e^\pm}\rangle$$

or

$$\overline{\Delta\theta}_{scat} = \sqrt{\langle\theta^2\rangle} = \frac{1}{\sqrt{2}}\frac{21}{P_e} = \frac{15\ \text{MeV}}{P_e} \approx \frac{25\ \text{MeV}}{E_\gamma}$$

assuming $P_e \approx \frac{1}{2} P_\gamma = \frac{1}{2} E_\gamma$. The second error was the error which occurred in actually measuring the best line which represented the shower direction. This error was estimated by comparing the two measurements of all the good 2γ events, using the formula

$$\cos(\Delta\theta) = \cos\theta_x^{(1)} \cos\theta_x^{(2)} + \cos\theta_y^{(1)} \cos\theta_y^{(2)} + \cos\theta_z^{(1)} \cos\theta_z^{(2)}$$

where 1 and 2 represent measurements of the same angle. The result of these comparisons was

$$\overline{\Delta\theta} = .03 \pm .01 \qquad \text{or} \qquad \overline{\Delta\theta}_{meas} = \overline{\Delta\theta}/\sqrt{2} = .021 \pm .007 \approx .025$$

Note that we have not included any angular error which might be due to possible systematic effects such as local distortions in the lucite, rotation of the chamber, and so forth, because we estimated these would not result in an error as large as the intrinsic measuring error discussed above.

The other error which was present was the time-of-flight error caused by fluctuations in the measured counter times and this error was shown earlier to be

$$\overline{\Delta t}_{TOF} = (.5 \pm .1) \text{ nsec}$$

which is the standard deviation of the difference between the average counter triplet times for valid gamma events which have one upper triplet and one lower triplet, where $\Delta t_{TOF} = t_{TOF}^{C\,upper} - t_{TOF}^{C\,lower}$. A histogram of Δt_{TOF} is shown in Fig. 14. With the error in the difference of two triplet lines given by $\overline{\Delta t}_{TOF}$, then assuming normal errors, the error in each individual time is

$$\overline{\delta t}_{TOF} = \overline{\Delta t}_{TOF}/\sqrt{2} = (.35 \pm .07) \text{ nsec} \approx .4 \text{ nsec}$$

We checked the accuracy of our error estimates by doing a subsidiary test. This consisted of computing the minimum distance in the x-y plane between the measured gamma directions as they converged towards the vertex. We had computed this distance for each of the 27 good events and found it to be an average of about 2 in. For the sample of computations, we used one or two good measurements of each event. We then computed an expected minimum distance in a special way. First, we took each of the fitted good events and we made each into an ideal two gamma event by modifying the values of $\cos \theta_{x_2}$ and $\cos \theta_{y_2}$ of the second gamma to make the event exactly coplanar:

$$\cos \theta_{x_2}^{copl} = - \cos \theta_{x_1} \sin \theta_{z_2} / \sin \theta_{z_1}$$

$$\cos \theta_{y_2}^{copl} = - \cos \theta_{y_1} \sin \theta_{z_2} / \sin \theta_{z_1}$$

We then used the values of $\cos \theta_{z_1}$ and $\cos \theta_{z_2}$ to compute a time-of-flight, t_{collin}, which would make the gammas exactly collinear in the center-of-mass:

$$t_{collin} = 125 \, (1 - \beta^2)$$

where

$$\beta = \left(1 + \cos \left(\theta_{z_1} + \theta_{z_2}\right)\right) / (\cos \theta_{z_1} + \cos \theta_{z_2}) \, .$$

We then modified the new direction cosines by combining them with angular error composed of remeasurement error and coulomb scattering error

$$\overline{\Delta\theta} = \sqrt{(.025)^2 + (.025/E_\gamma)^2}$$

according to the following formulas

$$\cos \theta_{z_i}^{new} = \cos \theta_{z_i} \cos \Delta\theta_i - \sin \theta_{z_i} \sin \Delta\theta_i \cos \phi_i$$

$$\cos \theta_{x_i}^{new} = \left(\cos \theta_{x_i}^{copl} \sqrt{\sin^2 \theta_{z_i}^{new} - \sin^2 \Delta\theta_i \sin^2 \phi_i} - \cos \theta_{y_i}^{copl} \sin \Delta\theta_i \sin \phi_i\right) / \sin \theta_{z_i}^{new}$$

$$\cos \theta_{y_i}^{new} = \left(\cos \theta_{y_i}^{copl} \sqrt{\sin^2 \theta_{z_i}^{new} - \sin^2 \Delta\theta_i \sin^2 \phi_i} + \cos \theta_{x_i}^{copl} \sin \Delta\theta_i \sin \phi_i\right) / \sin \theta_{z_i}^{new}$$

where $\Delta\theta_i$ was normally distributed with mean 0 and standard deviation $\overline{\Delta\theta}$ and ϕ_i was uniformly distributed between 0 and 2π. Using the new direction cosines we computed a minimum distance in the same manner as before. For each good event we had generated five Monte Carlo events and calculated the average minimum distance for the five. We then divided the measured minimum distance for each event by the average value obtained from the Monte Carlo simulation and we plotted this ratio in Fig. 25. Assuming this ratio was distributed as a folded normal restricted to positive values, we plotted a corresponding curve with a standard deviation given by $\sigma = E\{\text{min dist}\}/.793$, where $E\{\text{min dist}\}$ is the expected minimum distance. Note that the agreement is quite good, but the

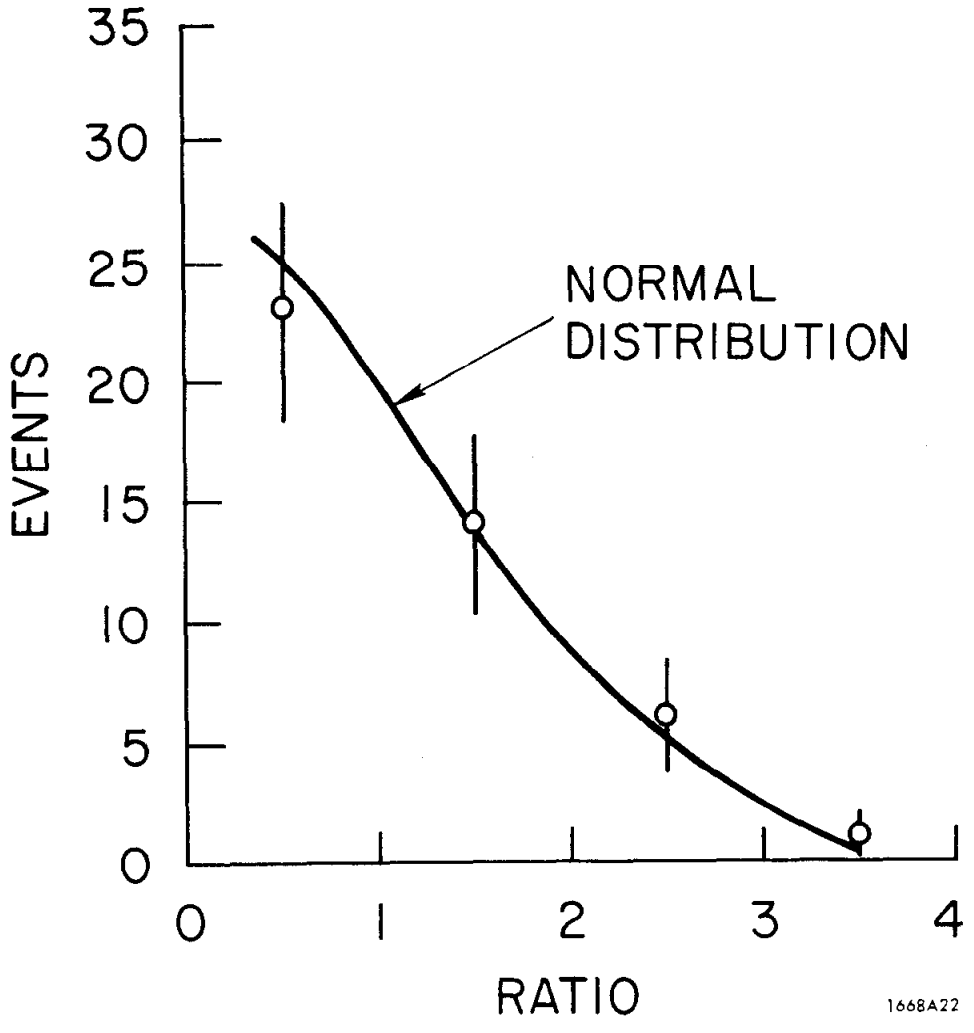

FIG. 25--Distribution of minimum distance ratio.

resolution of the calculations and measurements made in this comparison is only good to about 20%. Thus we can take the angular errors as $\overline{\Delta\theta}_{meas} = .025 \pm .005$ and $\overline{\Delta\theta}_{scat} = (.025 \pm .005)/E_{\gamma}$.

We next calculated the predicted distribution of $\cos \theta^{cm}_{\gamma_1\gamma_2}$ by using the Monte Carlo procedure described above. In other words, for each good event we generated a corresponding ideal event. We then modified its direction cosines with the angular errors given above and modified the collinear time-of-flight with a gaussian error of standard deviation $\overline{\delta t}_{TOF} = .4$ nsec, and fitted the Monte Carlo event in the standard way. To obtain enough statistics we generated ten Monte Carlo events for each good event that we used. We obtained the following results:

Runs 4 and 6: $$\epsilon\left(\cos \theta^{cm}_{\gamma_1\gamma_2} < -.96\right) = 1 - \frac{45\pm7}{170} = .73 \pm .04$$

Run 7: $$\epsilon\left(\cos \theta^{cm}_{\gamma_1\gamma_2} < -.96\right) = 1 - \frac{18\pm4}{190} = .90 \pm .02$$

The efficiency for Run 7 was higher because the tight collimator constraints on the x and y coordinates of the fitted vertex meant that the fit was less sensitive to the measured direction cosines.

Weighting the two values according to the number of K^0_L decays, as given in the normalization, we obtained an average efficiency

$$\bar{\epsilon}\left(\cos \theta^{cm}_{\gamma_1\gamma_2} < -.96\right) = .66\,(.73 \pm .04) + .34\,(.90 \pm .02) = .80 \pm .04$$

A similar calculation, with the timing error increased to $\overline{\delta t}_{TOF} = .5$ nsec, gave $\bar{\epsilon}(\cos \theta^{cm}_{\gamma_1\gamma_2} < -.96) = .75 \pm .04$, so the average efficiency is not critically dependent on the timing error. Also similar calculations were made, modifying the angular errors within the 20% ranges given above, and the average efficiency

was not effected, except within the statistical error given above. The weighted Monte Carlo distribution of $\cos \theta^{cm}_{\gamma_1\gamma_2}$ is given in Fig. 23.

We now verify that the events which we have selected by the collinearity requirement, exhibit other properties of valid $K^o_L \rightarrow 2\gamma$ decays. In Fig. 26 we have plotted the decay point distributions and the kaon momentum distributions for the good events, and these distributions agree quite well with the corresponding Monte Carlo curves.

Next we calculate the coplanarity in the lab frame of the two gamma decays by using the formula

$$\sin \theta_{copl} = \cos\left(\vec{P}_K, \vec{P}_{\gamma_1} \times \vec{P}_{\gamma_2}\right) = \frac{\left(\vec{P}_{\gamma_1} \times \vec{P}_{\gamma_2}\right) \cdot \vec{P}_K}{\left|\left(\vec{P}_{\gamma_1} \times \vec{P}_{\gamma_2}\right) \cdot \vec{P}_K\right|}$$

which has a zero value for two gammas coplanar to the beam direction. We have assumed that the beam is perfectly horizontal, which is experimentally valid to at least .5 ft/250 ft = .002 rad. In Fig. 27 we have plotted the coplanarity for the good events, and this is strongly peaked about $\sin \theta_{copl} = 0.0$ with a standard deviation of about .01 due to the angular errors discussed earlier.

We define a collinear time, t_{collin}, as the time-of-flight necessary to transform from the lab frame to a frame where the polar cosines, $\cos \theta^{cm}_{z_i}$, have equal and opposite value, which means that if the event was coplanar in the lab it would be exactly collinear in this new frame. In Fig. 28 we plot the difference $\delta t = t_{TOF} - t_{collin}$, where t_{TOF} is the measured time-of-flight. The plot shows a peak which is shifted slightly to the side $\delta t > 0$, but is consistent with $\delta t = 0$ to within the error in t_{TOF} of $\overline{\delta t}_{TOF} \simeq .4$ nsec.

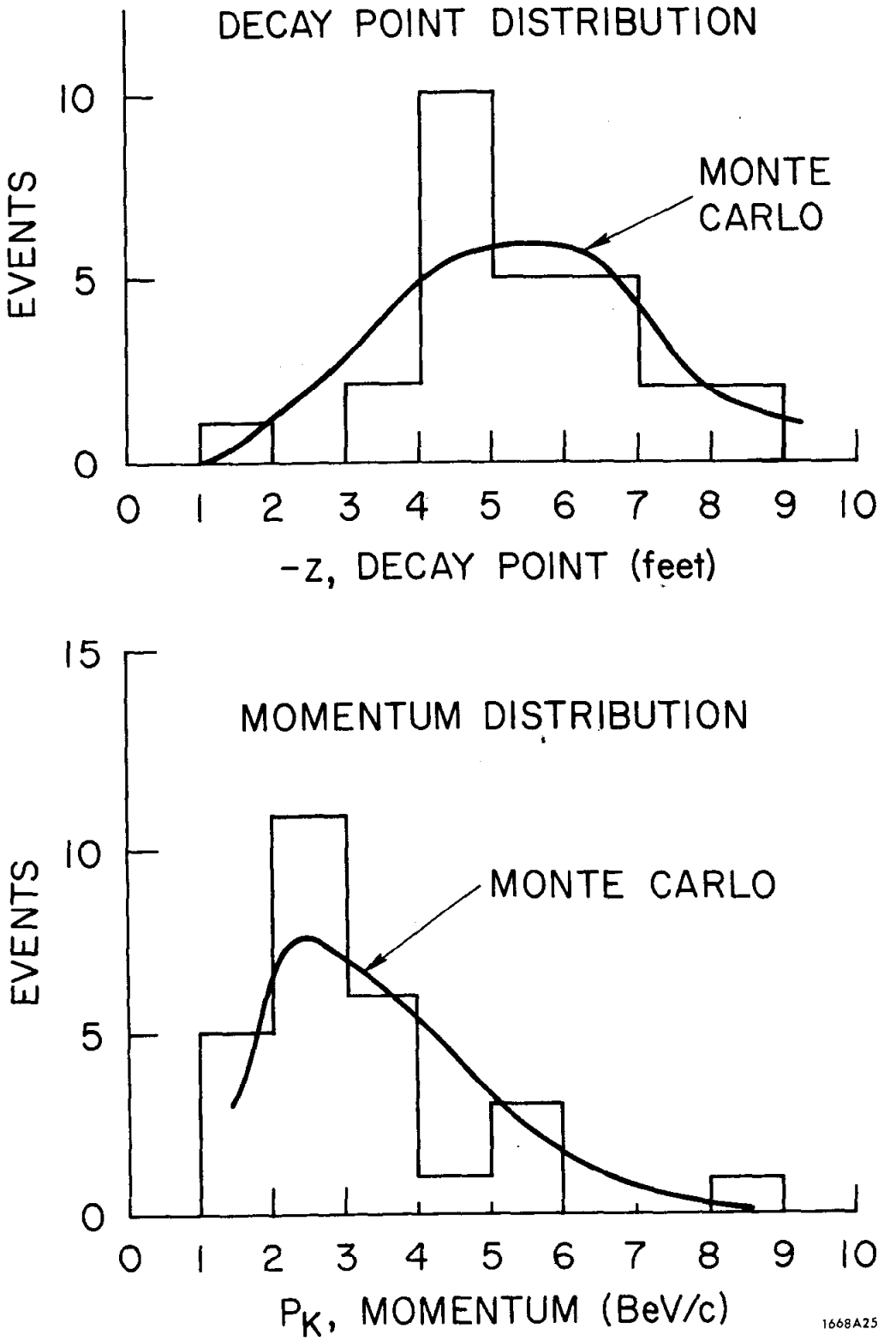

FIG. 26--K_L^o decay point and momentum distributions for good 2γ events.

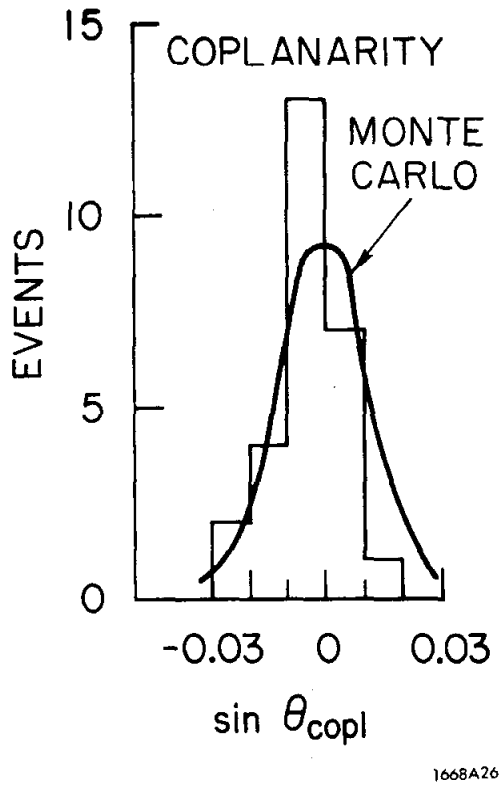

FIG. 27--Coplanarity distribution for good 2γ events.

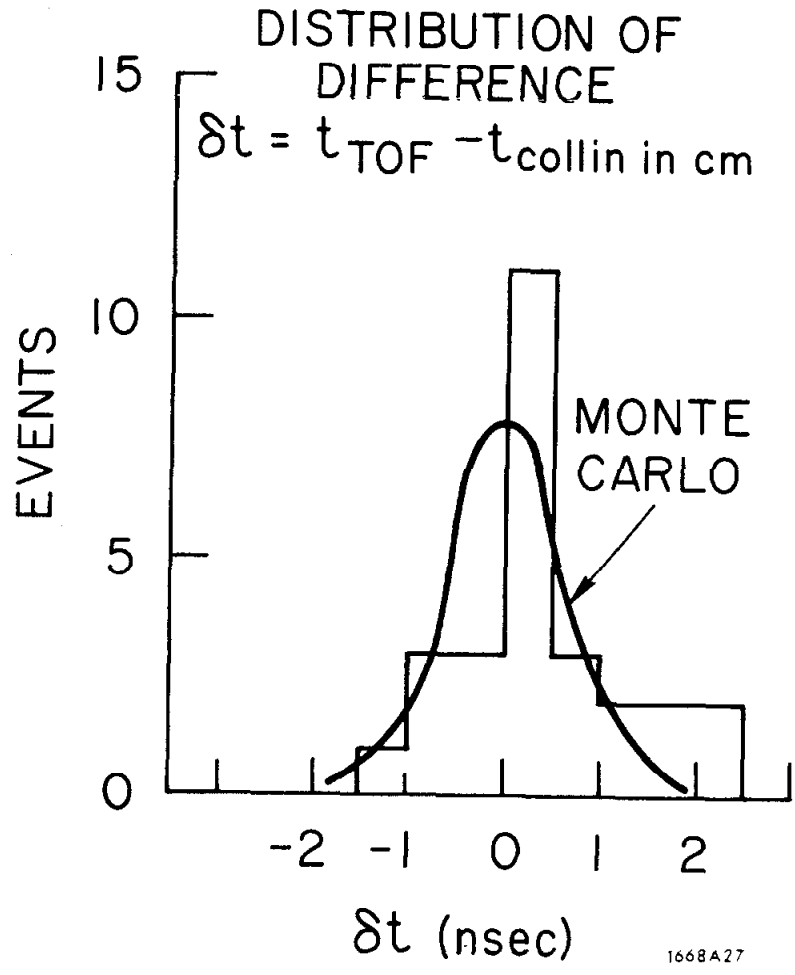

FIG. 28--Time-of-flight difference distribution for good 2γ events.

We calculate the invariant mass of the decay particle using a formula based on the measured gamma energies and direction cosines:

$$M_K = \sqrt{2E_{\gamma_1} E_{\gamma_2} \left(1 - \cos \theta^{lab}_{\gamma_1\gamma_2}\right)}$$

where

$$\cos \theta^{lab}_{\gamma_1\gamma_2} = \cos \theta_{x_1} \cos \theta_{x_2} + \cos \theta_{y_1} \cos \theta_{y_2} + \cos \theta_{z_1} \cos \theta_{z_2} \ .$$

Another determination is based on the measured time-of-flight:

$$M_K = \left(E_{\gamma_1} + E_{\gamma_2}\right) / \gamma(t_{TOF})$$

where

$$\gamma(t_{TOF}) = \sqrt{125/t_{TOF}}$$

The distribution of these mass plots allows us to verify that the decaying particle actually has the mass of a kaon and this is shown in Fig. 29. In some of the events with high energy showers, not all the energy was deposited in the shower counters and hence the measured energy tended to be lower than the true value, leading to lower mass values. Hence, the mass plots are centered somewhat below the kaon mass of .498 BeV. Corresponding Monte Carlo curves have been generated, starting with ideal 2γ events and computing an invariant mass after folding in the angular and timing errors discussed earlier, along with a gamma energy error as discussed in Appendix A.

3. Background Estimates

In an attempt to understand the origin of all the unlatched 2γ events which have been observed and to estimate the background of non 2γ decays which is present in the region of events where $\cos \theta^{cm}_{\gamma_1\gamma_2} < -.96$, we have considered

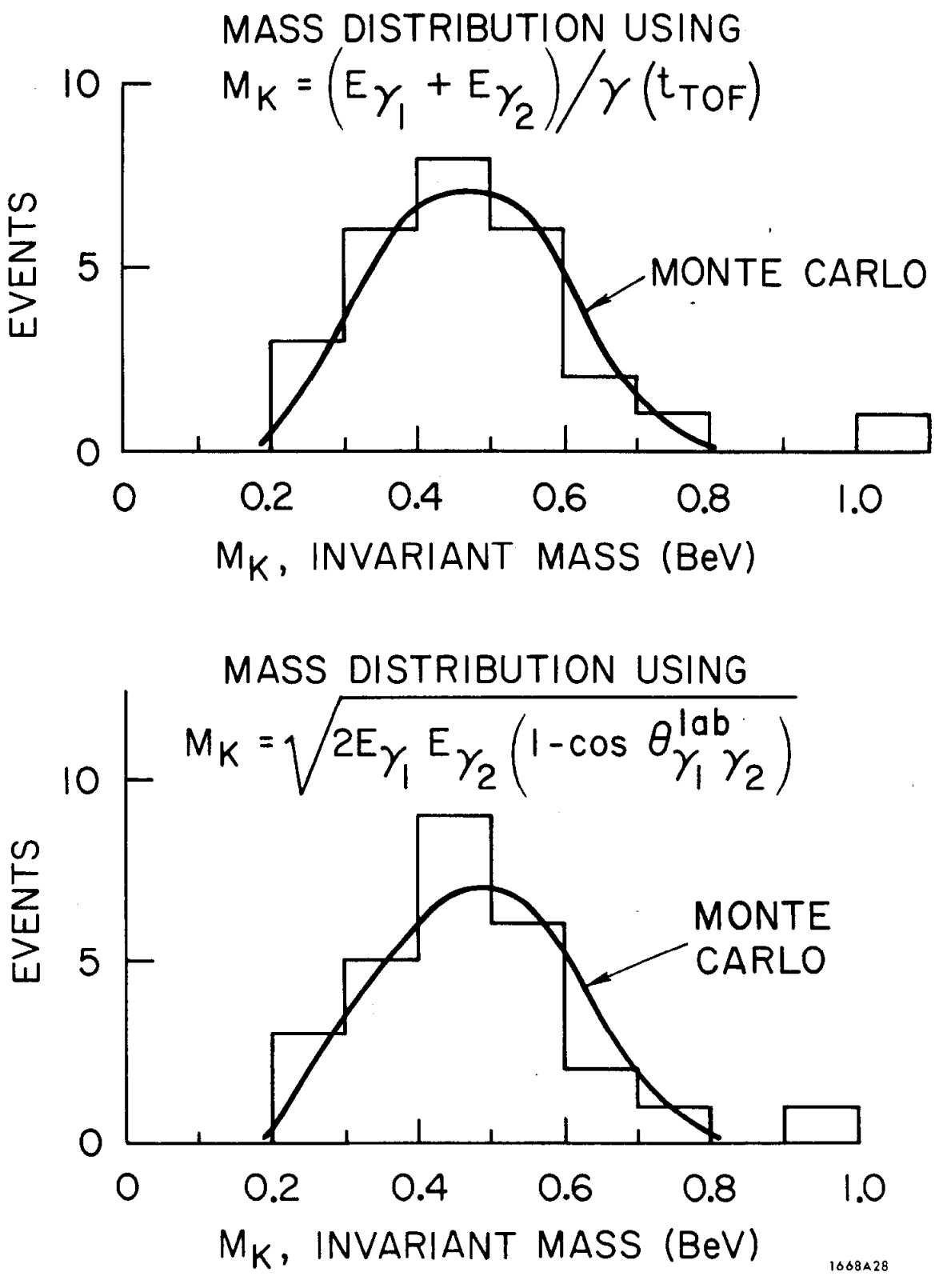

FIG. 29--Invariant mass distributions for good 2γ events.

several possible sources. There are two K_L^o decay modes which can simulate the 2γ decay, namely the $2\pi^o$ and $3\pi^o$ modes. Either of these decay modes looks a 2γ decay if only two gammas convert and shower in the chamber. The remaining gammas must either go through the latches or the chamber without converting. In order for these fake decays to be considered as valid candidates, the two observed gammas must be coplanar in the lab frame and collinear in the center-of-mass frame to the same degree as the genuine 2γ events.

We have generated Monte Carlo $2\pi^o$ and $3\pi^o$ decays which yield events with two converted gammas in the chamber, each in opposite quadrants, with no latches fired and with the proper trigger of $\bar{B} \cdot \bar{V} \cdot C$. For these events we calculated the collinearity and binned the events as a function of $\cos \theta^{cm}_{\gamma_1\gamma_2}$. These distributions are essentially flat, but diminish to zero as $\cos \theta^{cm}_{\gamma_1\gamma_2}$ approaches +1. The total number of such simulated 2γ events for a given number of $2\pi^o$ or $3\pi^o$ decays is particularly sensitive to the conversion probability in the chamber and also to the value of $|\eta_{00}|^2 \equiv \Gamma(K_L^o \to 2\pi^o)/\Gamma(K_S^o \to 2\pi^o)$, which gives the rate $\Gamma(K_L^o \to 2\pi^o)$. We used the values, as discussed earlier, of .5 conversion probability in the lead and 3.2 conversion lengths in the chamber. In the region $\cos \theta^{cm}_{\gamma_1\gamma_2} < -.96$, we estimate < 1 simulated 2γ event originating from 30,000 triggered $3\pi^o$ events, and ~ 1 simulated 2γ event originating from 250 triggered $2\pi^o$ decays. The number of $2\pi^o$ and $3\pi^o$ decays chosen corresponds to the total number of kaon decays calculated earlier ($\simeq 400,000$), and assumes a value of $|\eta_{00}| \simeq 2.5 \times 10^{-3}$.[16,17,33]

Another possible source of background are kaon interactions in the decay volume which produce a π^o that decays into two gammas which shower in the chamber. Such events can in principle be distinguished from true 2γ decays by

computing the invariant mass of the decay particle

$$M_X = \sqrt{2\, E_{\gamma_1} E_{\gamma_2} \left(1 - \cos \theta^{lab}_{\gamma_1\gamma_2}\right)}$$

because any particle having $M_X \lesssim .25$ BeV could not have been a kaon within the resolution of our experiment, as seen from the mass plots in Fig. 29. However, this determination of the mass is sensitive to the accuracy of the formula we use to compute E_γ.

Although we have attempted to estimate the size of the background in the above cases, it is not possible to know if we have considered all possible sources. Hence, we will make a total background estimation by simply assuming that the average background present in the event distribution given in Fig. 23 extrapolates into the region of $\cos \theta^{cm}_{\gamma_1\gamma_2} < -.96$. There are 53 events in the region $-.96 < \cos \theta^{cm}_{\gamma_1\gamma_2} < -.50$, which includes $\left(\frac{1}{.80} - 1\right)(\sim 25) \simeq 6$ good events as predicted by $\bar{\epsilon}\left(\cos \theta^{cm}_{\gamma_1\gamma_2} < -.96\right) = .80$. Thus the average background per bin is $\left[(53-6) \pm 7\right]/23 \simeq 2 \pm .3$, and in the region $\cos \theta^{cm}_{\gamma_1\gamma_2} < -.96$, the background is $2\,(2. \pm .3) = 4. \pm .6 \simeq 4 \pm 1$.

As a further check on the amount of background, the latched 2γ events were all measured and the collinearity $\cos \theta^{cm}_{\gamma_1\gamma_2}$ has been plotted on Fig. 24. We note that there are only 7 events in the region $\cos \theta^{cm}_{\gamma_1\gamma_2} < -.96$. The number of unlatched 2γ events in that region is 27, of which 4 have been estimated to be background leaving 23 above the background. Using the fractions of unlatched events given in Table 1 for each run, we calculate the expected number of latched real 2γ events as

$$(23 \pm 5) \cdot \left[.66(.13) + .34(.20)\right] = 3.7 \pm .8$$

Thus there are

$$(7 \pm 2.6) - (3.7 \pm .8) = 3.3 \pm 2.7$$

events which can be interpreted as background, which is consistent with the background being linearly extrapolated into the region $\cos \theta^{cm}_{\gamma_1\gamma_2} < -.96$. This is further evidence against any mechanism which could produce a large number of false 2γ events in that region.

C. Branching Ratio Calculation

The determination of the branching ratio $BR_{\gamma\gamma} = \Gamma(K^o_L \rightarrow 2\gamma)/\Gamma(K^o_L \rightarrow \text{all})$ depends on the following quantities: the number of observed events which satisfy all the criteria for selection as a genuine 2γ decay, the efficiency for a triggered 2γ decay to satisfy all these criteria, the efficiency for an observed 2γ decay to trigger the detection apparatus, and the total number of kaon decays which occurred during the same time which the 2γ events were triggered.

The number of observed 2γ decays which satisfy all the selection criteria, including the basic requirement that $\cos \theta^{cm}_{\gamma_1\gamma_2} < -.96$, is 27 for all runs. The background has been estimated as 4 events, and hence

$$N_{\gamma\gamma}\left(\cos \theta^{cm}_{\gamma_1\gamma_2} < -.96\right) = (27 \pm 5) - (4 \pm 1) = 23 \pm 5$$

where the error is statistical. The efficiency for a triggered 2γ decay to satisfy the selection criteria is

$$\bar{\epsilon}\left(\cos \theta^{cm}_{\gamma_1\gamma_2} < -.96\right) = .80 \pm .04$$

The efficiency for an observed 2γ decay to trigger the detection apparatus has been calculated by using a Monte Carlo simulation which generated 2γ decays in the same way that $3\pi^o$ decays were generated previously. The average

efficiency for observing two gamma rays in the spark chamber which satisfied the basic triggering requirement of $\bar{B} \cdot \bar{V} \cdot C$ was calculated for each run, integrating over the entire momentum spectrum and decay region

Run 4: $\epsilon_{\gamma\gamma} = .155 \pm .01$

Run 6 and 7: $\epsilon_{\gamma\gamma} = .171 \pm .01$

The average weighted according to the number of kaon decays in each run is

$$\bar{\epsilon}_{\gamma\gamma} = .47\ (.155 \pm .01) + .53\ (.171 \pm .01) = .163 \pm .01$$

The total number of kaon decays was determined to be

$$N(K_L \rightarrow \text{all}) = 396,000 \pm 16,000$$

Thus the branching ratio is

$$BR_{\gamma\gamma} = \frac{\Gamma(K_L^o \rightarrow 2\gamma)}{\Gamma(K_L^o \rightarrow \text{all})} = \frac{N(K_L^o \rightarrow 2\gamma)}{N(K_L^o \rightarrow \text{all})}$$

$$= \frac{\left[N_{\gamma\gamma}\left(\cos\theta^{cm}_{\gamma_1\gamma_2} < -.96\right)/\bar{\epsilon}\left(\cos\theta^{cm}_{\gamma_1\gamma_2} < -.96\right)\right]/\bar{\epsilon}_{\gamma\gamma}}{N(K_L^o \rightarrow \text{all})}$$

$$= \frac{[(23 \pm 5)/(.80 \pm .04)]/(.163 \pm .01)}{(396,000 \pm 16,000)} = \frac{177 \pm 41}{396,000 \pm 16,000}$$

$$= (4.5 \pm 1.0) \times 10^{-4} .$$

CHAPTER VI

CONCLUSIONS

The branching ratio which we have obtained of $BR_{\gamma\gamma} = (4.5 \pm 1.0) \times 10^{-4}$ is consistent with the other determinations of this number, which were discussed earlier and are summarized in Table 4, and with the currently accepted weighted average of $BR_{\gamma\gamma} = (5.2 \pm .5) \times 10^{-4}$.[16] The result is also consistent with the theoretical predictions of the models based on an intermediate state of neutral pseudoscalar bosons.

We believe the experimental method employed here for measuring this decay mode is intrinsically the most straightforward and also free of any systematic effects which could possibly cause a large error in the answer. The main limitation on the accuracy of the result is statistical, although some improvement could have been made if our resolution of measured quantities, such as the time-of-flight and gamma direction cosines, could have been improved, because the statistics and the efficiency factors would have been increased.

TABLE 4

SUMMARY OF $K_L^o \rightarrow 2\gamma$ MEASUREMENTS

Date	Group	Method	Normalization	Total 2γ Events	Branching Ratio, $BR_{\gamma\gamma}$	Reference
1967	Illinois	Spark Chamber Shower Counter	$\pi\mu\nu_\mu$, $\pi e\nu_e$, $\pi^+\pi^-\pi^o$	32	$(6.7 \pm 2.2)\times 10^{-4}$	1
1968	Princeton (1)	Spark Chamber Spectrometer	$3\pi^o$	90	$(5.5 \pm 1.1)\times 10^{-4}$	2
1968	Princeton (2)	Spark Chamber Spectrometer	$3\pi^o$	115	$(4.7 \pm 0.6)\times 10^{-4}$	3
1968	CERN-Orsay	Heavy Liquid Bubble Chamber	$3\pi^o$	16	$(5.3 \pm 1.5)\times 10^{-4}$	20
1970	Particle Data Group	Weighted Average			$(5.2 \pm 0.5)\times 10^{-4}$	16
1970	Stanford	Spark Chamber Shower Counter	$3\pi^o$, $\pi\mu\nu_\mu$, $\pi e\nu_e$	23	$(4.5 \pm 1.0)\times 10^{-4}$	

APPENDIX A

GAMMA ENERGY CALIBRATION

We have derived an empirical formula for gamma energy in terms of PH^{C}_{MI}, the pulse height in the trigger counters, PH^{P}_{MI}, the pulse height in the shower counters, and N_g, the number of gaps traversed by a shower in the spark chamber. This was done by using the sample of 27 good two gamma events. The energies of the gammas were determined theoretically from the fitted gamma direction cosines and the time-of-flight of the kaon. First, we assumed conservation of transverse momentum and divided up the kaon momentum as determined by time-of-flight into the z-components of momenta of the two gamma showers:

$$P_{\gamma_1} \sin \theta_{z_1} = P_{\gamma_2} \sin \theta_{z_2}$$

$$P_K = P_{\gamma_1} \cos \theta_{z_1} + P_{\gamma_2} \cos \theta_{z_2}$$

or

$$E^{trans}_{\gamma_1} = P_{\gamma_1} = P_K \frac{\sin \theta_{z_2}}{\sin \left(\theta_{z_1} + \theta_{z_2}\right)}$$

$$E^{trans}_{\gamma_1} = P_{\gamma_2} = P_K \frac{\sin \theta_{z_1}}{\sin \left(\theta_{z_1} + \theta_{z_2}\right)}$$

Second, we determined the photon energies by using only the polar direction cosines and assuming the gammas were coplanar. This allowed us to transform with velocity β to the center-of-mass frame where the gammas were collinear, and then assign each gamma $m_K/2$ energy and transform back to the lab frame.

The formulas we used were

$$\beta = \frac{\left(1 + \cos\left(\theta_{z_1} + \theta_{z_2}\right)\right)}{\cos\left(\theta_{z_1} + \cos\ \theta_{z_2}\right)}$$

assuming

$$\cos\ \theta_{z_i}^{cm} = \frac{\cos\ \theta_{z_i} - \beta}{1 - \beta \cos\ \theta_{z_i}}$$

Thus

$$E_{\gamma_i}^{collin} = P_{\gamma_i} = \frac{m_K}{2}\left(1/(1-\beta^2)\right)\left(1 + \beta \cos\ \theta_{z_i}^{cm}\right)$$

For each gamma in each of the good events, both formulations gave momenta which were the same to within 10%.

In order to do the calibration, we analyzed the data on the gamma showers in two steps. First, we estimated the energy lost in the trigger counters per unit of PH_{MI} as

$$\Delta E^c \sim 2(1.2\ \text{MeV/gm/cm}^2)\left\{\frac{1}{2}\ (11.35\ \text{gm/cm}^3)\ (.64\ \text{cm})\right.$$

$$\left. + (2.7\ \text{gm/cm}^3)\ (1.27\ \text{cm}) + (1\ \text{gm/cm}^3)\ (4\ \text{cm})\right\}$$

$$\simeq 2.4\left\{4 + 3.5 + 4\right\} \sim 30\ \text{MeV} = .03\ \text{BeV}$$

where the 2 represents an electron and a positron, 1.2 MeV/gm/cm^2 represents a typical ionization loss through material, and the quantities in brackets represent the amount of material traversed assuming the conversion took place half way through the 1/4-in. thick lead and was followed by 1-1/2 in. of scintillator and wood and the first 1/2-in. thick aluminum plate. The average value of PH_{MI}^C

was about 2 in PH_{MI} units, and thus the average energy lost was about .05 BeV, a small amount, but significant for the low energy showers.

Second, we looked at all showers which had traversed the entire chamber (at least the last thirty-seven gaps) and then plotted E_γ^{theor}, the theoretical gamma energy given by the formulas above, vs pulse height in units of PH_{MI}. This sample of events is shown in Fig. A.1, where we have drawn an approximate best fit line to the data points. From the intersection of the best fit line with the E_γ^{theor} axis, we obtained the average energy loss through the entire chamber and also through the lead and trigger counters. This yielded an energy loss of $E^{gap} = (.025 \pm .002)$ BeV/gap. From the slope of the best fit line, we obtained the shower counter contribution to the energy, because the trigger counter and gap contributions were essentially the same for every gamma. This yielded a shower counter energy of $\Delta E^P = (.28 \pm .04)$ BeV per unit of PH_{MI}.

Thus the formula for the gamma momenta is

$$E_\gamma^{meas} = .030\ PH_{MI}^C + .025\ N_g + .280\ PH_{MI}^P\ (BeV)\ .$$

As a measure of the error in our formula we have plotted

$$\delta E = \frac{E_\gamma^{meas} - E_\gamma^{theor}}{E_\gamma^{theor}}\ ,$$

where E_γ^{meas} is the measured energy and E_γ^{theor} is the theoretical energy. In Fig. A.2a we used $E_\gamma^{theor} = E_\gamma^{trans}$ and in Fig. A.2b we used $E_\gamma^{theor} = E_\gamma^{collin}$; and both histograms show a standard deviation of $\overline{\delta E} \simeq .35$, which is roughly the error expected in high energy ($\sim$ 1 BeV) shower measurements.

As a final indication of the reliability of our formula, we have plotted E_γ^{meas} vs E_γ^{collin} in Fig. A.3, which shows that it is fairly good except for very high

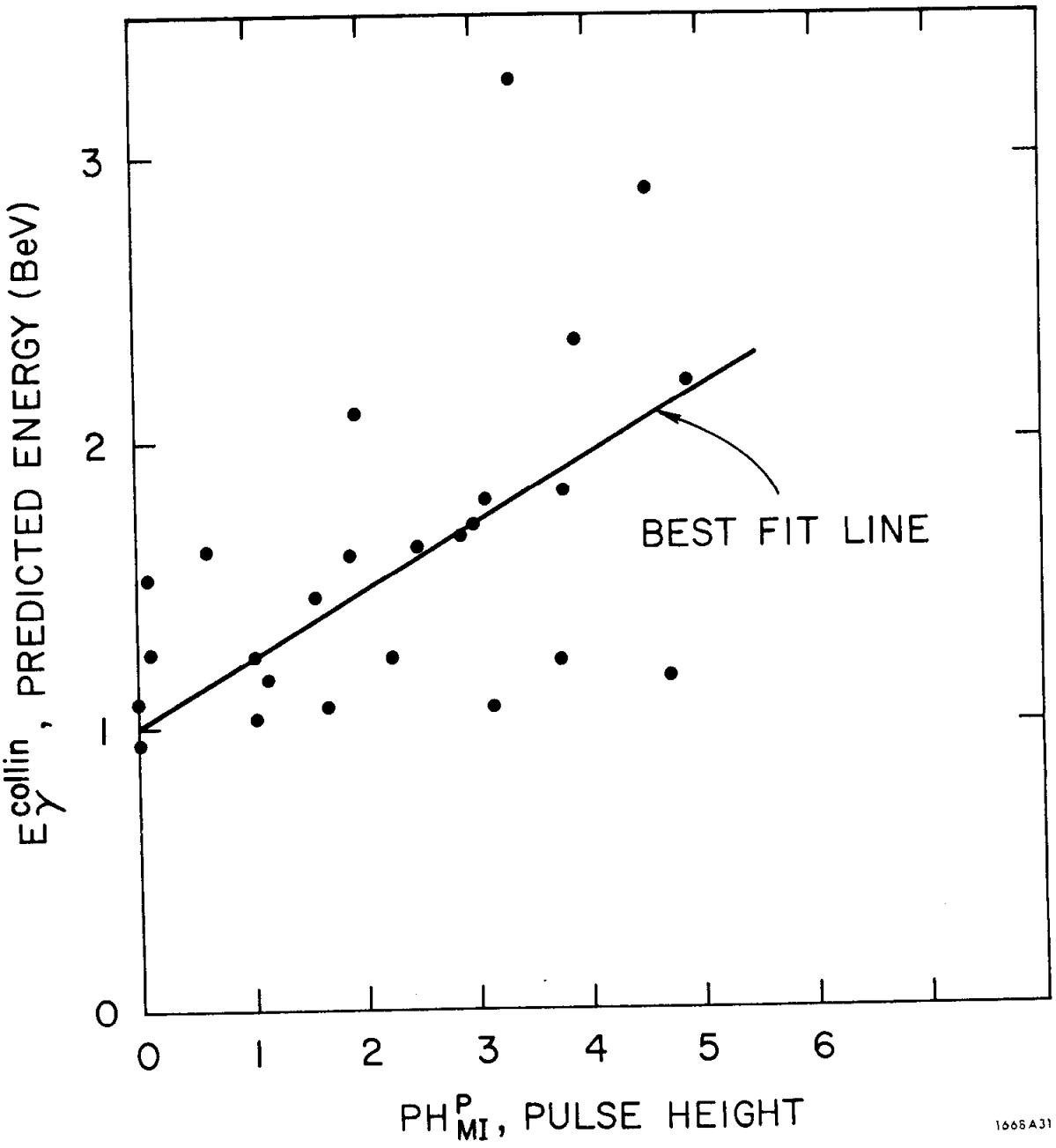

FIG. A.1--Predicted energy vs shower pulse height for gammas showering through chamber.

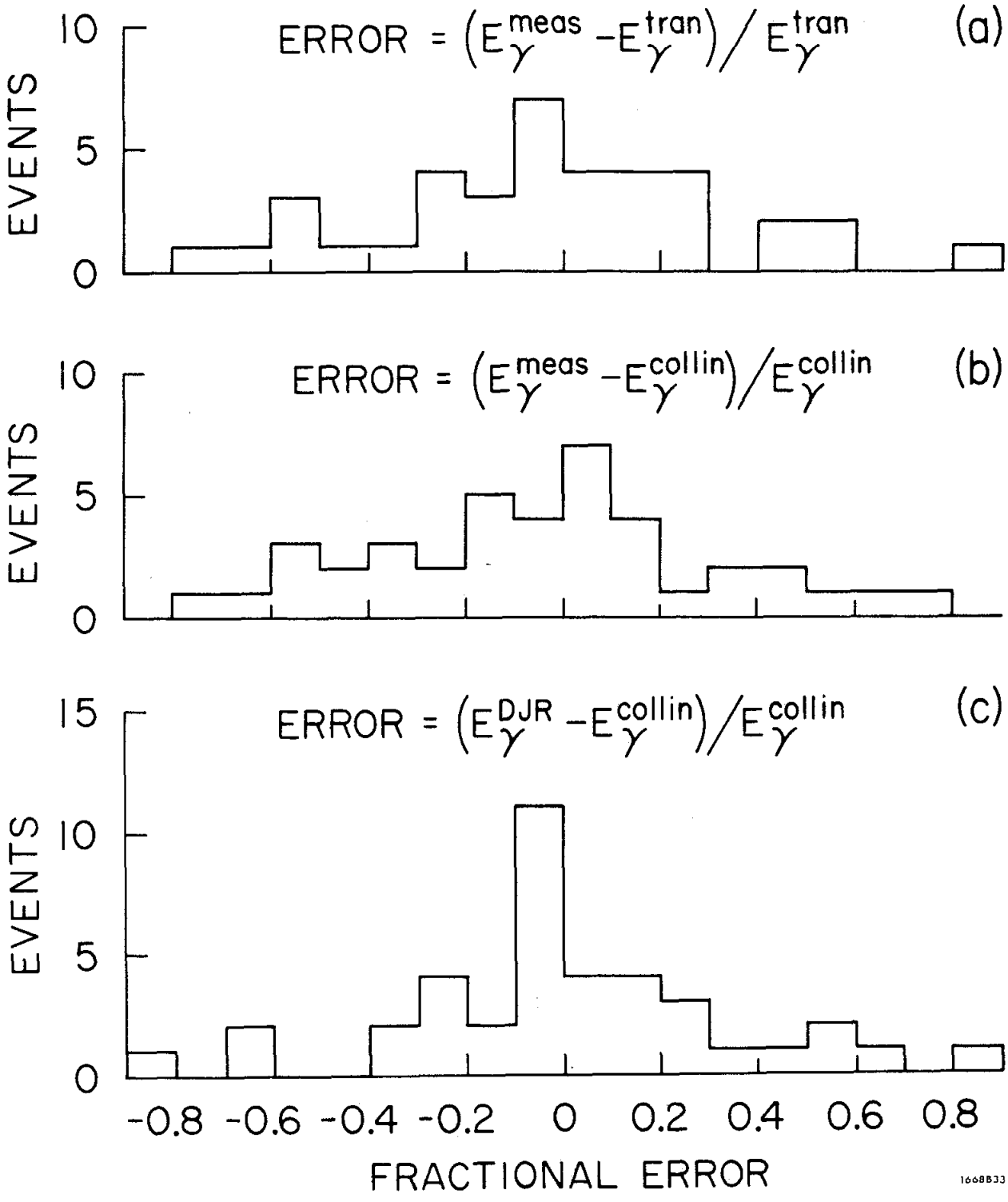

FIG. A.2--Distributions of fractional error in gamma energies.

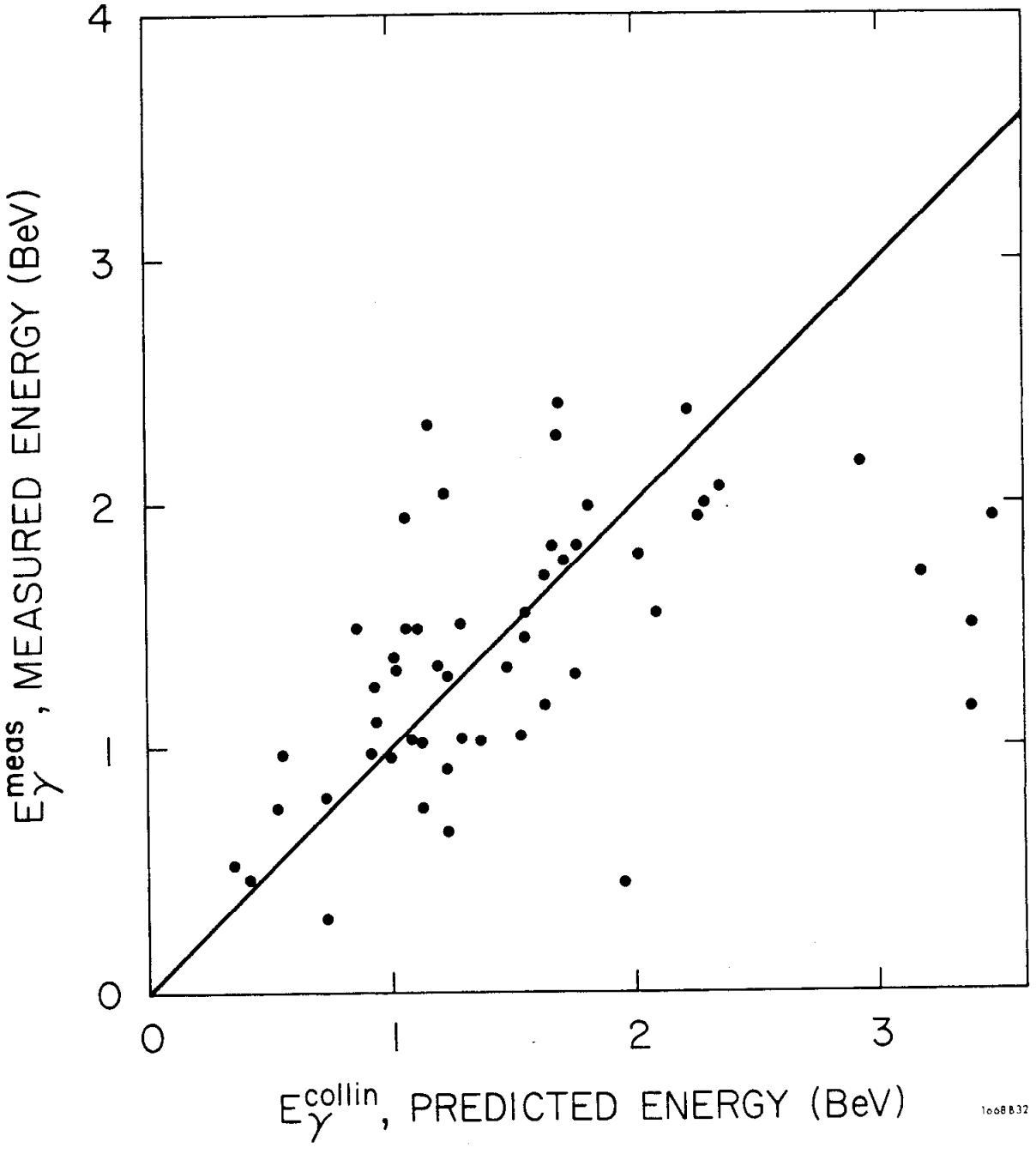

FIG. A.3--Measured energy vs predicted energy for good 2γ events.

energy showers, where it underestimates the true energy because the shower counters do not absorb all the energy.

An independent formula for the gamma momentum was used by D. J. Raymond,[33] which has the form

$$E_\gamma^{DJR} = a\ PH_{MI}^{C} + (b_1 + b_2 N_g)\ N_g + c\ \sqrt{1 + z_{cp}/10}\ \ PH_{MI}^{P}\ (BeV)$$

where a, b_1, b_2, and c are constants and z_{cp} is the z component of the gamma conversion point in inches and $z_{cp}/10$ is roughly the number of conversion lengths traversed before the conversion. The factor $\sqrt{1 + z_{cp}/10}$ is used to compensate for lower values of PH_{MI}^{P} which occur when a shower does not start developing until far into the chamber. Using a least squares fit of E_γ^{DJR} to E_γ^{collin} for the good 2γ events, we obtained the coefficients a = .027, b_1 = .016, b_2 = .00024, and c = .22. In Fig. A.2c we have plotted $\delta E = \left(E_\gamma^{DJR} - E_\gamma^{collin}\right)/E_\gamma^{collin}$, and this histogram shows a standard deviation $\overline{\delta E} \simeq .3$.

APPENDIX B

PION INTERACTION STUDY

To verify the accuracy of one of the parameters used in our Monte Carlo program for the leptonic decays, we calculated the number of pion interaction lengths in the spark chamber and then compared it with the experimentally observed number. The calculation was based on the total absorption cross section for pions interacting in the chamber. First we computed the average total cross section, $\bar{\sigma}_T$, by integrating the total cross section σ_T, over the energy spectrum of pions as given in the Monte Carlo simulations of the $\pi\mu\nu_\mu$ and $\pi e\nu_e$ decays. We assumed that the energy dependence of the pion cross section in aluminum and G10 was the same as that for carbon, for which experimental data was available.[36] In Fig. B.1 we show the total cross section in carbon, σ_T^C, as a function of pion kinetic energy, T_π. At higher energies, i.e., $T_\pi < 0.5$ BeV, σ_T^C approaches the geometrical cross section, $\sigma_{geom}^C = \pi(\hbar/m_\pi c)^2 A^{2/3} = .0628 \cdot A^{2/3} = .33$ barns.[16] Thus we obtained for both the leptonic decays that

$$\bar{\sigma}_T^{Al} = (1.20 \pm .02)\, \sigma_{geom}^{Al}$$

The total amount of material contained in the forty 1/2-in. thick plates of aluminum and G10 was $\ell_{Al} + \ell_{G10} = 70 + 45 = 115$ gm/cm^2, where we have neglected a 2% correction due to the average incidence angle at which the pions passed through the chamber. Using geometrical cross sections, the interaction length for aluminum is $L_{int}^{Al} = A/N\sigma_{geom}^{Al} = 80$ gm/cm^2 and the interaction length for G10 is approximately[34]

$$L_{int}^{G10} = \frac{\sum w_i A_i}{N \sum w_i \sigma_{geom}^i} = 76 \text{ gm/cm}^2$$

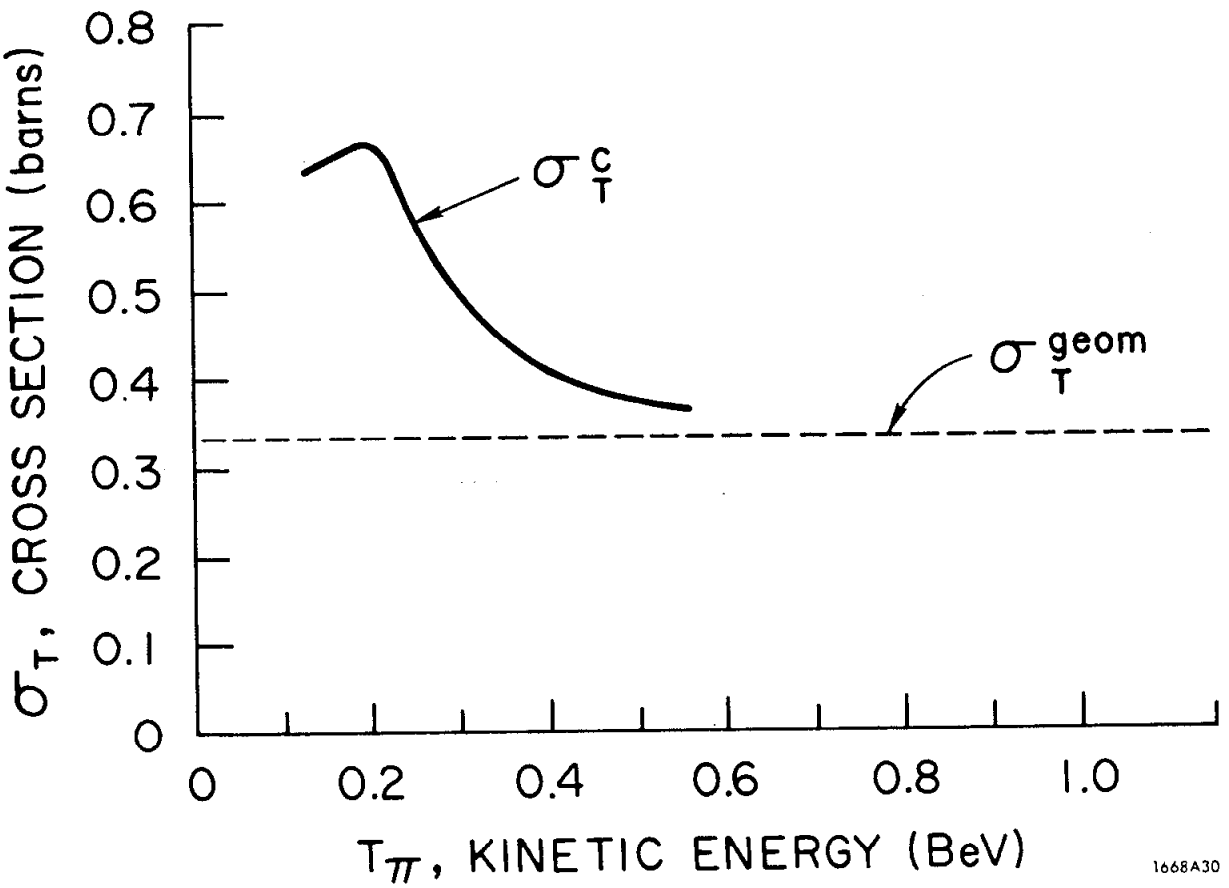

FIG. B.1--Pion interaction distributions.

where N is Avogadro's number and w_i is the fraction of the element with atomic weight A_i and cross section σ^i_{geom}, as given by the known composition of G10.[24] Thus the interaction length for the chamber is $L^{ch}_{int} = (78 \pm 2)$ gm/cm$^2 \simeq L^{Al}_{int}$ using geometrical cross sections, and is

$$\bar{L}^{ch}_{int} \cong L^{ch}_{int} \frac{\sigma^{Al}_{geom}}{\bar{\sigma}^{Al}_{T}} \simeq (78 \pm 2)/(1.2 \pm .02) = (65 \pm 2) \text{ gm/cm}^2$$

using the average energy dependent cross sections. The estimated number of interaction lengths contained in the chamber was thus

$$115/(65 \pm 2) = 1.8 \pm .06$$

For comparison, we experimentally measured the number of pion interaction lengths in our spark chamber. We did this by using the sample of measured monitor events which satisfied our selection criteria and obtaining a distribution of the pion interaction point. We distributed the interaction point into four bins which were each nine gaps wide, namely gaps 4-12, gaps 13-21, gaps 22-30, and gaps 31-39, and a fifth bin which included all tracks which did not interact before gap 40. These distributions were obtained using 482 $\pi\mu\nu_\mu$ events and 234 $\pi e\nu_e$ events from Runs 4, 6, and 7. In Fig. B.2 we have displayed these distributions in both differential and integral form, where a differential bin contained the number of pions which interacted within the gaps of that bin, and an integral bin contained all the pions which interacted after the first gap of that bin.

A pion interaction length is defined as the amount of material a pion must penetrate such that the differential number of interacted pions is reduced by a factor of 1/e, or such that the total number of uninteracted pions is reduced by a factor of 1/e. The number of interaction lengths for a chamber of forty plates

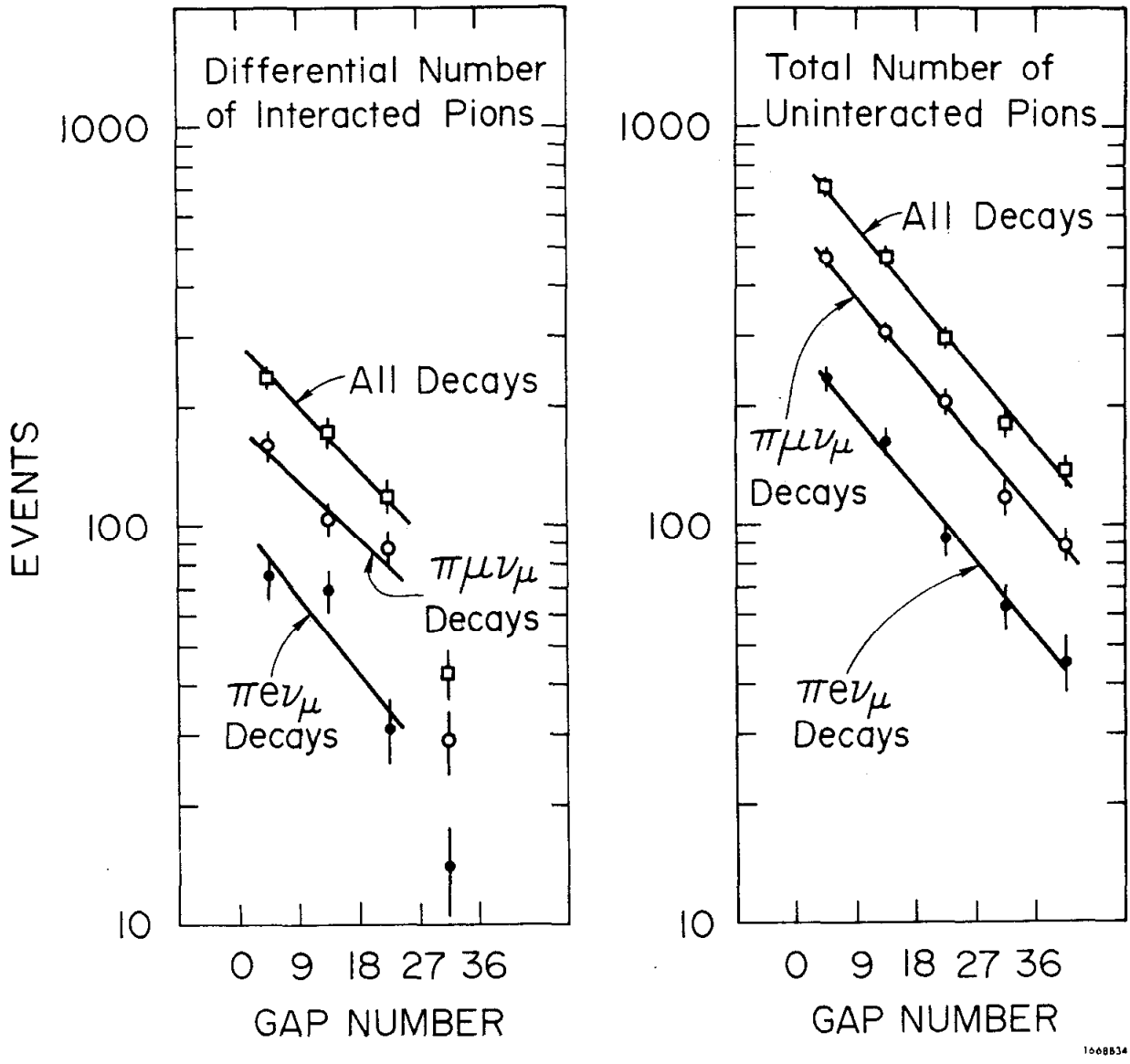

FIG. B.2--Pion total absorption cross section in carbon.

can be determined from the slopes shown in Fig. B.2. However, the differential slopes were not as accurate because for high energy pions it was difficult to observe a pion interaction in the last few gaps and hence the last data point was low. Thus we used the integral slopes because they included a fifth data point for uninteracted pions and also because there was greater statistical accuracy in all of the data points. Using the combined totals for the $\pi\mu\nu_\mu$ and $\pi e\nu_e$ events and computing the number of interaction lengths for forty plates, we obtain

$$\left(\frac{40}{36}\right) \ln \frac{(700 \pm 26)}{(131 \pm 11)} = 1.9 \pm 0.1$$

A similar calculation for the $\pi\mu\nu_\mu$ events yields 1.85±0.1 interaction lengths, and for the $\pi e\nu_e$ events yields 1.9±0.2 interaction lengths. These values are in good agreement with the calculated number.

REFERENCES

1. J. Todoroff, "Measurement of the two-photon decay of the K_L^o meson," Thesis, University of Illinois (1967), unpublished.
2. P. Kunz, "Measurement of the $K_L^o \rightarrow \gamma\gamma$ branching ratio," Thesis, Princeton University (1968), Elementary Particles Laboratory Report No. 46.
3. J. Pilcher, "Experimental study of some radiative decay modes of the K_L and K_S mesons," Thesis, Princeton University (1968), Elementary Particles Laboratory Report No. 49.
4. J. Dreitlein and H. Primakoff, Phys. Rev. 124, 268 (1961).
5. S. Oneda and S. Hori, Phys. Rev. 132, 1800 (1963).
6. C. Bouchiat, J. Nuyts, and J. Prentki, Phys. Letters 3, 156 (1963).
7. S. Oneda, Y. S. Kim, and D. Korff, Phys. Rev. 136B, 1064 (1964).
8. V. K. Ignatovich and B. V. Struminsky, Phys. Letters 24B, 69 (1967).
9. L. M. Sehgal and L. Wolfenstein, Phys. Rev. 162, 1362 (1967).
10. H. Stern, Nuovo Cimento 51A, 195 (1967).
11. D. F. Greenberg, Nuovo Cimento 56A, 597 (1968).
12. C. A. Savoy and A. H. Zimerman, Nuovo Cimento 57A, 201 (1968).
13. R. Rockmore, Phys. Rev. 182, 1512 (1969); 187, 2125 (1969).
14. B. R. Martin and E. de Rafael, Nucl. Phys. B8, 131 (1968).
15. S. Oneda and J. Pati, Phys. Rev. 155, 1621 (1967).
16. Particle Data Group, "Review of particle properties," Rev. Mod. Phys. 42, 87 (1970).
17. M. Banner, J. W. Cronin, J. K. Liu, and J. E. Pilcher, Phys. Rev. 188, 2033 (1969). Earlier references can be found in this paper.

18. V. Barger, Nuovo Cimento 32, 127 (1964).

19. L. Criegee, J. D. Fox, H. Frauenfelder, A. O. Hanson, G. Moscati, C. F. Perdrisat, and J. Todoroff, Phys. Rev. Letters 17, 150 (1966).

20. R. Arnold, I. A. Budagov, D. C. Cundy, G. Myatt, F. Nezrick, G. H. Trilling, W. Venus, H. Yoshiki, B. Aubert, P. Heusse, E. Nagy, and C. Pascaud, Phys. Letters 28B, 56 (1968).

21. R. B. Neal, The Stanford Two-Mile Accelerator, (W. A. Benjamin, Inc., New York, 1968).

22. A. D. Brody, W. B. Johnson, D.W.G.S. Leith, G. Loew, J. S. Loos, G. Luste, R. Miller, K. Moriyasu, B. C. Shen, W. M. Smart, and R. Yamartino, Phys. Rev. Letters 22, 966 (1969).

23. D. Drickey, H. Ticho, D. Stork, C. Buchanan, D. Rudnick, P. Shephard, E. Dally, E. Seppi, L. Ettlinger, R. Zdanis, P. Innocenti, SLAC Proposal No. 44 (1968). Also see SLAC Proposals No. 32 and 27.

24. R. T. Walsh, General Electric Company, 1969, private communication.

25. W. A. Wenzel, "Spark chambers," Ann. Rev. Nucl. Sci. 14, 205 (1964).

26. J. W. Cronin, "Spark chambers," from Bubble and Spark Chambers; Principles and Use, ed. R. P. Shutt (Academic Press, New York, 1967), p. 315.

27. D. Porat and K. Hense, Nucl. Instr. Methods 67, 229 (1969).

28. PDP-9 User Handbook, Digital Equipment Corporation, Maynard, Massachusetts (1968).

29. S. Wojcicki, "Software description," (1968) unpublished.

30. B. B. Rossi, High-Energy Particles (Prentice-Hall, Inc., Englewood Cliffs, New Jersey, 1952).

31. D. M. Ritson, Techniques of High Energy Physics (Interscience Publishers, New York, 1961).

32. Incremental Magnetic Tape Recorder, Model 1600/360, Operation and Maintenance Manual, Kennedy Co., Altadena, California.

33. D. J. Raymond, "CP violating decay of the neutral kaon into two neutral pions," Thesis, Stanford University (1970), unpublished.

34. J. H. Hubbell, "Photon cross sections, attenuation coefficients, and energy absorption coefficients from 10 keV to 100 GeV," National Bureau of Standards, Washington, D. C. (1969).

35. S. W. MacDowell, Nuovo Cimento 6, 1445 (1957).

36. A. E. Ignatenko, CERN Symposium 1956, II/45, p. 313.